Fakultät für Elektrotechnik und Informationstechnik

Heinz Nixdorf-Lehrstuhl für Medizinische Elektronik

Inkjet-printed flexible and disposable biochips with SWCNT sensors for multiparametric microphysiological measurements

Dipl.-Ing.Univ. Nada Mzoughi

Vollständiger Abdruck der von der Fakultät für Elektrotechnik und Informationstechnik der Technischen Universität München zur Erlangung des akademischen Grades eines

Doktor-Ingenieurs

genehmigten Dissertation.

Vorsitzende(r): Prof. Dr. Dr.h.c. Alexander W. Koch
Prüfer der Dissertation:
1. Prof. Dr. Bernhard Wolf
2. Prof. Dr. Franz Kreupl

Die Dissertation wurde am 30.08.2016 bei der Technischen Universität München eingereicht und durch die Fakultät für Elektrotechnik und Informationstechnik am 20.02.2017 angenommen.

To my mother Monia Mabrouk,
my father Mahmoud Mzoughi
and my brother Aymen.

Thank you for your love, continuous support and encouragement

Abstract

In recent years, printed and organic electronics have gained increasing attention due to their potential for bendable, light weight and low cost devices. Combining new materials with novel manufacturing methods offers the opportunity for a wide range of new applications where the conventional electronics reaches its limits. Here we present a proof-of-concept demonstration of all inkjet-printed, low cost and disposable biochips on flexible substrates that present an attractive alternative to the conventional rigid biochips from an economic point of view. These flexible biochips can be interesting for various applications such as in-vitro cell monitoring for diagnostics, toxicity tests and environmental monitoring. Successful inkjet deposition of electrically functional inks on different polymer substrates has been achieved. Obtaining conductive tracks using nanoparticles based inks without damaging the thermally instable substrates is challenging. Therefore, we investigated different sintering methods and compared the obtained electrical and mechanical performance of the printed tracks. Using a combination of silver, CNTs and polymer based tracks we could fabricate printed biochips that are biocompatible, bendable and robust enough in aqueous media to allow reliable and reproducible cell measurements. Due to their nanoscale nature and remarkable properties, using SWCNTs for biosensing applications can offer new opportunities in detecting biochemical targets. Novel SWCNT based sensors for the detection of pH and dissolved oxygen concentration changes can simply be integrated into the biochips either using drop-casting or inkjet printing and offer the advantage of simple impedimetric measurements without the need for a reference electrode. The suitability of these sensors for the monitoring of cells metabolic activity has been demonstrated with and without cells.

Acknowledgements

I would like to thank my advisor Prof. Dr. rer. nat. Bernhard Wolf for his mentorship and the possibility to work under his direction on this interdisciplinary and very exiting topic. I also would like to express my sincere gratitude to my supervisor Dr. Helmut Grothe who has guided me through my journey at TUM since my bachelor thesis. Without his generous help, patience and much appreciated advice none of this work could have been possible.
Special thanks to Frau Remm for the both enjoyable and productive collaboration.
Next, I would like to thank all my colleagues at the Heinz-Nixdorf Chair for Medical Electronics especially Yazay Eminaga, Senta Stein, Franz Demmel and Walter Wirths that were a source of support and motivation to me. Also thanks to Ingrid Franz for her dedication and support.
Further, I am thankful to the students that have positively contributed to my work especially Tayfun Günay, Hao Wu, Lena Zeithöfler, Alfred Ng Han, Eyüp Karakoc and Touba Jamal Khalaf.
Finally, I would like to thank Mr. Klaus Petersen from Mitsubishi Polyester Film, Ms. Stefanie Eiden from Bayer Technology Services and Mr. Thane Gough from DuPont Teijin Films for generously providing us with free samples and for their support.

This work was sponsored by the German Federal Ministry of Education and Research (research project PRINTS, FKZ 16SV5393). Financial support by the Heinz Nixdorf Foundation is also kindly acknowledged.

Publications

Conference Proceedings

[1] N. Mzoughi, B. Neumann, H. Grothe, B. Wolf, “Inkjet-printed electrodes on PET substrate for biosensing applications”, *45. DGBMT Jahrestagung,* Freiburg, 27.–30. September 2011.

[2] B. Neumann, N. Mzoughi, H. Grothe, B. Wolf, “Inkjet Printing of Nanomaterials for Microsensors”, *45. DGBMT Jahrestagung*, Freiburg, 27.–30. September 2011.

[3] N. Mzoughi, B. Neumann, H. Grothe, B. Wolf, “Gedruckte Sensorik für multiparametrische Zell-Sensorchips”, *Jahrestagung BioMST e.V.,* Ilmenau, 19.-21-June 2012.

[4] N. Mzoughi, H. Grothe ,M. Remm, B. Neumann, B. Wolf, “Inkjet-gedruckte Leiterbahnen für die Herstellung bioelektronischer Einweg-Sensorchips”, *Entwicklerforum Medizinelektronik,* München, 25.04.2013.

[5] N. Mzoughi, H. Grothe ,M. Remm, B. Neumann, B. Wolf, “Inkjet-gedruckte, flexible bioelektronische Einweg-Sensorchips für das Zell Monitoring”, *Entwicklerforum Medizinelektronik,* München, 08.10.2014.

[6] N. Mzoughi, H. Grothe, M. Remm, B. Neumann, B. Wolf, “Inkjet-printed biochips for cell-chip applications”, *International Workshop on Flexible Bio- and Organic Printed Electronics,* Konya, Turkey, 1-3 May, 2014.

[7] Y. Eminaga, N. Mzoughi, J. Wiest, M. Brischwein, J. Clauss, H. Grothe, B. Wolf, “Implantable In-situ Calibrated Dissolved Oxygen Micro Sensor for Improved Long Term Stability in Smart Electronic Therapy Support Systems”, *International Workshop on Flexible Bio- and Organic Printed Electronics,* Konya, Turkey, 1.–3. May 2014.

[8] N. Mzoughi, M. Remm, B. Neumann, H. Grothe, B. Wolf, “ Inkjet-printed flexible and disposable biochips for in-vitro tumor diagnostics”, *International Exhibition and Conference for the Printed Electronics Industry LOPEC,* 3.–5 March 2015.

[9] N. Mzoughi, M. Remm, B. Neumann, H. Grothe, B. Wolf, “Inkjet-gedruckte, flexible Einweg-Sensorchips als Alternative zu den konventionellen Chips für das Zell Monitoring”, *9. Deutsches BioSensor Symposium,* München, 11.–13 March 2015.

[10] N. Mzoughi, M. Remm, B. Neumann, H. Grothe, B. Wolf, “Flexible Einweg-Sensorchips für das Zell Monitoring getestet mit lebenden Zellen”, 12. Dresdner-Sensor-Symposium, Dresden, 07.–09 December 2015.

Peer reviewed journals

[1] N. Mzoughi, A. Abdellah, Q. Gong, H. Grothe, P. Lugli, B. Wolf, G. Scarpa, “Characterization of novel impedimetric pH-sensors based on solution-processable biocompatible thin-film semiconducting organic coatings”, Sensors and Actuators B, vol. 171– 172, pp. 537– 543, 2012

Table of Contents

Chapter 1

Introduction

After the demonstration of the bipolar junction transistor in 1947 and the first integrated circuit in 1958 electronics have evolved a lot over the years. The transistors are getting smaller and faster allowing a shift in the way electronic devices are used from a specialized industrial system to an ubiquitous and personal level of communications and entertainment system.
Despite the tremendous progress of main stream electronics, their application opportunities still face limitations due to their rigid and brittle nature as well as the complex and expensive fabrication process. The discovery of conducting polymers in 1977 allowed the integration of new materials in electronics and triggered a new era of organic and printed electronics. The printing technology opened up new research and manufacturing opportunities that could not be achieved with conventional electronics. The possibility for large area fabrication of low-cost and flexible devices has positively affected several research fields and is of special interest for biomedical applications.

1.1 Background and motivation

Changes brought by urbanization and modern life such as smoking, fast food consumption and physical inactivity have been associated with several diseases, one of the deadliest among which being cancer. Cancer is a leading cause of death worldwide and constitutes a burden on society in more and less developed countries alike [1].
Although the incidence rates are expected to grow further in the next years, proper diagnosis at early stages increases the chance for cancer curing. Classical screening methods, however, suffer from various limitations such as poor sensitivity and specificity or lengthy assays. For example, a study has shown that 23.8% of women over 40 years old had at least one false positive mammogram [2] which may not only result in short term anxiety but also leads to overdiagnosis and overtreatment [3].
A more reliable and efficient alternative consists in using biochips and cell based assays for in-vitro medical diagnostics [4, 5].

Multiparametric sensor chips (figure 1.1) have been demonstrated as a powerful tool for the recording of cellular microphysiological patterns [6, 7]. Equipped with different integrated sensors like pH, pO_2, electrical impedance and temperature sensors, the biochips can deliver information about cell metabolism, growth, adhesion and morphological changes [7]. By monitoring these parameters, the response of the cells to external stimuli such as the addition of specific drugs can be observed.

(a) (b)

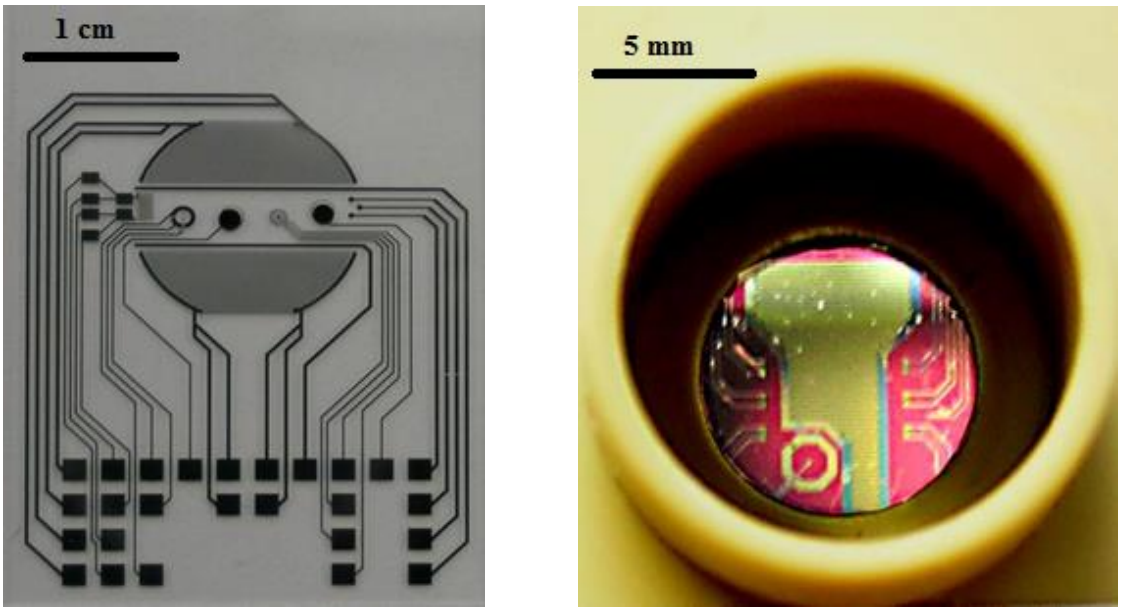

(c)

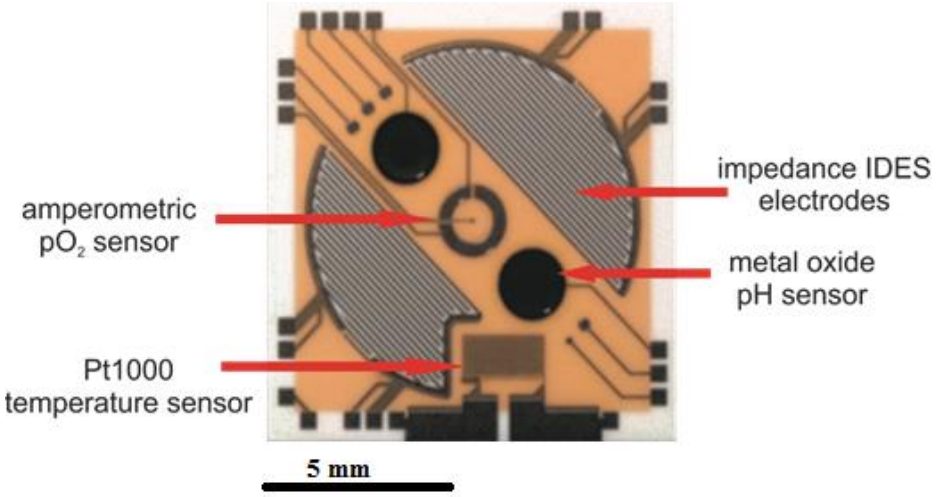

Figure 1.1: Multiparametric sensor chips for biomedical applications on glass (a), silicon (b) and ceramic (c) substrate. These chips are usually equipped with electrochemical impedance, pH, pO_2 and temperature sensors to monitor cell vitality (Heinz-Nixdorf Chair for Medical Electronics, TUM).

Sensorchip based cellular assays constitute a fundamental technique in scientific research and are relevant for a wide variety of applications including tumor chemo-sensitivity tests, pharmaceutical drug screening, point-of-care diagnostics and environmental monitoring. The impact of cellular assays on these various fields raised the need for automated and parallel measurements and led to the development of sophisticated platforms based on chip arrays such as the Intelligent MObile LAb (IMOLA) [8] or multiwell plates such as the Intelligent Microplate Reader (IMR) [9]. Combining multimodal sensor monitoring with parallel recording of cell samples, these platforms can generate enough data for statistical analysis in a single experiment and fulfill the requirements for online cell and tissue monitoring [10]. The IMR system, shown in figure 1.2, has been extensively investigated for parallel recording of cellular metabolic patterns and chemosensitivity tests [5, 9, 10].

This system comprises climate control to sustain an ideal environment for the cell samples during the experiments, automated fluid exchange to periodically refresh the culture medium, microscope optics to observe cell morphological changes and operate fluorescent optrodes as well as a unit for raw data evaluation.

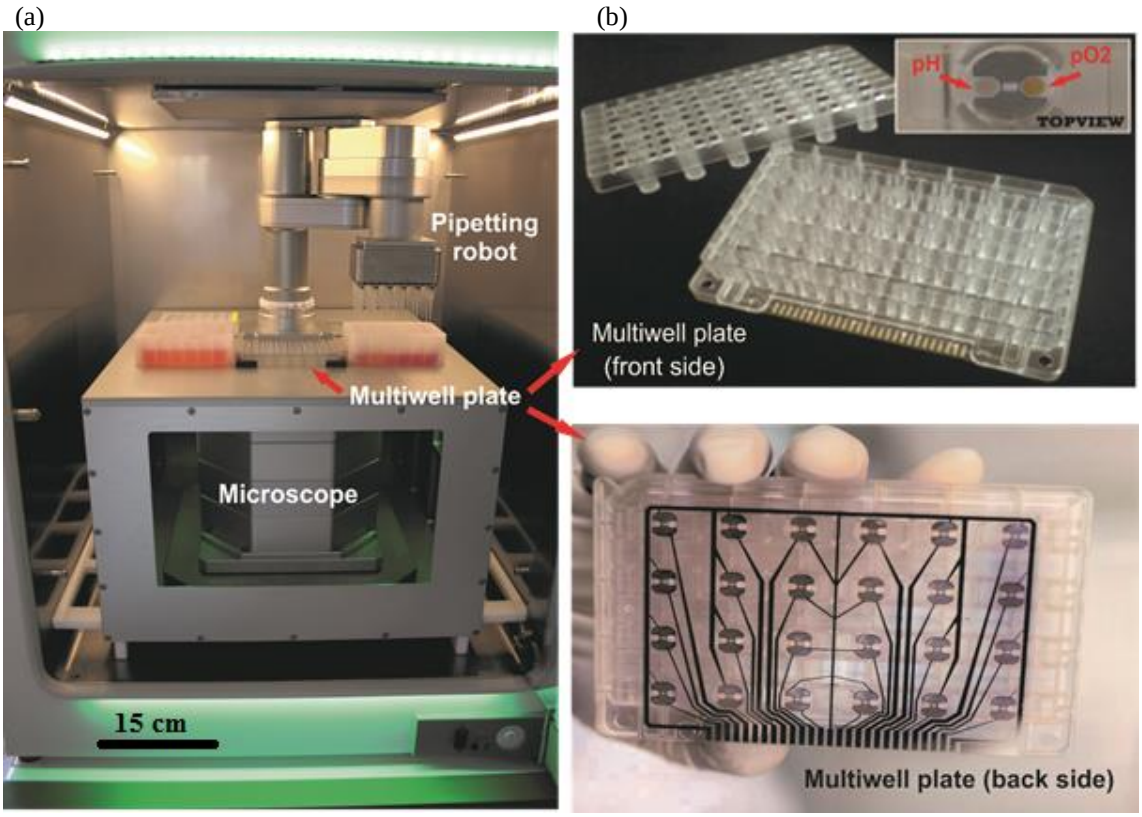

Figure 1.2: Intelligent Microplate Reader (IMR) (a) measuring platform with pipetting-robot for automated fluid exchange, a digital inverse microscope and a multisensoric multiwell-testplate (b) equipped with impedance sensors and optrodes for pH and dissolved oxygen sensing, (Heinz-Nixdorf Chair for Medical Electronics, TUM).

The core component of the IMR is the multiwell plate that is equipped with impedance sensors to deliver information about cell adhesion and morphology as well as optochemical sensors that are used to monitor cell metabolic rates such as extracellular acidification and cellular oxygen uptake over time. These are key parameters for an accurate evaluation of cell reactions to external stimuli such as anticancer-drugs. Marker-free and real time recording of cell metabolic activity in slices of human mamma carcinoma tissue has been successfully demonstrated [5]. Figure 1.3 shows an example of in-vitro measurements where the influence of two different chemotherapeutic agents (doxorubicin and chloroacetaldehyde) on the metabolism of human mamma carcinoma cells can be observed [11]. The cells were first left untreated for about 24 hours (relative metabolic rate ~100%) and then the chemotherapeutic agents have been added to the cell medium. The oxygen consumption and acidification rate of the cells exposed to doxorubicin stay rather constant over time whereas the metabolic activity of the cells exposed to chloroacetaldehyde (CAA) decreases and almost reaches zero after about 48 hours. It can be clearly seen that CAA is significantly more efficient than doxorubicin in this case.

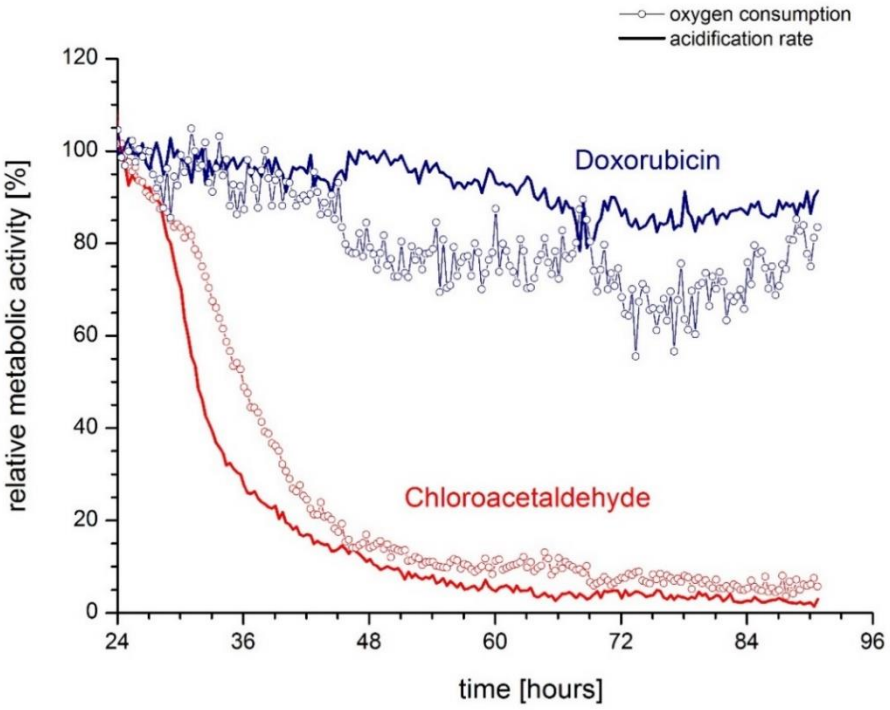

Figure 1.3: Relative metabolic activity of human mamma carcinoma cells under the influence of the chemotherapeutic agents Doxorubicin and Chloroacetaldehyde versus time. The in-vitro monitoring of the relative metabolic activity (oxygen consumption and acidification rate) shows that the metabolic activity of the cells exposed to doxorubicin (blue curves) stays rather constant over time while the metabolic activity of cells treated with chloroacetaldehyde (red curves) significantly decreases and almost reaches zero after 48 hours. The rapid and precise comparison of the performance of different drugs enables personalized in-vitro chemo-sensitivity tests [11].

As shown in figure 1.3, the biosensors used here do not have to deliver an exact value for pH and oxygen concentration but detect pH and oxygen concentration changes over time.

These assays allow a rapid and precise in-vitro comparison of the performance of different drugs at different concentrations and therefore offer the potential for an on-chip determination of the most efficient chemotherapeutic for each individual patient [5, 10, 11]. In addition to being more accurate and reliable than classical screening methods, the personalized in-vitro chemo-sensitivity tests can also be beneficial for cancer patients in terms of saving valuable time and minimizing the unwanted side effects caused by testing different chemotherapeutics.
This demonstrates the significant progress of sensorchip based assays and their importance for medical diagnostics and biological investigations. However, to exploit the full potential of this method, one major drawback needs to be addressed and that is the fabrication costs of the biochips and multiwell plates. Classical biochips are usually made using vacuum deposition and photolithography to create patterns of noble metals on rigid substrates such as glass [7], silicon [6] or ceramics [12] and are therefore rather expensive. This process involves multiple steps and is therefore time consuming and labor intensive. Expensive photolithography mask sets and vacuum equipment are required. The high temperatures needed for metallization and the corrosive solvents used for the etching process limit the choice of substrate. Large amounts of hazardous waste are usually generated that are not only environmentally destructive but also expensive to dispose of. All these factors together make the classical thin film technology a not very appealing process from an economic point of view. The high fabrication costs of the biochips, for example, limit the number of possible assays and constitute an inhibiting factor for mass production and better integration of the biochips in clinical applications.

Over the last decade, printed electronics has received substantial attention as a potentially low cost alternative to conventional electronics. The printing method is additive thereby reducing the number of fabrication steps, production time and material waste. Combined with the potential for large area roll-to-roll fabrication and high throughput processing, these are the key factors that result in cost-effective fabrication per unit area. In addition to the possibility for solution processing, printing allows to deposit materials at low temperatures so that unusual and low cost substrates such as paper, textile or plastic can be used. These new kinds of materials and substrates allow new capabilities in electronics. A new generation of light-weight, low-cost and flexible devices has been created. The success achieved in the fabrication of novel components such as stretchable thin film transistors [13] or bendable electroluminescent devices [14] paves the way for a new class of large-area electronics such as rollable displays [15] and flexible photovoltaic devices [16].
From a biomedical perspective, printed electronics are very interesting for the design of flexible sensors and diagnostic devices that are compatible with the soft, curvilinear and time dynamic human anatomy. Epidermal electronics that are mechanically invisible to the user have been developed for continuous on-body measurements [17]. Interesting application of the tattoo-like sensors include continuous and needle-free glucose monitoring (figure 1.4.a) [18] or epidermal pH sensors [19] that may be useful for in-situ wound monitoring [20]. Other applications include RFID tags that can be mounted on the skin [21] or sensors for bacteria detection in tooth enamel (figure 1.4.b) [22]. A low-cost and flexible organic pulse oxymeter (figure 1.4.c) has also been successfully demonstrated [23]. Another form of wearable diagnostic devices is textile electronics that can be integrated in the clothes. Textile electronics have been tested for various applications among which wearable electromyogram (EMG) for measurements of EMG signals [24] that can be useful for physical condition monitoring of athletes for example. Further innovative applications of flexible electronics include electronic skin for smart robots (figure 1.4.d) and edible food sensors [25].

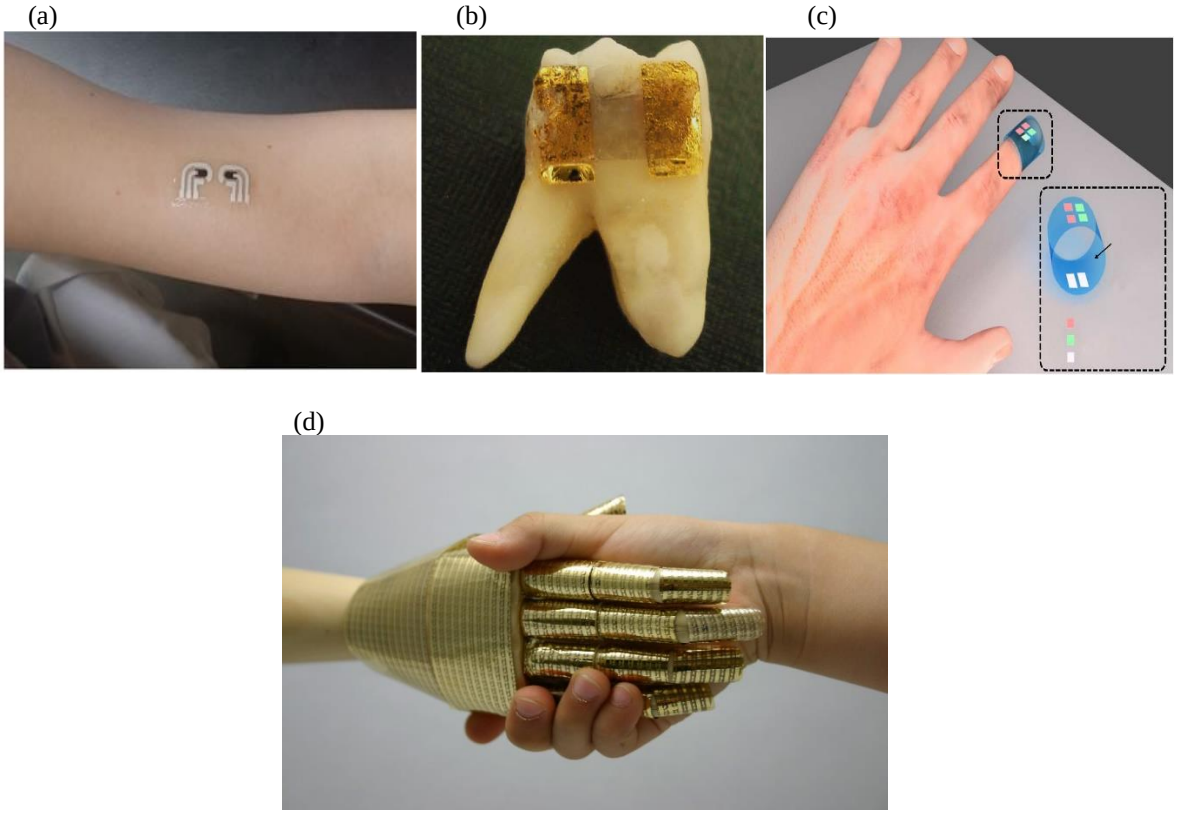

Figure 1.4: Examples of flexible electronics applications: tattoo-like sensor for needle-free glucose monitoring, reused with permission from [18] Copyright (2017) American Chemical Society (a), flexible biochips for bacteria detection in tooth enamel [22] (b), flexible and organic puls oxymeter [23] (c) (Figures 1.4.b and 1.4.c reused with permission, Copyright (2017) Nature Communications) and electronic skin (reused with permission: Takao Someya Group, university of Tokyo) (d) show the conformability of these novel devices with the human anatomy.

Printed and organic electronics has proven to be a successful method with a great potential for various applications, however, mainstream electronics is still to date faster, more mature and reliable. Therefore, printed electronics should not be considered as a replacement for conventional electronics but as a way to expand the application possibilities and market of electronics. Current research on this field is mainly focusing on the strong potential for low-cost and large area (R2R) fabrication of mechanically flexible devices. Due to the favorable features of printed electronics and the new opportunities this method has offered for research and industrial development, the printed electronics market is steadily growing and is expected to exceed $300 billion in the next twenty years [26].

1.2 Aim and outline of the thesis

Focusing on the cost effective aspect of printed electronics, the main objective of this research is to obtain printed, flexible and disposable biochips on polymer substrates (figure 1.5) that display suitable properties for cell monitoring applications and present a low-cost alternative to the conventional biochips. The first step towards this goal begins by choosing a printing method that is both suitable for prototyping as well as up-scaling towards large area fabrication. One of the most promising methods here is inkjet printing (chapter 2). To achieve the desired properties, different parts of the biochips are printed using different inks. Therefore, tracks printed using silver based inks (chapter 3), CNT based inks (chapter 4) and polymer inks (chapter 5) have been investigated. Combining the smart properties of these materials is crucial for the fabrication of inkjet-printed biochips that fulfill the requirements for cell-chip applications (chapter 6). Then, a possible application of these biochips for in-vitro cell monitoring is investigated using novel CNT based pH and oxygen sensors. To achieve these goals, it is necessary to first master the inkjet printing technique.

Chapter 2 gives an insight into the inkjet printing method as a potential method for prototyping and provides a comparison of the main printing techniques. Since achieving a good printing image is crucial for printed electronics applications, the challenges related to the printing of electrically functional inks on polymer substrates are addressed. The behavior of the generated droplets in flight and on the substrate are key factors for a good printing quality and need therefore to be optimized.

Chapter 3 covers the electrical and mechanical performance of inkjet-printed silver tracks on different polymer substrates. Sintering the silver nanoparticles to obtain conductive patterns without damaging the thermally instable polymer substrates imposes a significant challenge. Different sintering methods are investigated and the resulting electrical and mechanical performance of the printed track are compared.

In chapter 4, CNT based inks are investigated as a biocompatible alternative to silver for the printing of conductive patterns. Although CNT based tracks usually display a much higher resistivity than metal based tracks, various methods are explored to reduce their resistivity. The bendability and shelf life of the printed CNT based tracks in aqueous media are investigated to ensure their suitability for applications such as cell monitoring.

Polymer based inkjet inks are discussed in chapter 5. Since achieving a good printability using insulating polymer based inks can be challenging, the printability of different polymer based inks has been investigated. The polymer track are intended to present a biocompatible insulating coating for the silver based tracks, therefore, their insulating properties are investigated.

Combining the smart properties of the silver, CNT and polymer based tracks discussed in the previous chapters, successful fabrication of inkjet-printed biochips that display the desired properties for cell monitoring applications is presented in chapter 6. Novel CNT based pH and dissolved oxygen sensors can be easily integrated in the biochips and implemented for the monitoring of the metabolic activity of living cells. The performance of these sensors is first tested without cells.

After confirming their suitability for detecting pH and oxygen changes, the SWCNT based sensors are tested with living yeast cells.

Chapter 7 concludes the dissertation and addresses possible future work. The main findings of this work are summarized and a prospective about further development is presented.

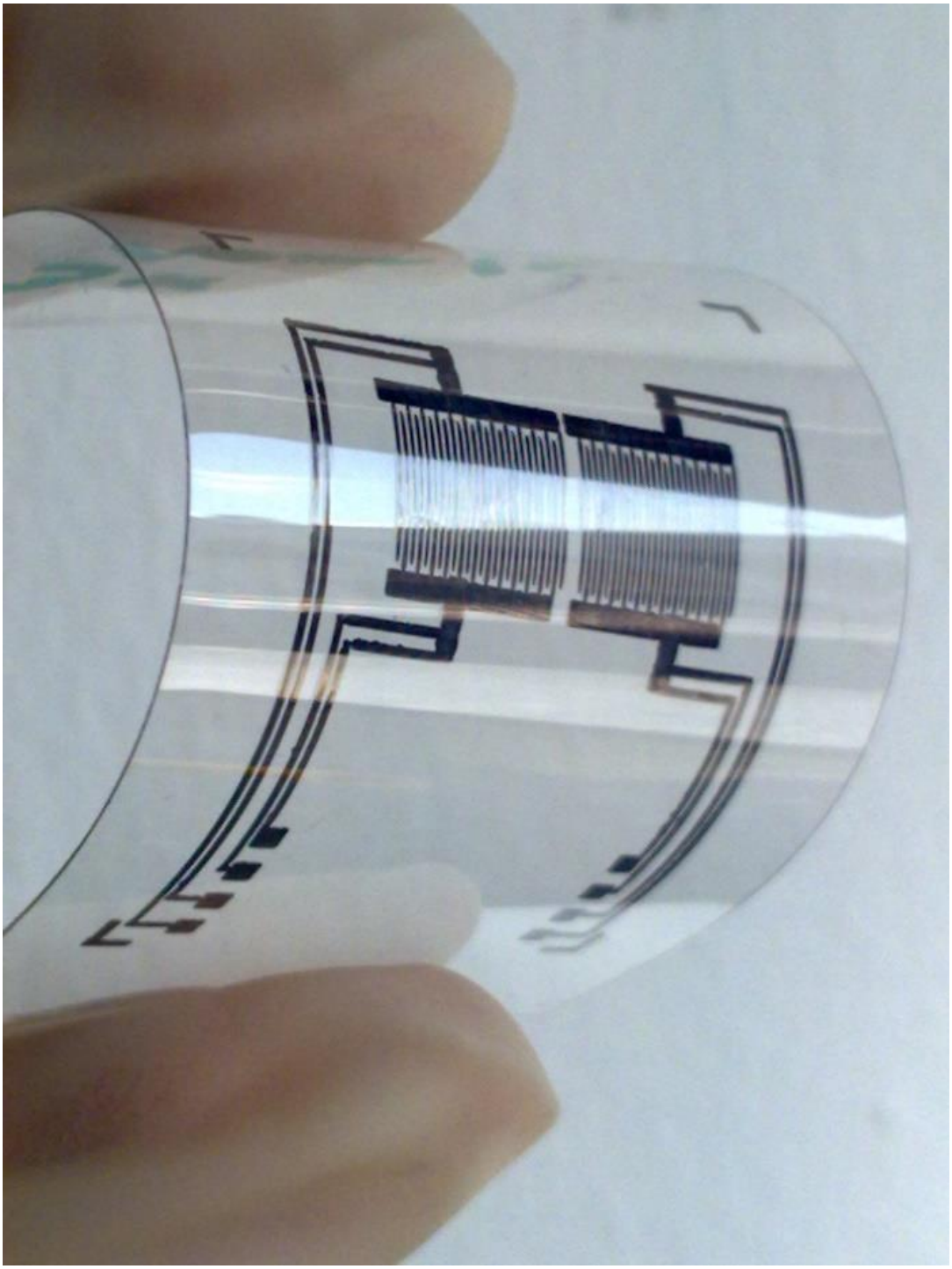

Figure 1.5: Inkjet-printed biochip on polymer substrate. These chips present a promising flexible and low cost alternative to the classical biochips shown in figure 1.1.

Chapter 2

Inkjet printing

2.1 Introduction to inkjet printing

Inkjet printing is a several centuries old method that has found its way from simple graphic art applications as a desktop printer to more interesting applications such as the fabrication of low cost electronics. The concept of inkjet-printed electronics may sound as simple as printing electrically functional inks instead of graphic art inks. However, the combination of the field of printing and the field of electronics involves tremendous challenges and requires a fundamental understanding of the inkjet technique.

2.1.1 Brief historical overview

The basics of the inkjet method go back to 1749 when Abbé Nollet studied the effect of static electricity on a stream of droplets (figure 2.1.a). In 1958 Lord Kelvin invented the very first practical inkjet device called “Siphon” (figure 2.1.b). The Siphon recorder shown in figure 2.1.b could produce a continuous stream of ink into a moving web of paper and was used to record telegraph messages [27].

(a) (b)

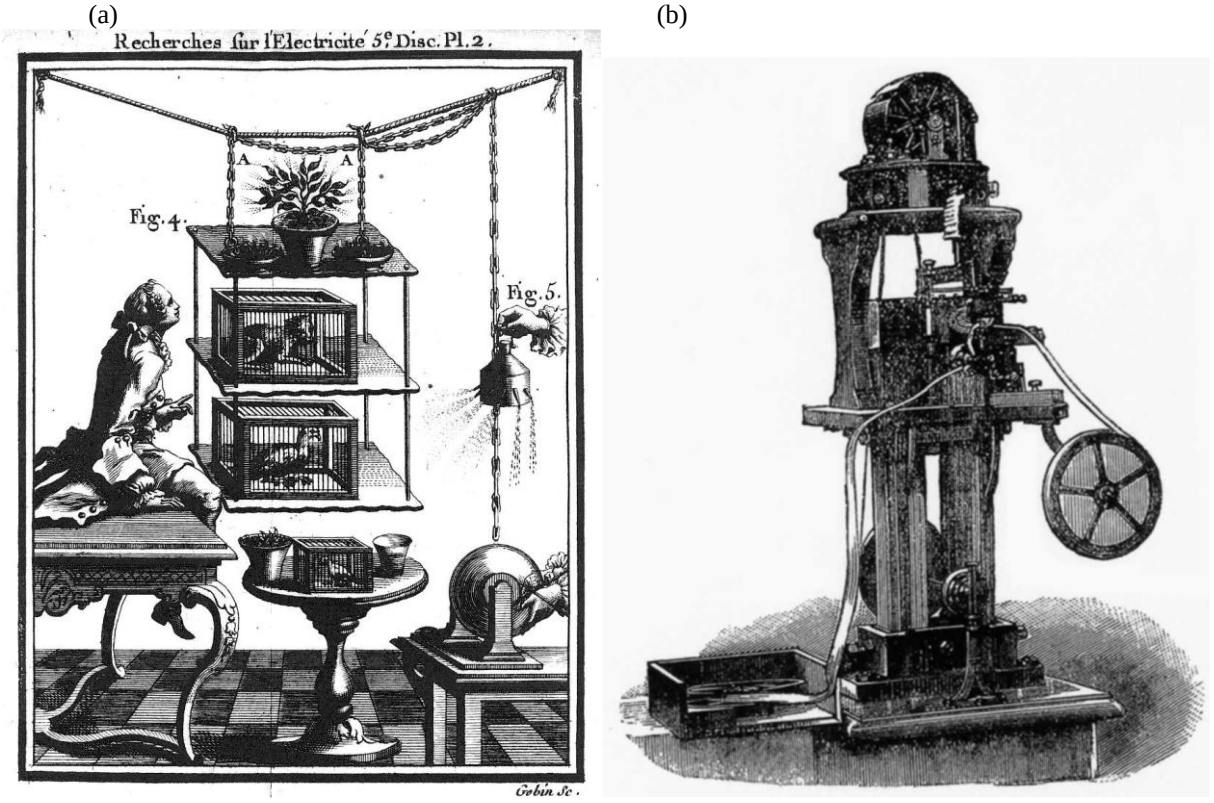

Figure 2.1: An illustration of Abbé Nollet showing the effect of static electricity on a stream of droplets, (Recherches Sur Les Causes Particulieres Des Phenomenes Électriques, 1749) (a), the Siphon recorder: the first practical inkjet device, (William Thomson, 1858, UK Patent 2147/1867) (b) reused with permission from [27].

Joseph Plateau and Lord Rayleigh are considered the founders of the modern inkjet technology. The Plateau-Rayleigh instability describes the break-up of a liquid stream into droplets (figure 2.2) as a result of the surface energy of a sphere being smaller than that of a cylinder while having the same volume [28].

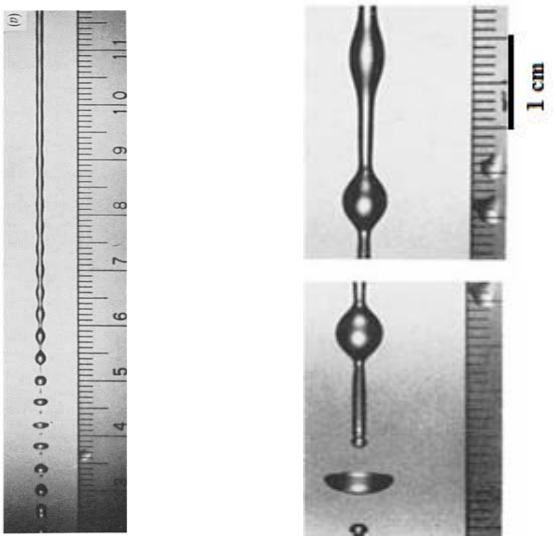

Figure 2.2: Typical photographs of water jet break-up: these break-up occurs because of Plateau-Rayleigh instability, reused with permission from [29].

Plateau derived a relationship between droplet size and jet diameter in 1865 while Rayleigh calculated a characteristic wavelength λ for a fluid stream and jet orifice diameter d as: $\lambda = 4.508*d$. The plateau-Rayleigh instability explains the spherical form of the droplets as the tendency of a liquid to form the shape with the smallest total surface area and lowest total energy. A continuous stream of liquid emerging from a circular nozzle will initially have a cylindrical form. Under the action of surface tension, disturbances with the wavelength $\lambda = 4.508*d$ will cause the jet-break up into spherical drops [27, 28, 30].
In 1965 Richard Sweet explained that with the effect of electrostatic forces, charged inkjet drops can selectively be deposited on the substrate [31]. This was the theoretical foundation for the continuous inkjet printing. In 1968 the first commercial continuous inkjet printer was introduced by the A. B. Dick Company under the name Videojet 9600. In 1946 Clarence Hansell patented his investigations on an inkjet device that uses vibrational waves to produce droplets only when needed (patent number US2512743 A) and this was the foundation for the drop on demand (DoD) inkjet printing. In 1971 the first DoD printer was released by the Casio Company under the name 500 Typuter [28].

2.1.2 Methods of drop generation

Although inkjet printing can basically be described as a digitally controlled droplet ejection from a print head on to a substrate, the droplet emission can be achieved by different methods. As described in the previous section, the inkjet methods can be classified in two main groups: continuous inkjet printing (CIJ) and drop on demand inkjet printing (DoD).

Continuous inkjet printing

As the name suggests, continuous inkjet printing is based on printing a continuous jet of liquid by forcing it under pressure through a nozzle. A disturbance is imposed on the jet usually by the vibration of a piezo crystal or by a resistive heat element causing the formation of drops with a homogeneous size and distance. The drops are then charged by passing through an electrostatic field.

The trajectory of the charged drops is monitored by a deflection field. The drops used for printing reach the substrate while the unneeded drops are deflected and get collected in the gutter, where they are recycled for reuse (figure 2.3).

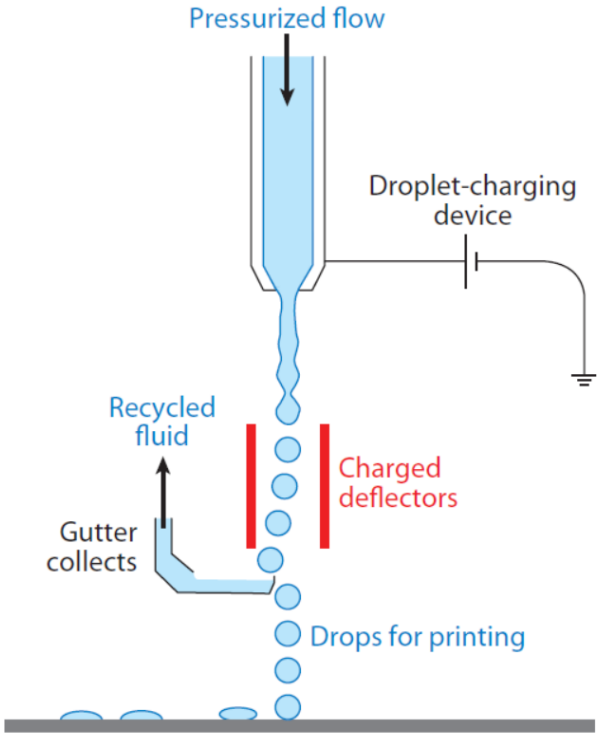

Figure 2.3: Principles of operation of a continuous inkjet system, reused with permission from [32]. The drops are charged by passing through an electrostatic field. The trajectory of the charged drops is monitored by a deflection field. The drops used for printing reach the substrate while the unneeded drops are deflected and get collected in the gutter, where they are recycled for reuse.

The continuous inkjet printing allows the emission of droplets at rather high frequencies usually between 50 and 175 KHz. This translates in a high printing speed. Also the droplets emerge from the nozzle with a high velocity between 10 and 30 m/s allowing the distance between the printing nozzle and the substrate to be relatively high.
This can be beneficial for industrial environments or for non-flat substrates. Another advantage of continuous inkjet is that it allows the printing of inks containing volatile solvents. The rapid drying of these solvents may enhance the adhesion of printed structures on the substrate.
The main disadvantages of the continuous inkjet method consist in the poor resolution, high maintenance requirements of the printing machine and the limitations caused by the fact that the inks need to be electrically chargeable [30, 33].

Drop on demand inkjet printing

As opposed to the continuous inkjet printing, here the printing nozzle fires only when needed (on demand). A pressure pulse is used to trigger the drop generation. Depending on the method used to create the pressure pulse, DoD can be divided in different subcategories. The two most common drop on demand subcategories are thermal inkjet (also called bubble jet) and piezoelectric inkjet [30]. A schematic presentation of the working principle of these two methods can be seen in figure 2.4.

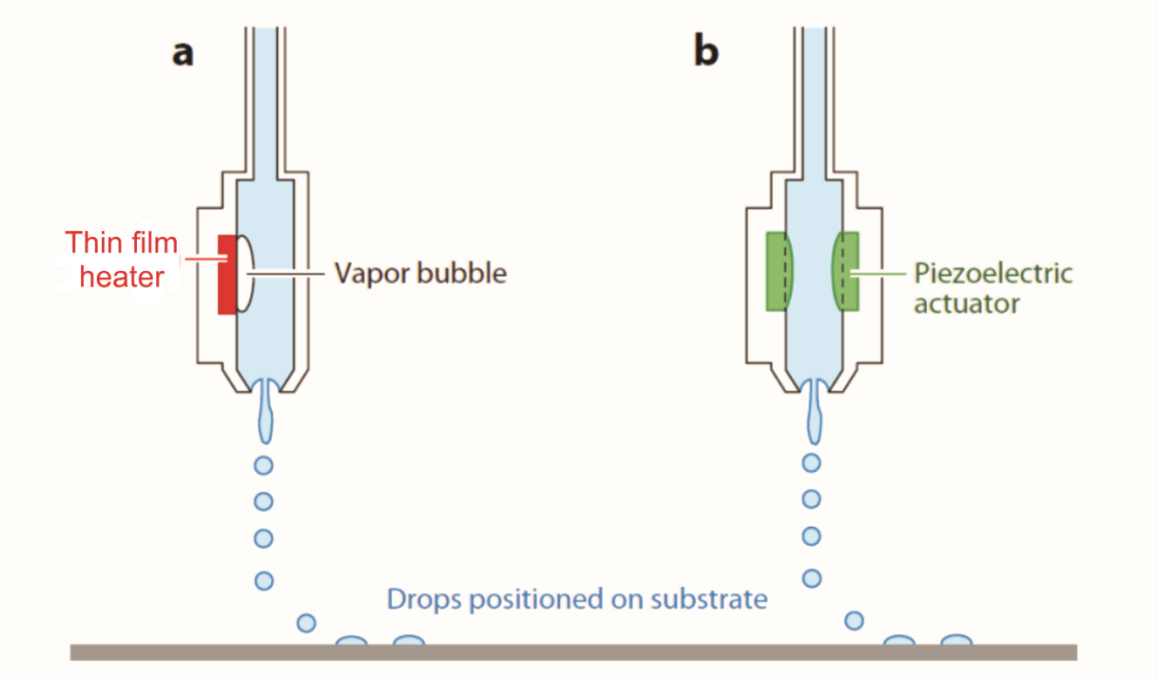

Figure 2.4: Schematic presentation of the working principle of thermal inkjet printing (a) where the droplet formation is generated by a vapor bubble induced by a thin film heater, and piezoelectric inkjet printing (b) where the droplet formation is generated by a piezoelectric actuator, reused with permission from [32].

Thermal inkjet printing

The thermal inkjet method is based on using a thin film resistive heater to cause the vaporization of a small layer of the ink adjacent to the heater. The rapid heating and vaporization of the ink causes a vapor bubble to grow resulting in fluid displacement that forces a drop to leave the nozzle. During the heating process the heater usually reaches temperatures about 350 to 400 °C for a few microseconds. After the droplet emission the heater is switched off and the void in the chamber is refilled with fresh replacement ink in preparation for the next drop emission. The advantages of inkjet include the potential for very small drop sizes and the rather low print head costs since the actuator is a simple resistive element.
The thermal inkjet has several limitations and reliability issues. The reliability issues include heater breakdown due to cavitation or heat stress and jetting failure due to ink viscosity increase. A typical problem with thermal inkjet is called “kogation” and is caused by the ink scorching that creates a solid coating on the surface of the heater. This can reduce the efficiency of the heater and may lead to poor printing quality. The inks for thermal inkjet have to be formulated in a way that the kogation-problem is minimized. Also the inks have to withstand the heating and vaporization process. This limits the choice of the solvents that can be used so that most of the thermal inkjet inks are water based [30, 33, 34].

Piezoelectric inkjet printing

In this printing method a piezoelectric ceramic is used to translate an electrical signal into a mechanical deformation in the nozzle and generate the pressure pulse needed for the drop formation. Lead zirconate titanate (PZT) is commonly used as a ceramic material for piezoelectric inkjet printing because of its strong piezoelectric effect [30].
In 1984 Bogy and Talke published an explanation of the working principle of piezoelectric inkjet print heads (figure 2.5) upon application of a basic rectangular driving waveform [35] and this was thoroughly further investigated by Wijshoff [27]. Upon application of a positive voltage, the piezoelectric element contracts enlarging the diameter of the ink channel. This creates a negative pressure wave that

propagates as two half amplitude waves in opposite directions. Because of its relatively large diameter, the supply tube can be considered as an open end with a transmission coefficient of 0 and a reflection coefficient of -1 while the nozzle tip can be considered as a closed end with a transmission coefficient of 0 and a reflection coefficient of 1. The wave that reaches the supply tube is reflected as a positive pressure wave while the wave that reaches the nozzle tip is reflected without changing sign. The two waves will meet while the driving voltage is set to 0. The piezo element goes back to its original form and the ink channel reduces back to its original diameter. This leads to the suppression of the negative wave and amplification of the positive wave. Upon reaching the nozzle tip (closed end), the amplified positive wave gets reflected with its maximum amplitude leading to droplet emission.

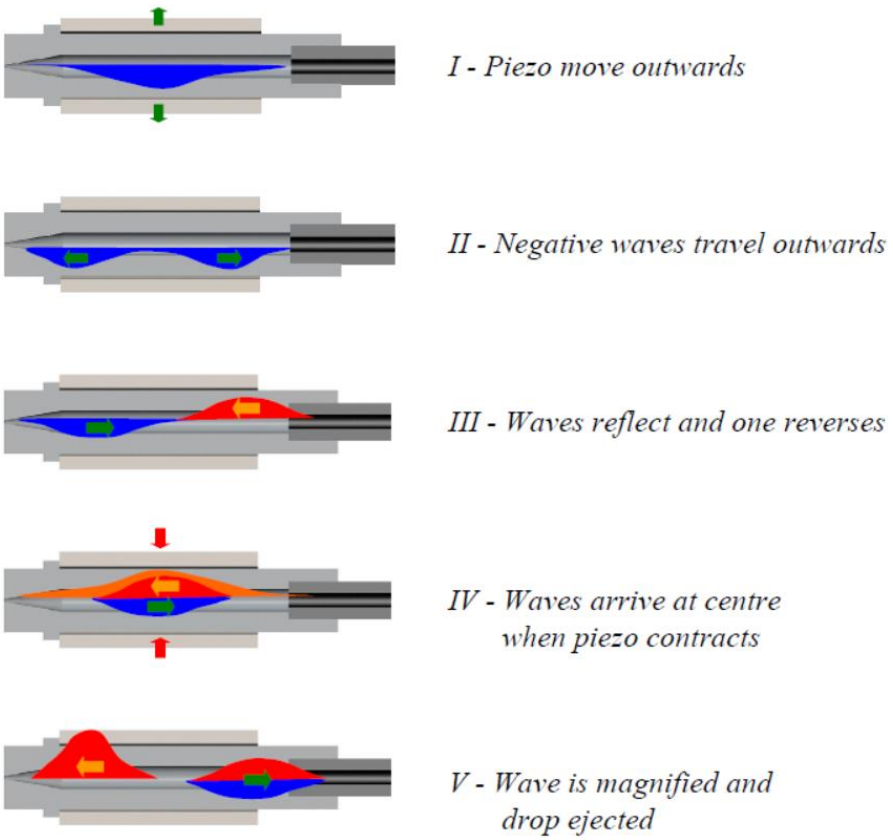

Figure 2.5: schematic presentation of the pressure wave propagation in the nozzle leading to droplet emission in a piezoelectric print head, reused with permission from [28]. Upon application of a positive voltage, the piezoelectric element contracts enlarging the diameter of the ink channel. This creates a negative pressure wave that propagates as two half amplitude waves in opposite directions. The wave that reaches the supply tube is reflected as a positive pressure wave while the wave that reaches the nozzle tip is reflected without changing sign. The two waves will meet while the driving voltage is set to 0. The negative wave is suppressed and the positive wave is amplified. Upon reaching the nozzle tip, the amplified positive wave gets reflected with its maximum amplitude leading to droplet emission

Although the fabrication costs of piezoelectric print heads are rather high in comparison with thermal inkjet, this is compensated by a longer shelf life (no kogation) and the highest level of ink development freedom among all inkjet methods. Also the driving waveform can be customized to control the droplet size and velocity. Therefore, piezoelectric inkjet is currently the method of choice for most emerging industrial applications and has predominated in the printed electronics applications [30, 33].
Figure 2.6 presents an overview of the different inkjet technologies as well as the key players using these techniques [33].

(a)

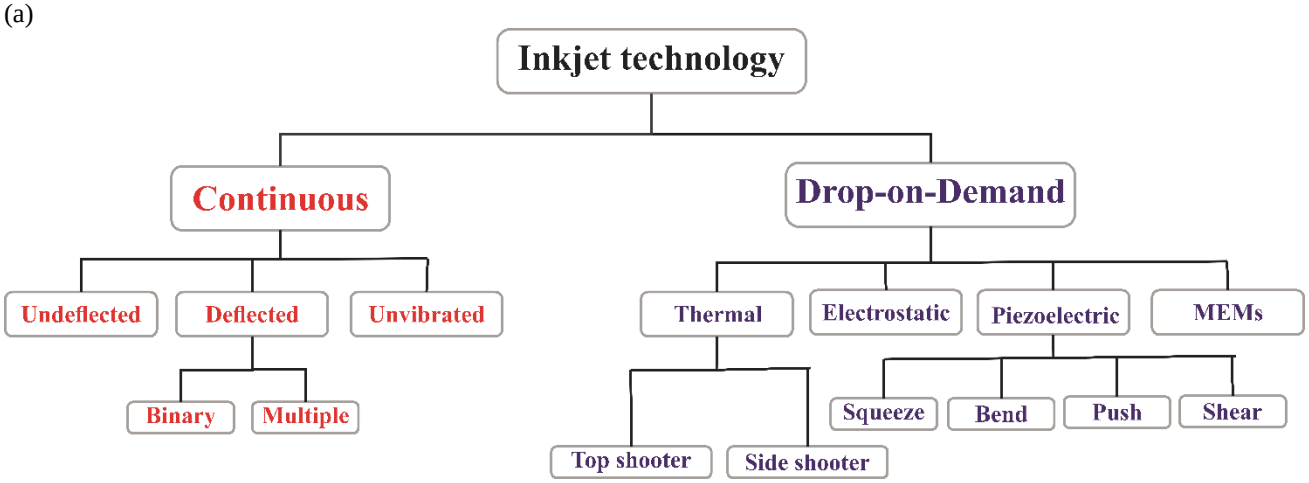

(b)

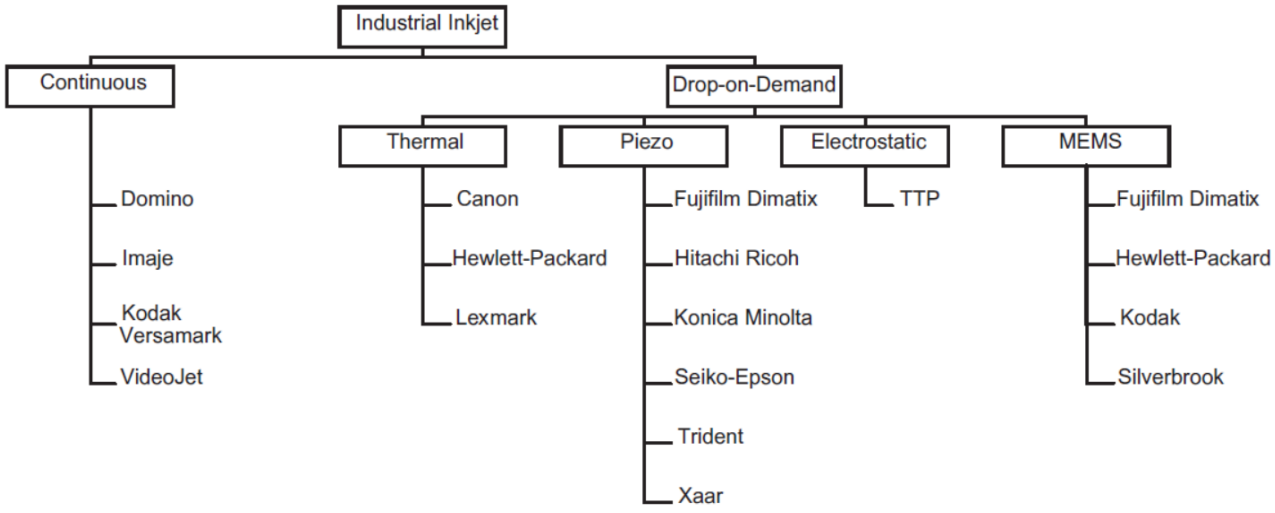

Figure 2.6: Classification of inkjet printing technologies, adapted from [28] (a), and major players using the different inkjet methods, reused with permission from [33] Copyright @ 2017 World Scientific Publishing (b).

2.1.3 Overview of the main printing techniques

In addition to inkjet printing, different printing techniques have already been investigated for the fabrication of flexible electronics. The most common patterning techniques that are suitable for roll to roll large area fabrication include screen printing, gravure, flexography and offset-lithography. Each one of these methods has specific characteristics and suitable application possibilities.

Screen Printing

Screen printing is one of the oldest and most common printing methods. The screen printing process consists of pushing the ink through a screen comprising a fine mesh of polymer, metal or carbon fibers (figure 2.7).
The pattern is defined by filling certain openings of the mesh with a stencil material. A squeegee is used to coat the screen with the ink and brings it in contact with the substrate so that the ink can be squeezed through the openings of the screen to define the desired pattern on the substrate [36].

(a)

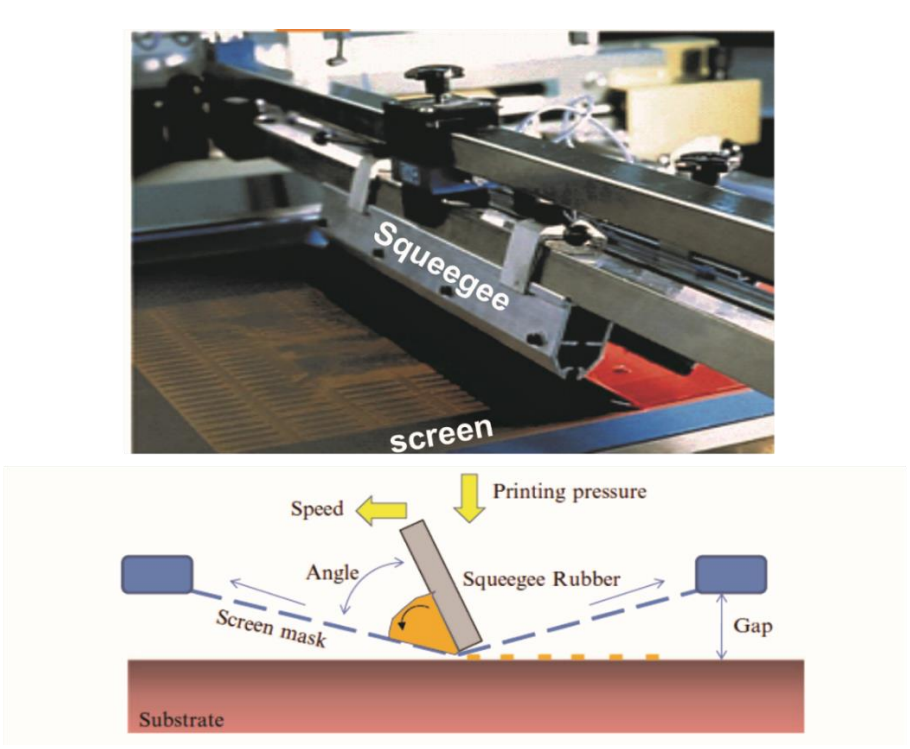

(b)

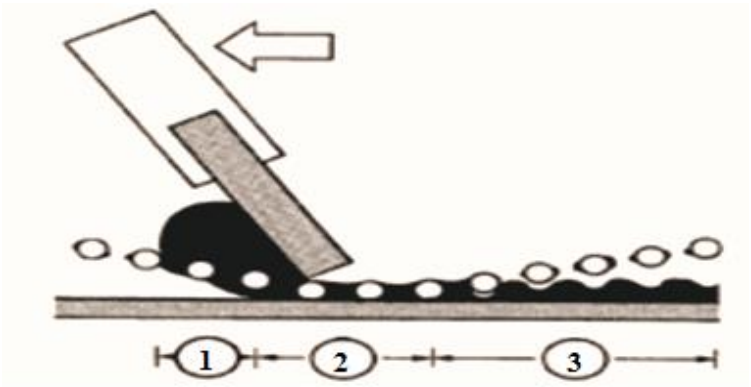

Figure 2.7: Image of a screen printer and working principle of screen printing: a squeegee is used to coat the screen with the ink and brings it in contact with the substrate so that the ink can be squeezed through the openings of the screen to define the desired pattern on the substrate [37] (a). The three phases of the printing process are: 1) filling of mesh openings with ink, 2) contact phase, 3) snap off, adapted from [38], reused with permission (b).

The inks for screen printing need to have a high viscosity and this leads to the most distinct feature of screen printing in comparison with other printing techniques: the high aspect ratio of printed structures. Screen printing tends to produce high thickness films usually in the range of several tens of microns. Using a thick screen mesh, the film thickness can reach 100µm with a single pass of printing. This cannot be achieved with any other printing method [37]. The film thickness can be controlled by the thickness of the screen and the viscosity of the ink. It should also be noted that inks with low viscosity cannot be used because of uncontrollable flow of the ink on the substrate. The result is that thin layers cannot be achieved with screen printing. The resolution of screen printing is determined by the size of the mesh and is typically about 100µm. A reasonable fine resolution for mass production screen printing is about 50µm however a resolution of about 10µm has been demonstrated at the laboratory scale [36, 37].

As a result of recent developments, a resolution of 20µm could be achieved with a mesh with 12µm wire diameter from Asada [38]. An alternative to conventional flat screen printing that has a much better printing speed but with a limited resolution is rotary screen printing.
Screen printing was used to fabricate the very first organic thin film transistor [36]. Other interesting applications of screen printing are disposable sensors for environmental monitoring [39] or biomedical sensors such as sensors for glucose monitoring [40, 41]. One of the main disadvantages of screen printing is the inhomogeneous layer thickness caused by the mesh pattern. Also, the limitation to higher layer thickness can be unpractical for applications where only thin layers are wanted.

Gravure printing

Gravure printing is a fast and high throughput printing method based on a gravure cylinder with etched or engraved cells that may vary in size and depth. The cells can be filled with ink using the doctor blading method. The sharp blade removes excess ink leaving the right amount of ink in the cells and the pattern can then be transferred on to the substrate (figure 2.8). An alternative to the conventional gravure method is the offset gravure printing where the ink is first transferred on to a soft rubber cylinder also called plate cylinder and then placed on the substrate under a given pressure. The advantage of the offset-gravure method is that it is suitable for three-dimensional substrates because of the softness of the rubber cylinder [37]. The main disadvantage of gravure printing is the high cost of the metal cylinder. The degradation of the doctor blade and the possible swelling of the rubber cylinder in contact with organic solvents can also have a negative impact on the printing quality.

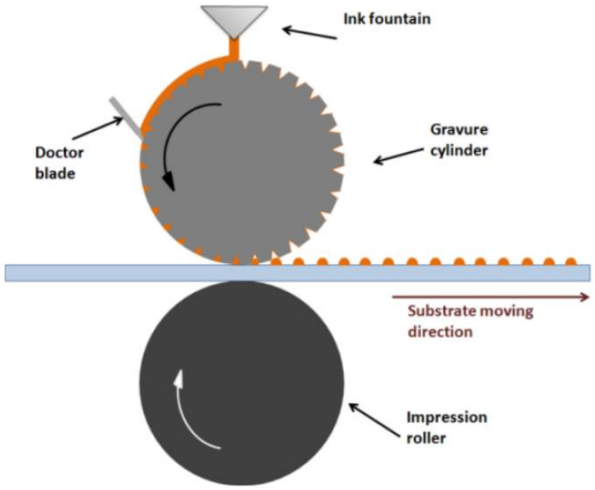

Figure 2.8: Working principle of gravure printing, reused with permission from [42]. A gravure cylinder with etched or engraved cells which can be filled with ink using the doctor blading method. The sharp blade removes excess ink leaving the right amount of ink in the cells and the pattern can then be transferred on to the substrate

A typical resolution for gravure printing is about 50µm [42] and it could be reduced in recent years to 10µm [43]. The gravure method is usually used to print high quality magazines. Gravure printing has also been explored as a fabrication method for large area electronics [44], organic thin film transistors [43] and organic light emitting diodes [45].

Flexography

Similar to gravure printing, flexography is also a high-throughput method. The printing cylinder contains protruding ink-receptive regions that are separated with non-printing wells [36]. This cylinder is usually made of a soft rubber material and is called plate cylinder. The ink is first transferred from the hard anilox roll to the plate cylinder and then placed on the substrate (figure 2.9).

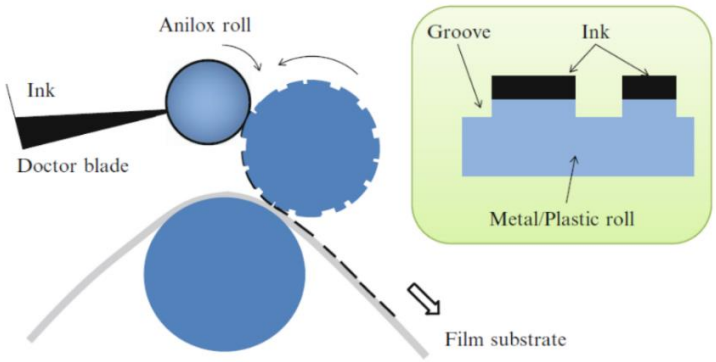

Figure 2.9: Working principle of flexography printing, reused from [37] with permission of Springer Nature. . The printing cylinder contains protruding ink-receptive regions that are separated with non-printing wells. The ink is first transferred from the hard anilox roll to the printing cylinder and then placed on the substrate

The advantage of flexography in comparison to gravure printing or screen printing is that it is suitable for low viscosity inks so that thin patterns can be achieved. The plate cylinders are also not expensive but are prone to degradation due to organic solvents. Flexography is commonly used for the fabrication of packages where lower printing quality can be tolerated. Research has also been conducted to integrate the flexography process into the fabrication of printed electronic components such as flexible organic transistors [46] or ring oscillators [47].

Offset lithography

Offset lithography is the most widespread commercial printing method. The plate cylinder has oleophilic/ ink-accepting (image) areas and hydrophilic/ ink-repelling (non image) areas. First the plate cylinder is dampened with water. This prevents the transfer of the oil based ink to the nonprinting areas. When the cylinder plate is coated with the ink, the ink sticks only to the image areas. The pattern is then transferred to an intermediate cylinder called blanket cylinder and then finally printed on the substrate by pressing the blanket cylinder to the impression cylinder (figure 2.10).

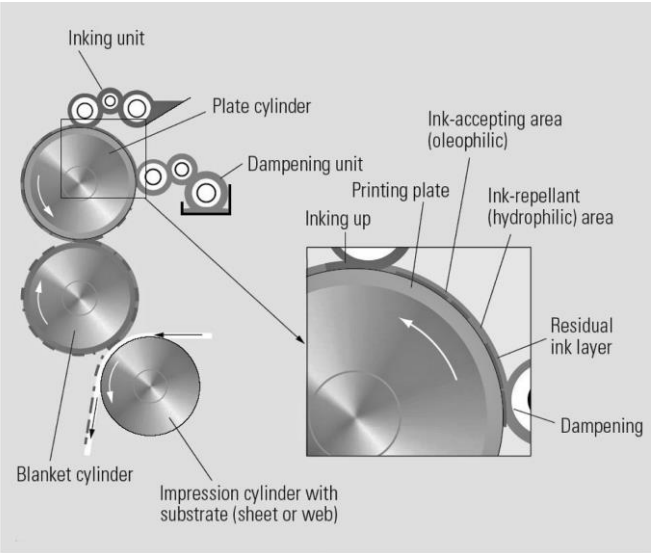

Figure 2.10: Working principle of offset lithography [36] Copyright Wiley-VCH Verlag GmbH & Co. KGaA. Reproduced with permission. Original figure from H. Kipphan: Handbook of print media technologies, reused with permission of Springer Nature. The plate cylinder has oleophilic/ ink-accepting (image) areas and hydrophilic/ ink-repelling (non image) areas. When the cylinder plate is coated with the ink, the ink sticks only to the image areas. The pattern is then transferred to an intermediate cylinder called blanket cylinder and then finally printed on the substrate by pressing the blanket cylinder to the impression cylinder.

The offset lithography process has been implemented for the fabrication of organic thin film transistors with channel lengths of 30 to 200µm [36] and capacity-type humidity sensors [48]

Other unpatterned large area printing techniques include slot die, wire bar and curtain coating [49]. There are also fine printing techniques such as nanoimprint and microcontact printing that have gained increasing attention because they allow the fabrication of sub-micrometer structures. However these techniques are still primarily used in research [37, 49].

2.1.4 Features of inkjet printing

The inkjet method has several advantages in comparison to other printing techniques and is therefore particularly attractive for printed electronics applications:

Digital input: one of the most interesting features of inkjet printing is that it is a digital method. The digital input allows for on-the-fly design changes and presents a significant cost advantage over methods that involve the use of a physical mask or template. This is also interesting for research because it allows for rapid prototyping. Also, on-the-fly distortion correction may result in more accurate alignment on large area substrates.

Non-contact printing: the non-contact ink deposition allows the use of substrates that are fragile, non-planar (rough or texturized) or even non-solid. It also eliminates problems associated with contact-based printing such as accidental contamination and print quality degradation due to the abrasion of print form over time.

Compatibility: inkjet printing allows the use of inks with low viscosity, usually in the range of 1 to 20 mPas. A wide variety of materials can therefore be deposited using inkjet printing. This can be useful for materials with limited solubility or materials that do not allow the use of binders because they may degrade their electronic functionality. This can be the case for some conductive polymers such as poly-3-hexylthiophene (P3HT) that might also be too expensive to formulate into a paste. Also, the low viscosity allows the deposition of thin material layers similar to main stream electronics. This is very important for applications that do not tolerate thick layers as is the case for the fabrication of cell-chips. Thicker electrodes lead to a non-homogeneous cell growth on the biosensors and are therefore unwanted.

Scalability: inkjet printing is modular and has a good potential for up-scaling. Several print heads can be placed side by side to print wider patterns or one after the other to print different materials in sequence.

Resolution: currently a line and space width as low as 20µm [26] is achievable with commercially available print heads such as the print heads from Dimatix with a nozzle diameter of 9µm. Lower resolution (<10µm) has been demonstrated at research scale [33].

As a result of these advantages, inkjet printing is one of the commonly used techniques for printed electronics application. It is interesting for both research and industrial applications because it is excellent for prototyping and can also be up-scaled for large area and roll-to-roll fabrication. However it should be noted that inkjet with a maximum printing speed of about 30m/min is not a fast printing technique especially in comparison with gravure printing or flexography that allow printing speeds up to 1000m/min.
Although the inkjet method is very appealing for challenging applications such as printed electronics, successful printing requires careful optimization of various parameters.

2.2 Printing Image: Droplet behavior in flight and on the substrate

Although the inkjet method can simply be defined as the deposition of small ink droplets on a random substrate, there are several important parameters that both frame and constrain this printing method. The accurate placement of equal sized droplets and the interaction between the ink and the substrate are very important to achieve a good printing image. In this section different parameters are discussed that have to be optimized in order to obtain a stable jetting behavior and a good pattern resolution. Since one missing drop could lead to an open circuit and one misplaced drop can cause a short circuit, a good printing image and defect free patterns are key requirements for printed electronics.

2.2.1 Droplet behavior in flight

The droplet formation in a piezoelectric inkjet system is based on the propagation and reflection of pressure waves in the ink channel created by an electric pulse applied to the piezoelectric element as discussed in section 2.1.2. The formation of the droplets and their shape are influenced by the ink properties, the pulse form and the diameter of the printing orifice as well as other parameters such as the design of the print head or the length of the piezoelectric element [35] that will not be discussed here.
The first step towards stable jetting begins with the choice of a printable ink with a suitable viscosity, density and surface tension. Using the Weber number (We: defines the balance between inertial and capillary forces) and the Reynolds number (Re: defines the ratio of inertial to viscous forces), Fromm has identified the dimensionless numbers Ohnesorge (Oh) and Z to characterize the behavior of liquid drops [32; 50]:

$$We = \frac{v^2 \rho a}{\gamma} \tag{1}$$

$$Re = \frac{v \rho a}{\eta} \tag{2}$$

$$Oh = \frac{\sqrt{We}}{Re} \tag{3}$$

$$Z = \frac{1}{Oh} = \frac{\sqrt{a \rho \gamma}}{\eta} \tag{4}$$

where ρ, η and γ are the density, viscosity and surface tension of the ink respectively, v is the average velocity of the droplet and a is the radius of the printing orifice. Z is not dependent on the drop velocity. Fromm predicted that $Z > 2$ is necessary for stable drop formation. This value was later further refined by Reis and Derby who defined the range of Z for stable drop formation as: $1 < Z < 10$ [32, 51]. If the value of Z is too low, the viscosity of the ink leads to the dissipation of the pressure waves and inhibits the drop generation. If the value of Z is too high, satellite droplets form around the main drop and lead to a low print quality. The appearance of satellite droplets is specially unwanted in printed electronics applications because they are easily misdirected by aerodynamic and electrostatic forces. This may not only lead to the degradation of the printing image but they can also be responsible for device failure by creating an unwanted connection between the electrodes. A schematic presentation of the printable range of inks depending on We, Re and Z can be seen in figure 2.11.

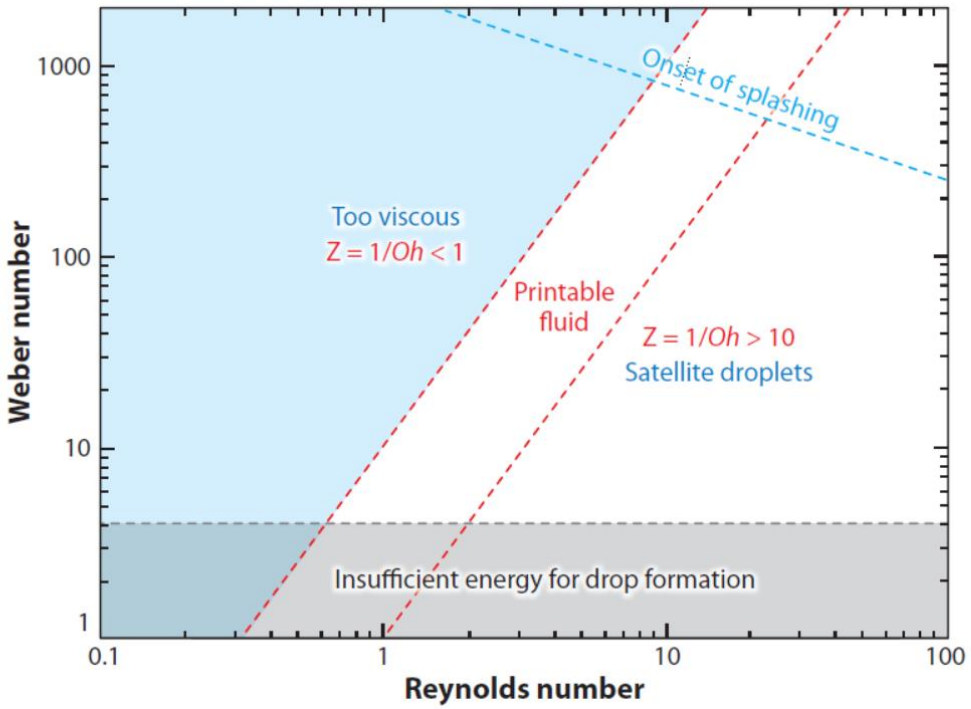

Figure 2.11: Weber number/ Reynolds number diagram representing the regime of fluid properties where inkjet printing is possible depending on the inverse Ohnesorge number Z, reused with permission from [32]. Stable drop formation is possible for 1 < Z < 10 [32, 51]. If the value of Z is too low, the viscosity of the ink leads to the dissipation of the pressure waves and inhibits the drop generation. If the value of Z is too high, satellite droplets form around the main drop and lead to a low print quality. For We<3 the energy is not sufficient for drop formation. The blue dashed line in the upper left part of the diagram indicates the onset of splashing.

Based on experimental research, Jang et al. have redefined the range of Z for stable droplet formation as: 4 < Z < 14 [50].
The influence of the nozzle diameter on the jetting stability does not only appear in the Weber and Reynolds numbers but it also affects the minimum velocity needed for droplet emission:

$$v_{min} = \sqrt{\frac{2\gamma}{\rho a}} \tag{5}$$

This equation can be translated to We > 4 for a possible droplet formation [32]. Jang et al. also noticed that the droplet volume increased with higher Z values [50].
Since most functional inkjet inks contain nanoparticles, the diameter of the printing orifice should be adjusted to the dimensions of the particles. Particles that are bigger than 5% of the nozzle diameter can cause clogging [34]. Depending on the application, either the bigger particles are removed, usually using a filter, or a bigger orifice diameter is used.
Also the diameter of the emitted drops is roughly equal to the diameter of the orifice from where they emerged, but can be influenced by other parameters such as the rheological properties of the ink (Z value) and the waveform of the input signal.
The drop generation is controlled by the electric pulse applied to the piezoelectric transducer (PZT). The design of the input waveform impacts the jetting behavior as well as the droplet speed and volume. The classical input signal usually has a trapezoidal form as it can be seen in figure 2.12.

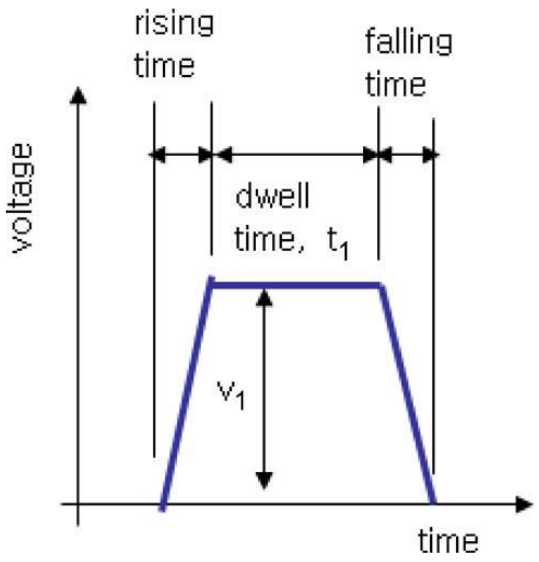

Figure 2.12: Trapezoidal input waveform for piezoelectric inkjet printing, reused with permission from [52], Copyright @ 2017 IEEE Xplore.

The rising and the falling sections of the waveform are responsible for the generation of the pressure waves as discussed in section 2.1.2 while the d_{well} section is related to the amplification or cancellation of the propagating waves.
The d_{well} time should be adjusted to allow the amplification of the positive pressure wave leading to droplet emission. An optimal value for dwell has been suggested as d_{well}= L/C where L is the length of the printing nozzle and C is the speed of sound in the ink [52].
The higher the magnitude of the voltage v_1 is the higher the speed [52] and the volume [53] of the droplets are. A minimum value for v_1 is needed for droplet formation while satellite droplets are created if the magnitude of v_1 is too high [52].
Alterations to the classical waveform have revealed interesting results. Kwon et al. demonstrated that a negative waveform is also suitable for inkjet printing but suggested that this waveform should be limited to inks with high jettability because it leads to a strong decrease of the droplet velocity [52]. Jang et al. have investigated a bipolar waveform and found that the second pulse cancels residual acoustic oscillation in the nozzle and may lead to a better printability of the ink. With the use of a waveform with two consecutive pulses, Nogushi et al. could reduce the droplet volume from 17pl to 1.4pl. The small drop volume was beneficial for the fabrication of thin film transistors with a high mobility and a good stability over several weeks [53]. The small volume of the droplets is also interesting for the fabrication of patterns with small feature size.

Once the droplet detaches from the nozzle, it begins its journey towards the substrate. For a good printing quality, it is important that the trajectory of the droplet is a straight line between the nozzle and the substrate. To achieve this requirement, two parameters need to be optimized: the printing height and the printing speed.

Inkjet is a non-contact printing method that requires a distance between the nozzle and the substrate. A minimum stand-off distance (MSD) is needed to avoid ink smearing on the substrate or damaging the nozzle tip. The MSD is also defined as the minimum flying distance of the droplet before it reaches a spherical form. If the droplet hits the substrate while its form is still not stable or has tails and satellites, the impact of the drop on the substrate will be unpredictable and may lead to a poor printing quality. Jang et al. determined the MSD for printable inks to be between 436µm and 650µm depending on their rheological properties [50].
On the other hand, if the distance between the nozzle and the substrate is long, the impact of aerodynamic and electrostatic forces on the droplet may lead to trajectory errors. Creagh et al. found that the drop placement error for a stand-off distance of 1mm can be about ± 10µm [54].

To allow the up-scaling of the inkjet method for industrial applications, high speed printing of large areas is needed.
It was noticed that for high speed printing unwanted satellite droplets are formed because of air entrapment in the nozzle or remaining meniscus oscillations caused by previous drops.
Some research groups have addressed this problem and shown that by optimizing the waveform or adjusting the viscosity of the ink printing at roll-to-roll compatible speeds is possible [52, 55; 56]. Most drop-on-demand inkjet printers can operate with frequencies in the range of 1 to 20 kHz [32].

2.2.2 Droplet behavior on the substrate: Line formation and stability

There are two main differences between using inkjet for graphic art applications and printed electronics: the impact of droplet spacing and the reaction of the solvent with the substrate. In the case of graphic arts the paper substrate is rather forgiving because it absorbs the solvent and the human eye averages out possible printing defects and the distance between the isolated drops. For the fabrication of printed electronics it is important to achieve continuous, straight and smooth lines. The solvent that is not absorbed by the polymer substrate evaporates affecting the shape of the printed line.
Soltman and Subramanian investigated the influence of drop spacing on the behavior of printed lines and identified five possible behaviors with decreasing drop spacing: individual drops, scalloped line, uniform line, bulging line and stacked coins [57]. Stacked coins appear only on a heated substrate when each drop dries individually regardless of overlap. This effect will not be discussed here.
If the droplets are placed too far from each other with a distance bigger than the diameter of a drop they will dry as isolated drops. A minimum overlap is needed for coalescence. With decreasing spacing the droplets merge but retain individual rounded contact lines creating a scalloped line. The scalloped lines are usually narrower than single droplets because the fluid expansion is partially arrested [57]. With further decreasing of the drop spacing the scalloping will be eliminated leading to a smooth und uniform line, which is the desired morphology. Stringer and Derby identified the maximum droplet spacing for a line with stable width as:

$$p_{max} = \frac{2\pi d_0}{3{\beta_{eqm}}^2\left(\frac{\theta}{(\sin\theta)^2} - \frac{\cos\theta}{\sin\theta}\right)} \tag{6}$$

with

$$\beta_{eqm} = \frac{d_{eqm}}{d_0} \tag{7}$$

With d_0 being the diameter of the droplet in flight, d_{eqm} the diameter of the droplet on the substrate and θ the contact angle of the droplet with the substrate [58].
At smaller droplet spacing bulging instability can occur. The periodically formed bulges are separated by regions of narrow lines. Duineveld explained this phenomenon as the axial flow of the ink back into the line causing regions of higher pressure and outflow [59].
Another instability observed by Duineveld is when overlapping drops do not merge to a stable line but form bigger drops instead as can be seen in figure 2.13. Dewetting is observed when the surface tension of the ink and the substrate are not matching [60, 61].

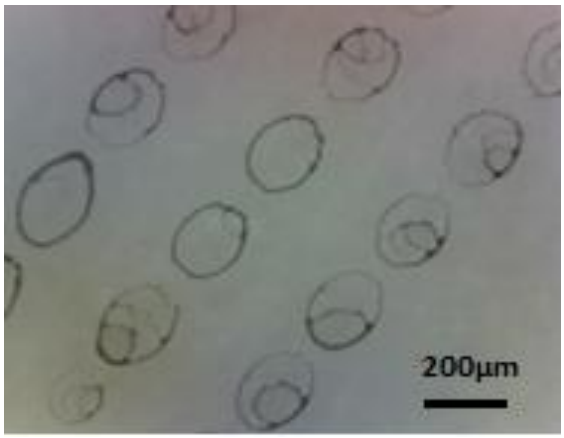

Figure 2.13: CNT ink printed on polymer substrate: if the surface tension of the ink and substrate are not matching dewetting can inhibit the formation of stable lines.

Also, the particles in the ink (in this case CNTs) tend to build a ring around the edges of the droplets. This is a commonly observed phenomenon when coffee droplets evaporate leaving a ring-shaped stain and is therefore called the coffee ring effect.
When a drop hits a substrate that does not absorb the solvent, the drop will spread and expand to a certain point and then gets pinned. Deegan et al. explained that if a drop evaporates on a substrate while having a pinned contact line, radial flow towards the edges of the drop takes place to avoid shrinkage of the drop. Because of the small surface area to volume ratio at the edges and the high surface area to volume ratio in the center the evaporation rate at the edges is higher than in the center. The higher evaporation rates at the edges trigger fresh solvent from the center to replace evaporated solvent at the edges [62]. Deegan also explained that the contact line pinning is caused by surface irregularities and is stronger with solute than without it. The radial flow of the solvent transports the solute towards the edges of the drop causing ring deposits as can be seen in figure 2.14.

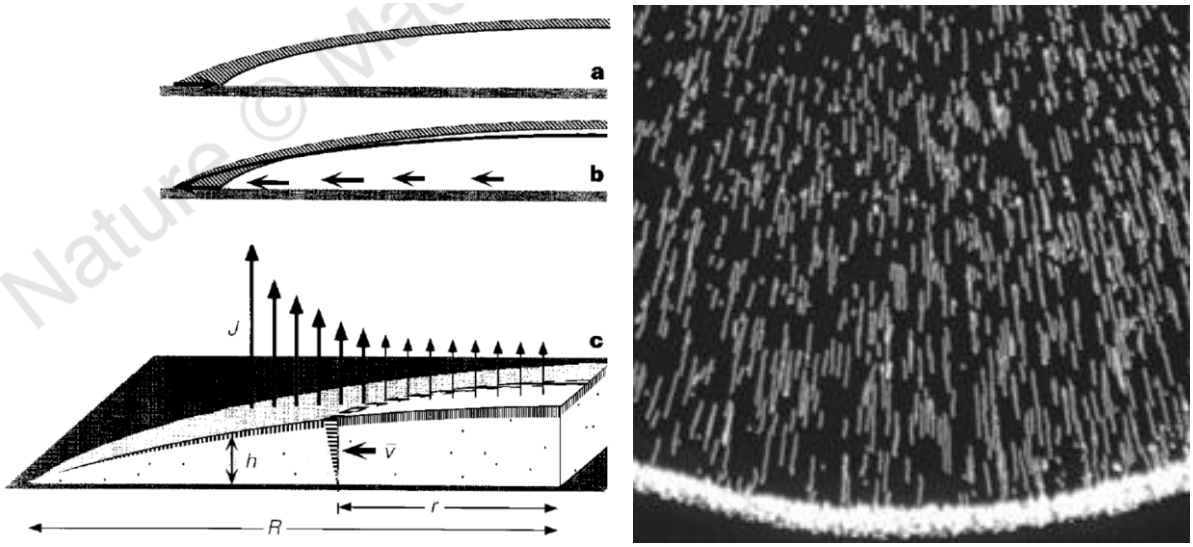

Figure 2.14: left: schematic presentation of the coffee ring effect: mechanism of outward flow during evaporation. The higher evaporation rates at the edges trigger fresh solvent from the center to replace evaporated solvent at the edges. The radial flow of the solvent transports the solute towards the edges of the drop causing ring deposits. right: Image of the droplet edge. The coffee ring effect causes particle transport towards the edges of a drying droplet. Original picture by Deegan et al who were the first to explain the coffee ring effect as being caused by a replenishing flow that originates in a drying droplets interior and travels towards the contact line, reused with permission from [62] Copyright @ 2017 Nature Publishing Group.

The deposition of material at the edges of printed structures is an unwanted behavior because it leads to a poor feature definition and the printed lines are not smooth. Several research groups have investigated methods to inhibit or reduce the coffee ring effect such as by cooling the substrate, raising the ambient humidity or reducing the droplet size [63].
Another method to suppress the coffee ring effect is by enhancing the Marangoni effect. Marangoni found that a surface tension gradient results in a circulatory flow that carries the particles towards the center of the drop. The Marangoni recirculation can either be temperature or surfactant-driven. The evaporative cooling of a sessile droplet into ambient air leads to a temperature gradient that induces a surface tension gradient. Hu et al. have shown that the temperature-induced Marangoni effect can reverse the coffee ring effect [64]. The temperature dependent Marangoni flow is suppressed in water but in this case the surfactant-driven Marangoni effect can be used to obtain a relatively uniform deposition of the particles by mixing a surfactant with the aqueous dispersion [65]. When the local concentration of surfactant molecules at the pinned contact line increases because of the coffee ring effect the surface tension of the drop decreases locally creating a surface tension gradient that leads to a recirculatory Marangoni flow.
We have investigated the effect of the surfactant-driven Marangoni effect and found that by adding triton x surfactant with a concentration of 0.1% to the CNT ink we could minimize the coffee ring effect and obtain more homogeneous lines (figure 2.15).

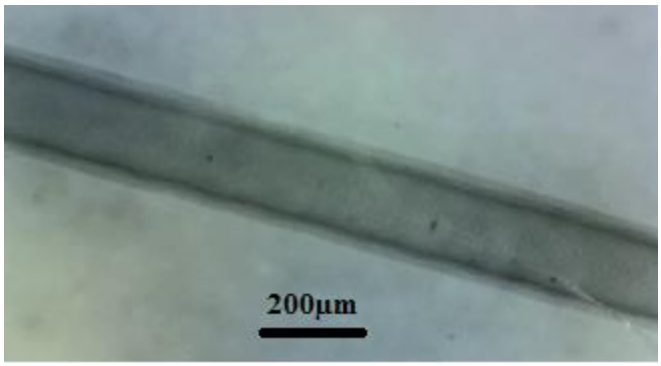

Figure 2.15: CNT line printed on PET substrate as in figure 2.13, however with the addition of a surfactant to the CNT ink.

We obtained similar results by modifying the surface tension of the substrate with a 5 minutes argon plasma treatment as can be seen in figure 2.16.

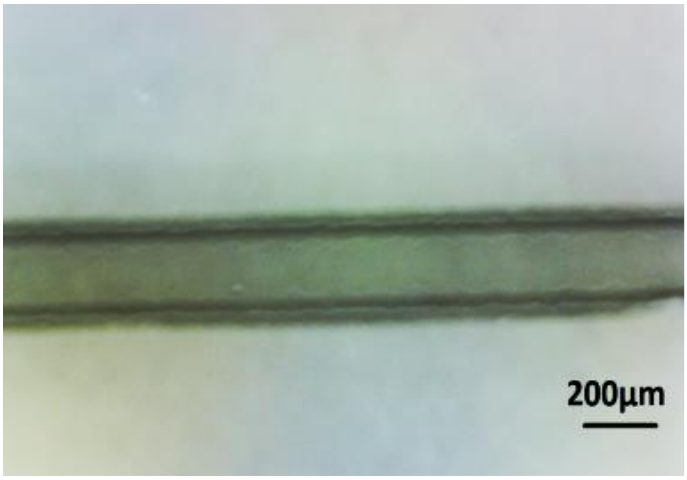

Figure 2.16: CNT line printed on PET substrate as in figures 2.13, however with a plasma pre-treatment of the polymer substrate.

We did not only test the effect of adding the surfactant to the ink but we also investigated the effect of a detergent based cleaning of the polymer substrates. Using Deconex to clean substrates is a well-known method especially for glass substrates. We submerged the polymer foils in a Deconex solution for one minute and then rinsed them under running distilled water. The substrates were then dried using a nitrogen gun. As can be seen in figure 2.17, we could obtain a good printing image with this method. Here the used ink has a higher concentration than in the previous figures because it was centrifuged and not filtered. The effect of the centrifugation will be discussed in more detail in chapter 4.

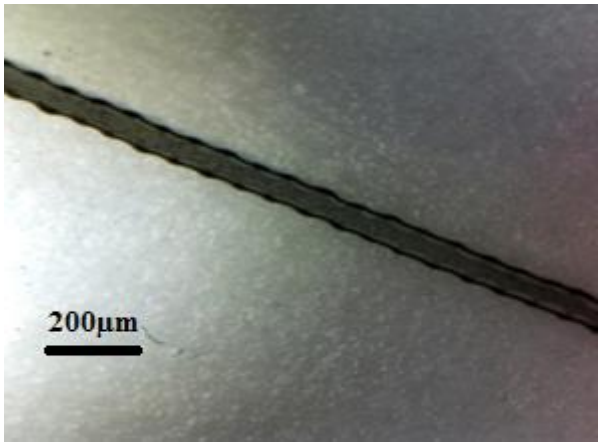

Figure 2.17: Printed CNT line on a PET substrate that has been cleaned using a detergent.

The coffee ring effect could not be completely eliminated but it was suppressed enough to obtain continuous and rather homogeneous lines.
It should be noted that the coffee ring effect is not always considered bad. Some research groups have utilized this primarily unwanted effect for innovative applications such as transparent conductive coatings based on interconnected silver [66] or CNT [14] rings for flexible solar cells, OLEDs and displays.

2.3 Conclusions

This chapter presented an insight into the inkjet method that is the main device fabrication technique used in this thesis. We highlighted the potential of inkjet printing and in particular piezoelectric inkjet printing for printed electronics applications compared to the main printing techniques. Being a digital and non-contact method, inkjet printing is attractive for both prototyping as well as large area fabrication. We also discussed the challenges associated with deploying the inkjet method for printed electronics applications. The fabrication of electronic devices necessitates the accurate deposition of a relatively large number of droplets and the formation of a flawless printing image. We have shown that an optimization of various parameters that affect the droplet behavior in flight and on the substrate is the key to a good printing image that fulfills the requirements for challenging applications such as printed electronics.

Chapter 3

Electrical and mechanical performance of printed silver tracks

Conductive patterns play a crucial role in the fabrication of printed electronic devices. Several conductive materials have been investigated for inkjet inks such as polymers [67, 68, 69], carbon nanotubes [70] and metal precursors [71, 72]. While the polymers and the carbon nanotubes that will be discussed in the next chapter have interesting properties and applications, their conductivity is rather limited in comparison with metal based inks. The most commonly used metals for direct writing of conductive patterns are silver [73, 74], copper [75] and gold [76]. Silver being less expensive than gold, more robust against oxidation than copper [75, 77] and having the lowest bulk resistivity (1.59μΩcm) is frequently the metal of choice for printed electronics applications. In addition to the good chemical stability, the silver inks have also the advantage of high metal loadings [78] that can be helpful for achieving high conductivity tracks. Due to these attractive properties, inkjet-printed patterns have found their way into different applications such as radio frequency identification (RFID) tags [21], organic thin film transistors (OTFTs) [79], organic solar cells [80] and light emitting diodes [74].
The two main types of silver precursor inks are the silver nanoparticles based dispersions [74] and the metal organic compounds (MOD) based solutions [73]. The as printed structures are not conductive and require a sintering step to render the precursor compounds conductive. The conventional sintering method is thermal sintering and consists in heating the whole sample at relatively high temperatures for at least 30 minutes [81]. Because of the prolonged treatment duration this procedure is not scalable for large area and roll to roll fabrication. Another major drawback of thermal sintering is that the high temperatures are damaging for the heat sensitive polymer substrates limiting the choice of substrates to rigid and expensive materials such as ceramic or glass. Several research groups have been investigating methods to obtain conductive structures with a short processing duration and low temperatures compatible with the commonly available low cost polymer foils such as polyethylene terephthalate (PET) and polycarbonate (PC) that have rather low glass transition temperatures. Alternative and selective sintering techniques allow the sintering of the metal precursors without affecting the sensitive substrates [72, 81].
The electrical and mechanical performance of the sintered tracks is important for a successful fabrication of printed electronic devices. Because metal inks are mainly used for contacts and wiring, a high resistivity can lead to unwanted power losses and reliability issues. Since the flexible polymer substrates are crucial for the large area fabrication of low cost devices, the printed patterns should also be flexible and able to withstand mechanical stresses to avoid device failure. The shelf life of printed tracks in aqueous media is also directly related to their reliability for applications where a contact with solutions is inevitable such as in cell monitoring applications.
In this chapter the sintering of inkjet-printed tracks from MOD and nanoparticles based inks using different sintering techniques is discussed and the obtained resistivities are compared. The adhesion of the sintered tracks to the substrate and their shelf life in aqueous media are also investigated.

3.1 MOD ink

The metal organic compounds (MOD) based inks have the advantage of being in the form of a solution rather than a dispersion which minimizes the risk of nozzle clogging due to particle agglomeration, makes them easier to print and is favorable for the fabrication of narrow tracks because it allows the use of nozzles with small diameter. Also, these inks do not require a colloidal stabilizer [81]. In the MOD inks the silver exists in its oxidized form. After printing it is necessary to sinter the printed tracks to reduce the silver cations to their elemental form and allow the in-situ formation of nanoparticles that can fuse together creating conductive patterns [72, 82].

The needed temperatures to decompose the organic component and trigger the sintering of the in-situ created nanoparticles are usually higher than 250°C and therefore not suitable for most low cost polymer substrates such as PET. Sintering at lower temperatures is possible but requires a prolonged treatment duration. Jahn et al. obtained a resistivity of about 25μΩ cm after a thermal treatment at 100°C for 5 hours [83]. Valeton et al. reported on room temperature sintering of MOD tracks using a combination of UV treatment and chemical treatment for 20 seconds with a hydroquinone solution [82]. This method is very interesting because it is suitable for almost all substrates and conductive tracks are achieved after a relatively short treatment.

Materials and Methods

Based on the work of Valeton et al. we tested the printability of a solution of silver neodecanoate in xylene with a concentration of 30wt%. The solution was filtered using a 0.45μm syringe filter and then printed using a nozzle with a 30μm diameter. The inkjet printing was performed using a piezoelectric Autodrop MD-P-822 system (Microdrop Technologies, Norderstedt, Germany) equipped with an AD-K-901 print head (Appendix A). During printing we used only red lighting to avoid the decomposition of the ink in the reservoir and the nozzle. A stable droplet formation was obtained with a voltage of 90V, a pulse width of 55μs and a printing speed of 5mm/s. Printing was performed on PET (substrate that has been cleaned using Deconex. To check the printing quality and measure the line width a USB camera (PCE MM 200 Microscope, PCE Group) was used. Continuous and smooth lines were obtained at a drop spacing of 70μm.
The printed samples were exposed to UV lighting for 10 minutes and then submerged in a hydroquinone solution. The samples were rinsed first in a water/ethanol solution (50/50), then in propanol and finally dried using a nitrogen gun.
A multimeter (Voltcraft digital multimeter VC-820) was used to measure the resistivity of the printed tracks. To test their shelf life in aqueous media, the samples were submerged in a PBS (phosphate buffered saline) solution at room temperature for several hours and their resistivity was checked periodically.

Results and discussion

With the above mentioned parameters we could obtain a good printing image and the continuous silver lines (figure 3.1) were about 100μm wide.

Figure 3.1: Line printed using a MOD silver ink on PET substrate. These continuous and smooth tracks are about 100μm wide.

After the UV exposure the structures started getting conductive but their resistivity was high. At this point the color of the samples has changed from white to brown. This color change is attributed to the formation of the latent image of free silver atoms. When the samples are submerged in the hydroquinone solution, a redox reaction takes place between the silver neodecanoate and the hydroquinone [82] sintering the samples and enhancing their conductivity.

The color of the samples changes again from brown to silver as can be seen in figure 3.2. In figure 3.2 the lines were inkjet-printed and the dots were placed with a spacing of 1 cm using drop casting for easier resistivity measurements.

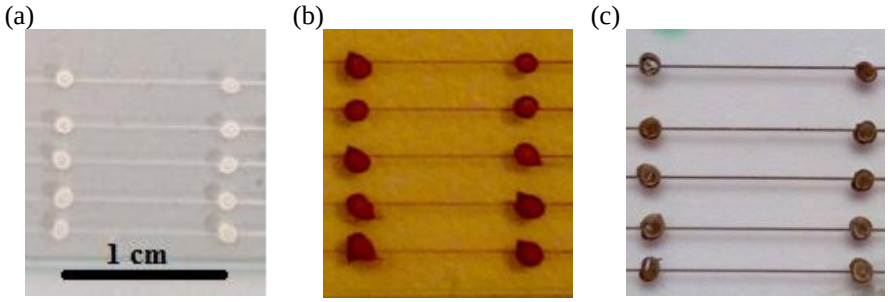

Figure 3.2: Inkjet-printed silver based tracks on PET substrate directly after printing (a), after UV radiation (b) and after chemical sintering with hydroquinone (c). The as printed lines are white and non-conductive. After UV irradiation the formation of the latent image of free silver atoms is indicated by the brown color. After chemical sintering with the hydroquinone solution the samples are conductive and show a silvery color.

The obtained resistivity after hydroquinone sintering of single layer printed samples was rather high, about 48 μΩ cm. The reason for the high resistivity may be the relatively low neodecanoate concentration in the ink. Also a height measurement using a profiler showed that the once printed lines were 40nm thick. Tracks printed using MOD inks can lose up to 90% of their volume after sintering due to decomposition of the organic compounds [83]. For this reason we increased the thickness of the lines by printing eight layers.
After 1 min of hydroquinone exposure we could measure a resistivity of about 14 μΩ cm for the thicker samples. This is similar to results achieved by Valeton et al. They measured a resistivity of about 15μΩ cm after 20 seconds of sintering. To investigate the influence of the duration of the hydroquinone treatment on the resistivity of the samples, we submerged them for longer periods of time in the hydroquinone solution. Figure 3.3 shows that a longer sintering duration leads to a lower resistivity.

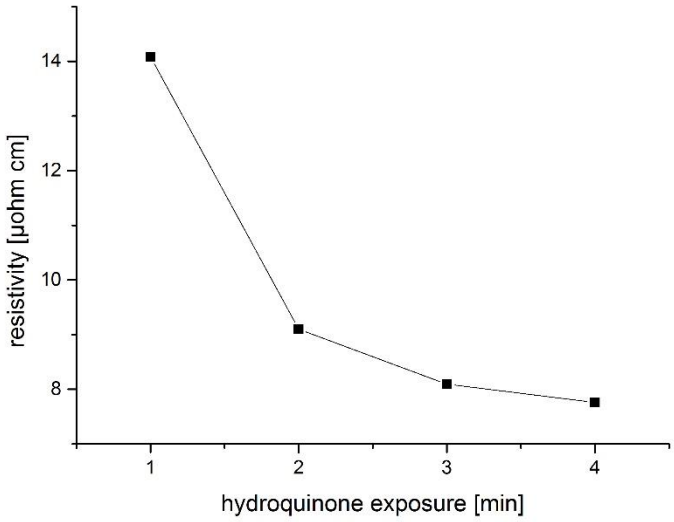

Figure 3.3: Resistivity of printed silver based tracks versus the duration of exposure to the hydroquinone solution. A longer exposure to hydroquinone leads to lower resistivity values of the printed silver based tracks.

After four minutes of hydroquinone exposure we could measure a resistivity of about 8 μΩ cm. This resistivity is still rather high in comparison with resistivity values obtained with thermal sintering at relatively high temperatures. Jahn et al. obtained a resistivity of 3.7 μΩ cm after a 30s treatment at 250 °C of the MOD tracks [83]. However, since high temperatures are very damaging for the PET substrate, this method is only suitable for high performance substrates. In a recent work Dong et al. have reported that by using a solution of silver oxalate in ethylamine they could sinter the on polyimide substrate printed tracks at 150°C for 30 minutes and obtain a resistivity of 8.6μΩ cm [73]. The low curing temperature may be attributed to the high silver content of 71wt% in the oxalate powder. We could not achieve conductive structures using thermal sintering at low temperatures that do not damage the PET substrate with the silver neodecanoate ink that only contains 8 to 11 wt% of silver in the neodecanoate powder.
The mechanical stability test showed that the chemically sintered MOD samples have a rather short shelf life in aqueous media. As figure 3.4 shows, the samples got damaged and started losing their conductivity after 44 hours in PBS.

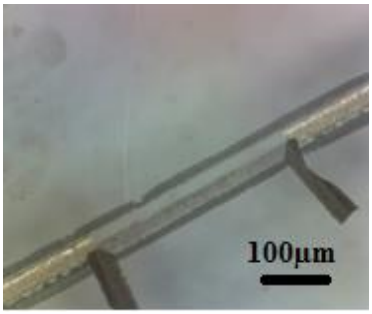

Figure 3.4: Printed silver based track on PET substrate after exposure to aqueous media. After being submerged in PBS for 44 hours the chemically sintered MOD samples get damaged and lose their conductivity.

Although we could obtain a good resistivity value of 8 μΩ cm without damaging the sensitive PET substrate using the hydroquinone sintering at room temperature, the shelf life of the samples in aqueous media is rather limited. The tracks printed from the MOD ink are not robust enough to be implemented in sensor chips for measurements in liquids.
The silver neodecanoate ink is sensitive to UV radiation and has therefore a rather limited shelf life. Also, the printing procedure has to be performed in a way to avoid UV radiation causing unwanted decomposition of the ink in the reservoir or the nozzle. Aqueous silver nanoparticles dispersions on the other hand have a better shelf life, are more environmentally friendly and allow metal loadings up to 70wt% [84]. Nanoparticle based inks are therefore a promising alternative for MOD inks.

3.2 Silver nanoparticle based ink

Whereas in MOD inks the silver salt is first printed on the substrate and the nanoparticles are then created in-situ by adding the reducing agent, in the nanoparticle based solutions already formed metal nanoparticles are dispersed in the ink. Nanoparticle dispersions have the advantage that they can be prepared using environmentally friendly solvents such as water and diethylene glycol. They can allow a higher metal concentration than MOD inks, are commercially widely available and were reported to have lower contact resistances [81].
To avoid agglomerations that may lead to nozzle clogging, protective agents are necessary to stabilize the nanoparticles. The stabilizers can be either polymers such as polyvenylpyrolidone and polyacrilic acid or low molar mass molecules such as long chained thiols and carboxylates [84]. They inhibit van der Waals attractions between the nanoparticles based on an electrostatic stabilization or a steric stabilization.

In case of the electrostatic stabilization, ions adsorbed at the particle surface form an electrical double layer creating Coulombic repulsion between the nanoparticles. The steric stabilization takes place when organic molecules act as a protective shield on the surface of the particles separating them from each other [85].
The stabilizing agents play an important and positive role enhancing the shelf life and printability of the ink by preventing unwanted agglomerations. However, after the deposition of the pattern on the substrate the protective shell around the nanoparticles prevents electrical conductivity by inhibiting direct contact between them and has to be removed. This is the reason why a post-printing step called sintering is required in order to obtain conductive patterns. The removal of the organic shell allows direct physical contact and leads to neck formation between the particles. Due to Ostwald ripening and surface to volume reduction bigger particles are formed and electrically conductive percolating paths are created upon sintering [86].
The conventional method to remove the stabilizers and obtain conductive patterns is thermal sintering. Usually high temperatures are needed for the decomposition of the organic shell and formation of conductive tracks. Due to extensive research in optimizing the inkjet inks during the last years, thermal sintering can be achieved at relatively lower temperatures of about 200 to 300°C depending on the size of the particles, the type of stabilizer used and the amount of organic additives [81, 84]. However, these temperatures are still not compatible with low cost substrates such as PET and the treatment duration needed for thermal sintering is rather long and not suitable for manufacturing scale and roll to roll fabrication.
Several research groups have been working on alternative sintering methods to achieve conductive patterns without affecting the thermally sensitive substrates and reduce the processing time [86]. Very interesting selective sintering methods have been developed such as chemical sintering [87], plasma sintering [88], microwave sintering [89] laser radiation [90], electrical sintering [91] and photonic sintering [80].
Since metal based inks are mostly used for electrical contacts and wiring, achieving a good electrical performance of the sintered tracks is necessary. High resistivities may lead to power losses, excessive heating and reliability issues of the printed devises. Although a conductivity of one tenth of bulk silver is considered sufficient for low performance applications, conductivities of up to 60% of bulk silver could be obtained using selective sintering techniques in a short processing time and validate the potential of these techniques for printed electronics [86]. Also, uniform sintering is important for reproducible large area fabrication processes. A good mechanical stability is necessary to ensure the reliability of the printed devices for the intended applications.
In this chapter we print silver nanoparticle based samples on different substrates and investigate the suitability of some of the innovative sintering methods to achieve conductive patterns on thermally instable substrates. We compare the obtained resistivities and investigate the mechanical stability of the sintered tracks and their shelf life in aqueous media.

Inkjet printing

Silver tracks were printed using an aqueous silver nanoparticles based ink (BayInk TPS CP, Bayer Technologies, Eindhoven) using a nozzle with 50µm diameter at a printing speed of 10 mm/s. The voltage was set to 80 V and the pulse width to 24µm.
At a droplet spacing of 90µm we could obtain continuous and smooth lines with a width of 120µm and a height of about 700nm.

3.2.1 Chemical sintering

Successful sintering of inkjet-printed nanoparticles at room temperature can be triggered using chemical agents such as the cationic polymer poly(diallyldimethylammonium chloride) (PDAC) [87] or the chloride ions (Cl-) in sodium chloride (NaCl) or hydrochloric acid HCl [92]. In case of the polymer PDAC or the sodium chloride a solution containing the sintering agent has to be placed on the printed tracks and may be destructive for the densely packed nanoparticles. On the other hand, since the vapor of the hydrochloric acid contains chloride ions sintering is possible without direct contact with the acid.

The chloride ions can cause a protonation of the stabilizing polymers and eliminate the electrical repulsion between the nanoparticles. They can also detach and replace the anchoring groups of the stabilizers from the surface of the nanoparticles causing a spontaneous coalescence of the densely packed nanoparticles and lead to conductive patterns [92].

Materials and methods

The printed samples were exposed to the vapor of hydrochloric acid (Hydrochloric acid fuming, 37%, Merck, Darmstadt) for 30 seconds and then dried for 5 minutes at 120°C in a convection oven.
The resistance of the samples was measured using a multimeter (Voltcraft digital multimeter VC-820). To test the influence of the thickness and width of the tracks on their shelf life in aqueous media, five times wider samples (by printing five adjacent lines) and thicker samples (five printing layers) were prepared. The samples were submerged in a PBS (phosphate buffered saline) solution at 37°C in the incubator and their resistivity was controlled using an impedance analyzer (SI 1260, Solartron Analytical, U.K).

Results and discussion

After a 30 seconds exposure to the vapor of the hydrochloric acid and a quick drying for 5 minutes at 120°C we could measure a resistivity of 12 μΩ cm.
For an easy and quick evaluation of the adhesion of the samples we first performed an adhesive tape test. This test showed that the chemically sintered tracks had a poor adhesion to the PET substrate and the samples got almost completely transferred on to the tape as can be seen in figure 3.5.

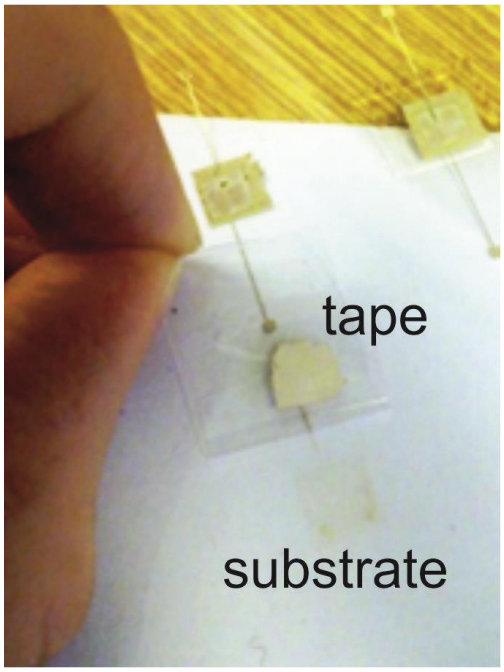

Figure 3.5: Adhesive tape test performed on printed and chemically sintered silver based samples on PET substrate. This test reveals the poor adhesion of the chemically sintered tracks to the PET substrate as they easily get transferred to the adhesive tape (for details of the adhesive tape test see figure 4.5).

The impedimetric measurements revealed that these samples had also a very short shelf life in aqueous media. However we found that the shelf life can be improved by using wider and thicker printed tracks as shown in figure 3.6.

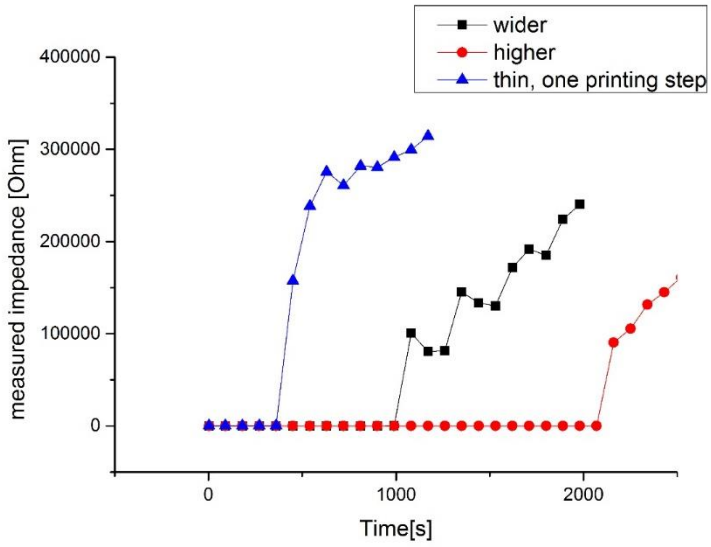

Figure 3.6: Measured impedance over time of a thin (one printing layer) silver based track, a thicker track and a wider track exposed to aqueous media. The impedance measurements show that thicker and wider tracks have a better shelf life in aqueous media than simple tracks printed using only one printing layer.

The thicker samples with five printed layers had about a five times longer shelf life than the tracks prepared using only one printing step.
The resistivity of 12 μΩ cm that we have obtained is similar to the resistivity values reported by other research groups using chemical sintering. Grouchko et al. have reported the lowest resistivity of 3.84 μΩ cm obtained at room temperature using an ink with nanoparticles they have synthesized and stabilized on their own. They also showed that the sintering step may be skipped using a "self-sintering" Ink with a built-in sintering mechanism [92].
Chemical sintering is a fast, easy and low cost method that does not require expensive equipment and leads to good resistivity values. However, the down-side of room temperature sintering is the poor adhesion of the structures to the substrate. Even with several printing steps, the limited shelf life of chemically sintered electrodes in aqueous media makes them not suitable for applications such as cell monitoring biochips.

3.2.2 Plasma sintering

In addition to being a well-established method for surface etching, treatment and activation, low pressure plasma has found its way into even more interesting applications in the field of printed electronics. Plasma treatment can not only be used to improve the wettability of substrates and enhance the printability but it was also proven to be an efficient method for the sintering of printed nanoparticles [93]. The plasma generation creates exited species such as ions, radicals and UV irradiation that cause chain scissions and the decomposition of the stabilizing agent. The decomposition products of the stabilizer can easily evaporate under the applied low pressure and conductive tracks can be achieved [94].

Materials and methods

To investigate the effect of plasma sintering, we printed dumbbell shaped structures on PET (Hostaphan GN4600, Mitsubishi Polyester Film) and PEN foils (Teonex Q65HA, DuPont Teijin Films) (Appendix B). The samples were then dried for 5 minutes at 160°C for the samples on PET substrate and 230°C for the PEN substrate. The plasma sintering was performed using a plasma asher (TePla 100-E Plasma system, Technics Plasma GmbH) capable of utilizing different process gases. Both argon and nitrogen plasma were performed at 300W. To test the effect of a combination of chemical pre-treatment and nitrogen plasma sintering, samples were first exposed to the vapor of hydrochloric acid for 30 seconds and then sintered with nitrogen plasma.

To investigate the mechanical stability of the printed samples, impedance measurements were performed using the IMOLA system (Appendix C) [95]. The sintered samples were placed in adapters that we prepared for this purpose and fresh PBS was regularly manually pipetted on the tracks to test their shelf life in aqueous media.

Results and discussion

Single layer printed samples on PET substrate with a thickness of 700nm showed a resistivity of 25μΩ cm after a 15 minutes exposure to argon plasma. To investigate the effect of the thickness of the tracks on their resistivity, 2 and 4 layer samples were also investigated. Since plasma sintering progresses from top to bottom [88], thicker samples need a longer plasma exposure duration. When the samples are sintered, they change color from dark blue to a more silvery color as shown in figure 3.7a. The bluish colors seems to be typical for unsintered and nonconductive samples printed using silver nanoparticles inks [88]. The 4 layer samples needed a 45 minutes plasma treatment and we could measure a resistivity of about 5μΩ cm. The thicker the tracks are, the lower their resistivity is (figure 3.7.b).

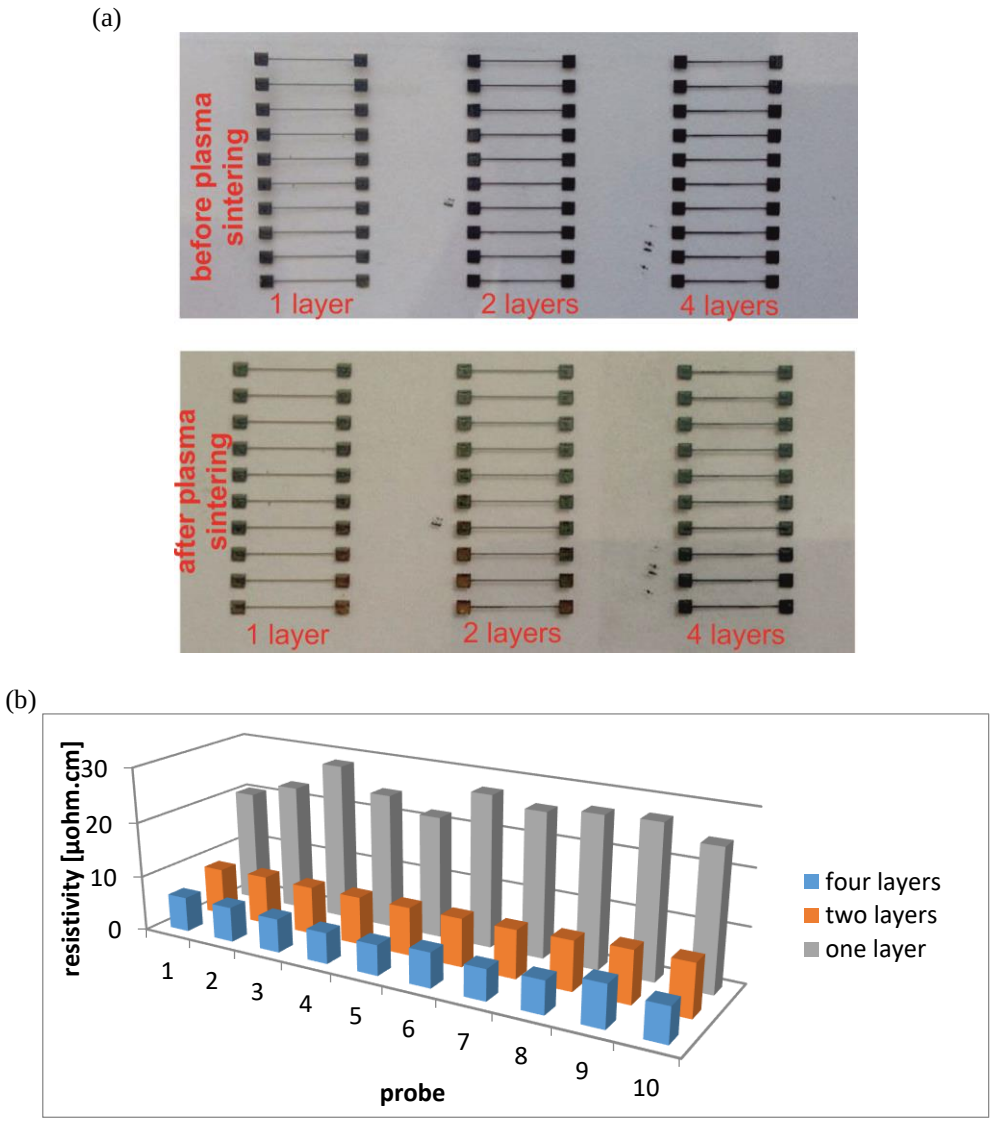

Figure 3.7: Silver based tracks (1, 2 and 4 printing layers) on polymer substrate before and after plasma sintering. When sintered, the printed silver nanoparticle based samples (track length: 1cm) change color from blue to a more silvery color (a), measured resistivity of ten samples with one, two and four printed layers: the thicker the samples are, the lower their resistivity is (b).

Another way to further decrease the resistivity is by increasing the sintering time. Niittynen et al. measured a resistivity of 15 μΩ cm for a single printed layer after 240 minutes of laser exposure [86]. However, it should be noted that such long plasma exposures can be damaging for the polymer substrates. The argon plasma post-printing process was rather successful for the silver based tracks. However, the argon plasma was found to be very damaging for CNT-based tracks. When samples based on silver and CNT tracks are exposed to argon plasma, the silver tracks get sintered as expected whereas the CNT samples get almost completely erased after 5 minutes. Since other research groups have reported positive sintering results with nitrogen plasma [96], we tested nitrogen plasma as an alternative to argon plasma sintering.
For this purpose, samples printed on PET and PEN foils were first dried for 5 minutes at 160°C for the PET substrate and 230°C for the PEN substrate. The samples were then exposed to the vapor of hydrochloric acid for 30 seconds before being sintered using nitrogen plasma for 15 minutes. Using this combination of chemical pre-sintering followed by nitrogen plasma sintering we obtained a resistivity of 9 μΩ.cm for samples on PET and 3 μΩ.cm on PEN substrate for one printed layer samples. The CNT samples were not damaged after the treatment with nitrogen plasma, on the contrary, the resistivity of these samples was rather reduced to about 80% after 20 minutes and to 65% after 40 minutes of treatment,which is eventually caused by nitrogen doping of the CNTS.
The impedance measurements in PBS revealed that the silver tracks sintered using argon plasma had a better adhesion to the substrate then the chemically sintered samples at room temperature. They had a shelf life of several weeks (up to 4 weeks) in aqueous media. No impedance measurements have been conducted yet for the samples sintered with nitrogen plasma but they showed a good adhesion to the substrate upon adhesive tape test. Since plasma sintering progresses from top to bottom and the bottom layer is responsible for the adhesion to the substrate, a longer sintering time of several hours may have a positive impact on the adhesion [86].
Low pressure plasma sintering using argon or nitrogen gas is an efficient method to achieve conductive silver based tracks with a good resistivity on thermally sensitive substrates for thin printed layers. However the lowest resistivities are obtained for thick structures with several printed layers and for long sintering durations. This is not only related to more material consumption and higher fabrication costs but the prolonged plasma exposure can be damaging the polymer substrates and makes the sintering process very slow. We observed that the PET and PEN foils started turning from colorless to opaque after an hour of plasma exposure witch is not suitable for applications where the substrate has to be transparent to allow optical microscopic investigations as is the case for cell monitoring applications. The combination of chemical pre-sintering and plasma sintering seems to be efficient and delivers a low resistivity rather quickly, however, this method might not be easy to integrate in large area fabrication. An emerging and very appealing alternative to low pressure plasma sintering that still has to be investigated is atmospheric plasma sintering [94, 96]. Atmospheric plasma sintering is a quick and substrate friendly method that promises potential cost savings. Tracks can be sintered at speeds compatible with R2R fabrication without the need for expensive vacuum related components so that the sintering process can be integrated in large area fabrication processes. However, this method is still in development and obtaining low resistivity values still requires multiple treatments.

3.2.3 Microwave sintering

Microwave flash sintering is one of the fastest selective sintering methods. In contrast to bulk metals which reflect the microwave radiation, metal nanoparticles are able to absorb and interact with it. The interaction of the nanoparticles with the microwave radiation is believed to be based on Maxwell-Wagner polarization that is caused by charge accumulation at the materials interface, electric conduction and eddy currents. However, the main reasons behind successful heating of metal nanoparticles using microwave radiation are still not yet fully understood [97]. The idea behind the microwave flash sintering is the that the nanoparticles are able to selectively absorb the microwave radiations, heat up and build conductive patterns while the polymer substrates are almost not absorbing the radiation and do not get affected by it. The polarization of dipoles in thermoplastic polymers below their Tg (glass transition temperature) is limited and makes the skin depth (the distance at which the incident power is reduced to half of its initial value) of the polymer foils almost infinite and hence transparent to microwave radiations [97].

Using microwave sintering may take several minutes to obtain conductive structures with a conductivity of about 5% of bulk silver. However, long exposure durations can be damaging for the polymer substrate underneath the heated up silver tracks.
Using a combination of a gentle pretreatment and microwave sintering can lead to lower resistivity values in a shorter treatment time and at lower power [89]. For this reason we investigated the suitability of a combination of chemical pre-sintering followed by microwave sintering to obtain conductive structures on thermally unstable substrates.

Materials and methods

Silver nanoparticles based samples printed on PET and PEN substrates were first exposed to the vapor of hydrochloric acid for 30 seconds and then sintered in a microwave with adjustable power (Ethos one, Milestone, Italy).
The mechanical stability of the microwave sintered samples was tested first by a simple adhesive tape test and then by exposure to an aqueous PBS solution.

Results and discussion

Using the combination of chemical pre-sintering and microwave sintering we could obtain conductive structures with a resistivity of about 6μΩ cm after 30 seconds at 100W on PET and PEN substrates. Perelear et al. obtained tracks with a conductivity of up to 40% of bulk silver using a combination of photonic pre-sintering and microwave sintering with a treatment duration of less than 15 seconds [89].
The downside of microwave sintering is that it still can be damaging for the polymer substrates even at relatively low power. We observed some printed line samples were so heated up that they damaged the underlying substrate.
The adhesive tape test revealed another disadvantage of the microwave sintering that is the bad adhesion of the sintered tracks to the substrate. The samples were strongly damaged and lost their conductivity upon adhesive tape test. When exposed to aqueous media, the microwave sintered samples were also damaged and started dissolving as shown in figure 3.8.

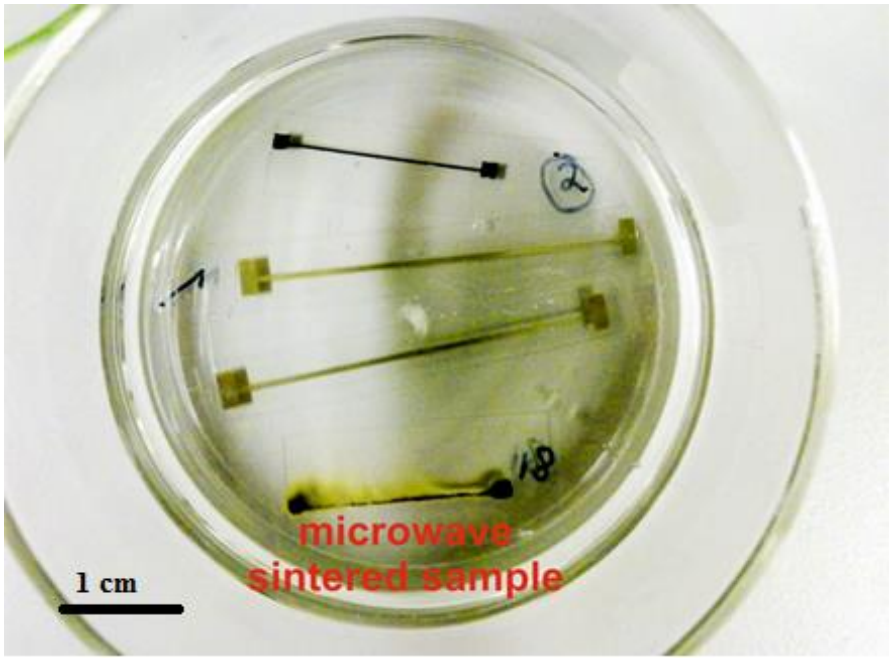

Figure 3.8: Printed silver and CNT based tracks on polymer substrate submerged in an aqueous solution. The microwave sintered samples dissolve upon exposure to aqueous media.

The combination of a gentle pre-treatment and microwave sintering is a very promising method to obtain a good conductivity rather fast and is scalable for large area R2R fabrication.
Although the polymer foils are not directly affected by the microwave radiation, dissipated heat from the sintered silver tracks may be damaging for the underlying substrate. Therefore, this method seems to be more suitable for high performance foils such as PI foils rather than low cost substrates such as PET or PEN.
Using another pre-sintering treatment such as photonic sintering instead of chemical pre-sintering may improve the adhesion of the sintered tracks to the substrate.

3.2.4 Photonic sintering

Photonic sintering is a fast and selective method that has that been reported to deliver good resistivity values with a treatment duration as short as 10 seconds [86].
For the photonic sintering an intense pulsed light with a broad spectrum in the visible range from ultraviolet (UV) to infrared (IR) is used to irradiate the printed sample. The short flashes have a pulse length from a few micro- to milliseconds.
The dark printed silver tracks absorb the intense irradiation, heat up and build conductive patterns. On the other hand, the colorless polymer foils do not absorb the irradiation as fast as the metal tracks and do not get damaged.
Photonic flash sintering allows sintering speeds up to 100 meter per minute and can lead to conductivity values up to 34% of the conductivity of bulk silver [89].

Materials and methods

Dumbbell shaped silver nanoparticle based samples were printed on PET substrate. The photonic sintering was performed by Novacentrix using a PulseForge 1200 (Novacentrix, Austin, USA).
The resistance of the samples was investigated with a two point measurement using a multimeter (Voltcraft digital multimeter VC-820). Impedance measurements using the IMOLA system were performed to investigate the shelf life of the sintered samples in aqueous media.

Results and discussion

The samples sintered using photonic flash sintering showed a resistivity of 13μΩ cm. These samples showed a good adhesion to the substrate and their resistivity did not change upon adhesive tape testing. Niittynen et al. reported similar resistivity values for a sintering time of 10 seconds and an energy of 3.5 kJ. The resistivity could be reduced to about 3.3 μΩ cm for a sintering time of 40 seconds and an energy of 14kJ.
They also reported a very good adhesion to the substrate upon adhesive tape test with a category of 5B or 4B according to ASTM D3359-B standard adhesion test [86].
The impedance measurements showed that samples sintered using photonic flash sintering were robust and had a shelf life of several weeks in aqueous media as shown in figure 3.9. With an applied voltage of 300mV in aqueous media, these samples had a shelf life of up to 11 weeks after which the experiment was stopped.

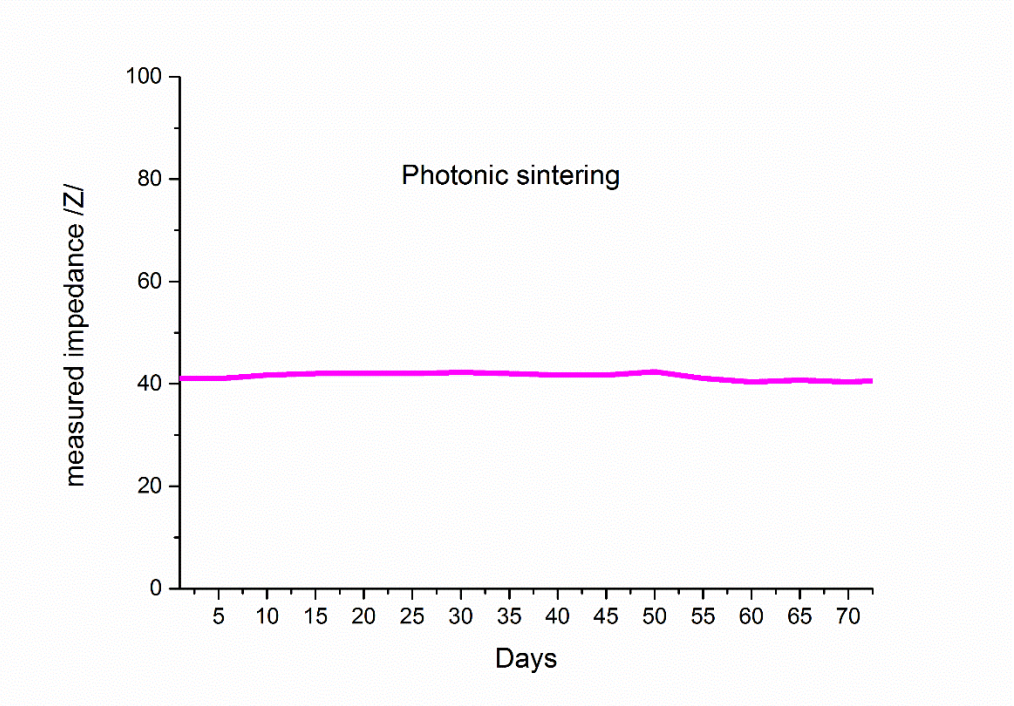

Figure 3.9: Measured impedance over time of inkjet-printed silver based tracks sintered using photonic flash sintering and exposed to aqueous media. The samples sintered using photonic flash sintering are robust and have a shelf life of several weeks in aqueous media.

Photonic flash sintering is a very efficient method that can lead to excellent conductivities in seconds and has a great potential to be integrated in large area R2R fabrication processes. The obtained mechanical stability is also very good compared with other sintering techniques. The tracks sintered using photonic sintering are good candidates for challenging applications such as the sensor applications in fluids under applied voltage.

3.2.5 Thermal sintering

Thermal sintering is the conventional and most commonly used sintering method [86]. It is an easy method where the whole sample is simply heated up, usually in a convection oven, to allow the decomposition of the organic stabilizing shell and the merging of the nanoparticles to create conductive percolating paths. While bulk silver melts at 960°C, silver nanoparticles have the ability to melt at much lower temperatures [87]. However, the decomposition of the stabilizer requires temperatures higher than 200°C which prevents thermal sintering at low temperatures and restricts the choice of substrates to expensive high performance substrates [84]. The curing temperature differs from one ink to another and depends on the metal loading, particle size, solvent system and the stabilizing agent [93]. The most commonly used polymer substrates for thermal sintering are polyimide (PI) substrates that typically have a brown or yellow color. In recent years colorless PI foils have been developed for applications where the substrate has to be transparent. We had the opportunity to test the suitability of colorless PI foils that can withstand temperatures up to 350°C for printed electronics applications.

Materials and methods

Silver nanoparticles based tracks printed on colorless PI substrate (I.S.T, Tokyo, Japan) were thermally sintered at 300°C for 60 minutes in a convection oven (B180, Nabertherm, Germany) with a slope of 15 minutes.
The resistivity of the tracks was measured with a two point measurement using a multimeter (Voltcraft digital multimeter VC-820). The shelf life in aqueous media of the sintered tracks has been investigated using impedimetric measurements in the IMOLA system.

Results and discussion

The thermally sintered samples at 300°C on PI substrate showed a resistivity of about 3μΩ cm. As mentioned above, the curing temperature strongly depends on the ink formulation and we could not achieve conductive tracks using thermal sintering at lower temperatures. Thermal sintering is a very efficient method and resistivity values as low as twice the resistivity of bulk silver are commonly obtained using this method [84, 86].
The thermally sintered samples had a good adherence to the substrate and were not damaged upon peel off test. The sintered tracks did not transfer to the adhesive tape and we measured a maximum resistivity change of about 1.6%. These results are similar to the results obtained by Niitynen et al. who found that thermally sintered tracks have a very good adhesion that can be classified in the category 4B/5B according to ASTM standard adhesion test (ASTM D-3359). The impedance measurements confirmed the good adhesion of the thermally sintered samples to the substrate and the impedance of the tracks in aqueous media was stable for several weeks as can be seen in figure 3.10.

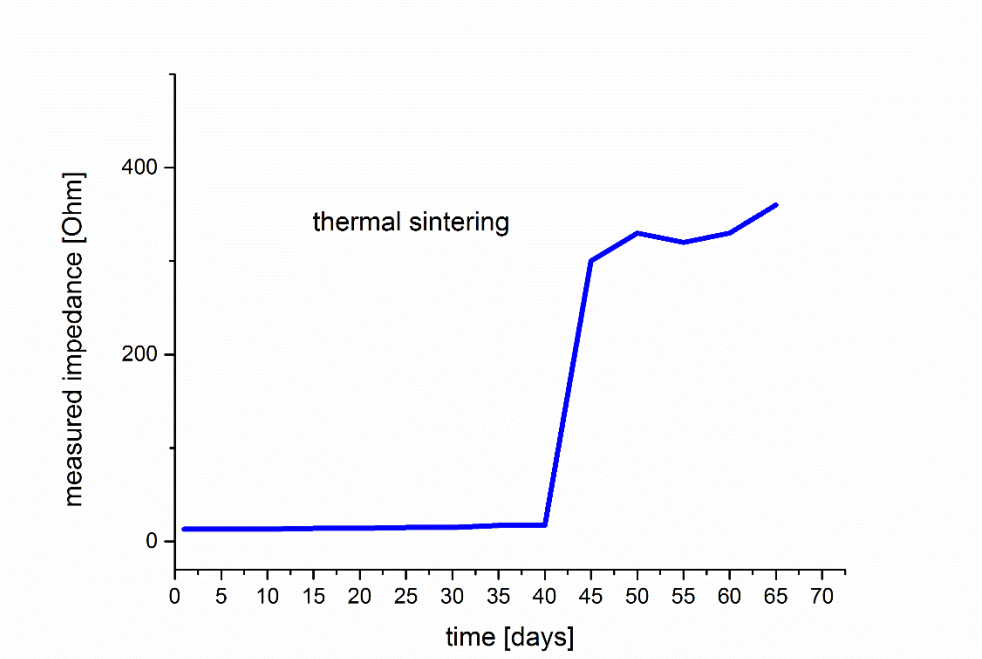

Figure 3.10: Measured impedance over time of inkjet-printed and thermally sintered silver based tracks exposed to aqueous media. These measurements show that thermally sintered silver tracks have a shelf life of several weeks in aqueous media.

3.2.6 Bendability

The commonly used substrates for the fabrication of printed electronics are the polymer substrates. Since the polymer foils are flexible, it is important that the printed tracks are also flexible to avoid device failure during handling or even during fabrication. The fabrication process has to be scalable for low cost and large area R2R fabrication where the printed tracks are bent already during production. Bendability is also important for applications where foldable devices are advantageous as is the case for flexible displays or sensors for medical implants, for example.

Materials and methods

For the bendability test we chose chemically sintered samples with a very poor adhesion to the substrate and samples sintered with photonic sintering with a very good adhesion to compare their performance.

The samples were bent with a bending radius of 1.5 cm and a cycle duration of 7 seconds using a motor while their impedance is measured using an impedimetric analyser (SI 1260, Solartron Analytical, UK). As can be seen in figure 3.11, no significant change in the impedance was measured for both samples for 9400 bending cycles after which the measurement was stopped.

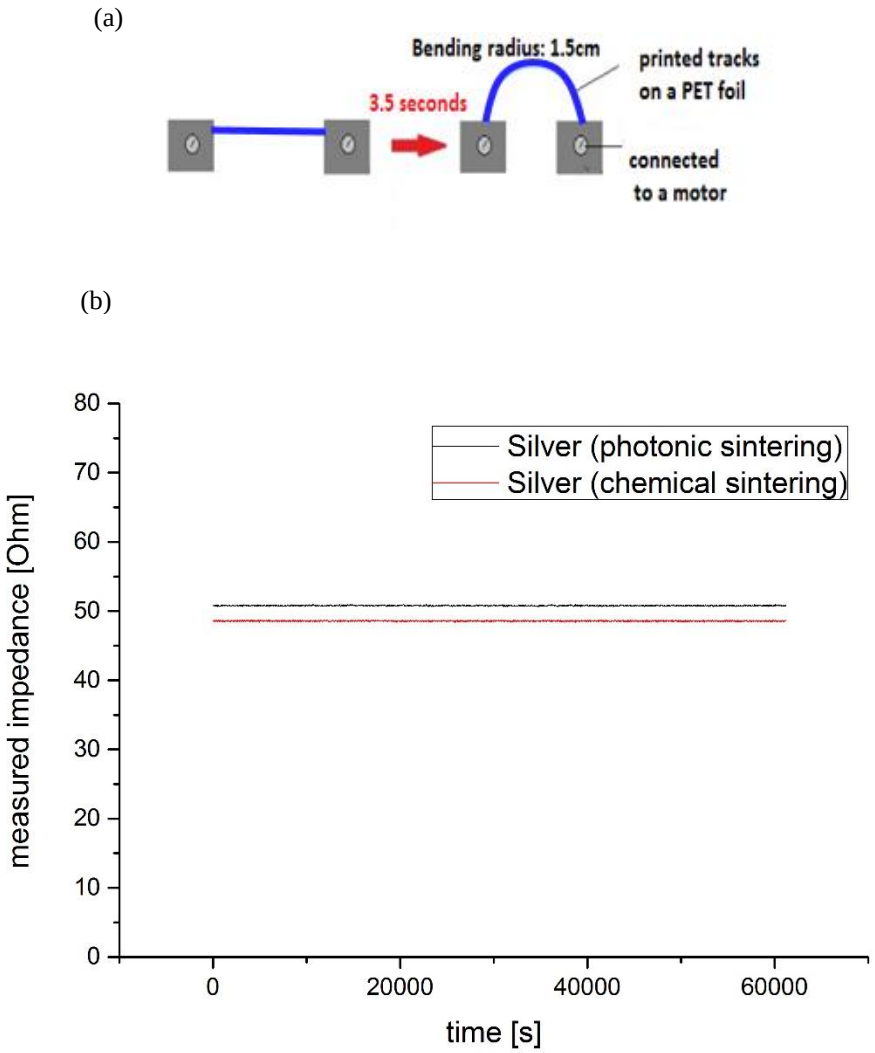

Figure 3.11: Setup for bendability test where a motor is used to bend the printed samples at a bending radius of 1.5 cm and a cycle duration of 7 seconds (a) Measured impedance over time of chemically sintered silver based tracks and silver tracks sintered using photonic flash sintering during the bending test. Although chemically sintered and photonic sintered silver samples have very different adhesion to the substrate, both samples showed a very good performance during the bendability test and no changes in the impedance were measured after about 17 hours (b).

Similar results were obtained by other research groups. Layani et al found that the resistance of printed silver nanoparticles based transparent arrays did not change even after bending at angles below 20° [66]. The resistance increase of silver nanowires based transparent layers was less than 2% after 1000 bending cycles and they are therefore an attractive replacement for ITO in the fabrication of flexible displays [26]. Valeton et al. have shown that the resistance of spin-coated silver samples on 50µm thick PET substrate was stable for up to 12000 cycles of an applied 2%strain and resistance increase begins only at the breaking point of the substrate [82].

3.3 Summary

We successfully printed and sintered MOD and silver nanoparticle based inks on different polymer substrates and then investigated the electrical and mechanical performance of the sintered tracks and their suitability for flexible printed electronics applications.
For the MOD based samples we could obtain a resistivity of 8μΩ cm without damaging the thermally instable PET substrate by using chemical sintering at room temperature with a hydroquinone solution instead of the classical thermal sintering. These samples have not been further investigated mainly because of the limited shelf life of the MOD ink and the poor mechanical performance of the printed tracks.
For the silver nanoparticles based samples we investigated and compared different sintering methods on PET, PEN and PI substrates and we could obtain resistivity values as low as twice the resistivity value of bulk silver without damaging the polymer substrates. Although very low resistivity values can be achieved, a full conversion to bulk silver is not possible because the evaporation and decomposition of the organic protective shell leaves a porous structure with many voids [86].
Similar to results obtained by other research groups, we found that the sintering method has a big influence on the mechanical stability of the sintered tracks. Choosing the right sintering method, the adherence of silver based tracks to the substrate can be significantly enhanced. The good adherence to the substrate was linked to a longer shelf life in aqueous media. Using photonic sintering we could enhance the shelf life of printed silver tracks in aqueous media at 38°C and with an applied voltage of 300mV up to eleven weeks. A summary of the obtained resistivity values and the influence of the sintering method on the shelf life of the silver samples in aqueous media is displayed in table 3.1. However, it should be noted that in addition to the sintering method, the sintering parameters, the substrate and the ink may have a strong influence on the performance of the printed samples.

Table 3.1 Overview of the resistivity values and shelf life in aqueous media of silver samples with different sintering methods

Method	Chemical sintering	Argon plasma sintering	Nitrogen plasma sintering (+ chemical pre-sintering)		Photonic sintering	Microwave sintering (+ chemical pre-sintering)	Thermal sintering
Substrate	PET	PET	PET	PEN	PET	PET/PEN	PI
Resistivity (one printed layer)	12 μΩ cm	25 μΩ cm	9 μΩ cm	3 μΩ cm	13 μΩ cm	6 μΩ cm	3 μΩ cm
Shelf life	-	+	Good adhesion	Good adhesion	++	-	+

Although printing several layers is linked to increased material usage and longer printing and sintering time, we observed a reduction in resistance with increased printed layer number for both MOD and silver nanoparticles structures of up to the factor 5 for four printed layers. We also found that thicker tracks have a longer shelf life in aqueous media than single layer tracks. However, the sintering method has a much stronger effect on the robustness of the printed patterns than their thickness.
Therefore we have investigated all sintering techniques for inkjet-printed structures that have been reported in the literature, to the best of our knowledge, with the exception of laser and direct current (DC) sintering. However, laser sintering has been reported to lead to a poor adherence to the substrate [97] and DC sintering is a very difficult method to scale up for R2R fabrication because a continuous direct contact with a power supply is necessary [26, 89].
We showed that using alternative sintering methods such as photonic sintering low resistivity values can be obtained rather fast without damaging the sensitive polymer substrates and the sintering time can be reduced from hours to seconds. Some of the alternative sintering techniques can lead to a mechanical stability that is as good as or even better than the mechanical stability obtained with thermal sintering. This demonstrates the potential of inkjet-printed electronics for R2R large area fabrication.

Chapter 4

Electrical and mechanical performance of printed CNT based tracks

The advantages brought by the liquid phase processing of printed electronics stimulate the development of novel materials and inks such as carbon based inks. Due to their desirable and unique properties combined with the potential for low-cost fabrication carbon nanotubes (CNTs) belong to the most investigated one dimensional nanoparticles and represent a promising alternative to noble and expensive metals.
In this chapter, we investigate the suitability of inkjet printing as a cost effective and scalable method for the deposition of conductive CNT-based patterns on flexible polymer substrates. The fabrication of low cost biocompatible electrodes is crucial for disposable biochips because it eliminates the need for the prohibitively expensive gold and platinum based electrodes.
One of the biggest challenges faced when fabricating CNT based tracks is the relatively high resistivity of the printed patterns. Here we report on different methods to reduce the resistivity of the printed CNT tracks to nearly one order of magnitude without affecting the stability of the jetting behavior or damaging the sensitive substrates. To ensure the suitability of the printed tracks for flexible biochips and cell monitoring applications we also investigated the shelf life of the CNT electrodes in aqueous media and their bendability.

4.1 Inkjet deposition of CNT based tracks on flexible polymer substrates

Carbon nanotubes (CNTs) are high aspect ratio nanocylinders that have unique properties such as high intrinsic current mobility, mechanical flexibility, optical transparency of the thin films and the potential for low cost fabrication. The exceptional properties of carbon nanotubes coupled with the possibility for solution deposition make them a promising material for flexible and printed electronics.
Carbon nanotubes can be visualized as seamless and hollow cylinders of one (single walled carbon nanotubes, SWCNTs) or more (multi walled carbon nanotubes, MWCNTs) layers of graphene.
The diameter of SWCNTs is typically in the range of 0.4 to 4 nm while the outer diameter of MWCNTs can reach up to several tens of nanometers. The length of CNTs ranges from less than 100 nm to several centimeters thereby bridging molecular and microscopic scale [98].
SWCNTs can be metallic or semiconducting depending on the orientation of the graphene lattice with respect to the tube axis, which is called chirality. Statistically seen, one third of the SWCNTs are metallic and the other two thirds are semiconducting [99]. Although each one of the coaxial shells of a MWCNT can either be metallic or semiconducting, MWCNTs are typically metallic [100].

Carbon nanotubes represent an interesting alternative to the conventional semiconductors and metal based conductors and have stimulated big interest in both fundamental research and practical applications.
The SWCNTs have been mainly implemented in applications where the ability to modulate the carrier concentration is beneficial such as in organic thin film transistors, medium scale flexible circuits, displays, radio frequency devices and sensors [99, 101]. SWCNT based sensors for biochips will be discussed in detail in chapter 6.
On the other hand, MWCNTs are rather interesting for applications where the electrical conductivity is a primary metric and all CNTs should ideally be metallic such as in interconnects or electrodes [102].

Although metallic SWCNTs are also suitable candidates for these applications, MWCNTs offer several advantages. MWCNTs do have similar current carrying capacity as metallic SWCNTs while being easier to fabricate due to easier control of the growth process [100]. MWCNTs are also low-cost and do not require complicated processes to separate the metallic and semiconducting tubes as is the case for SWCNTs

CNT based transparent electrodes (TE) represent one of the main applications for CNTs and CNT films in flexible LEDs are at the market entry stage [26].

In this work we describe the patterning of CNT based electrodes on plastic substrates using the inkjet method. The main challenges that we address here are the printability of CNT based inks and the high resistivity of the printed CNT patterns. We investigate different methods to lower the resistivity of the printed CNT tracks and then investigate their mechanical stability and shelf life in aqueous media.

Inkjet printing

Similar to the silver nanoparticles discussed in the previous chapter, CNTs also tend to agglomerate. For a stable jetting behavior, it is therefore important to remove any agglomerates and unwanted bigger particles that may cause nozzle clogging.

The classical method to remove the agglomerates from the ink before printing is by using a filter. However, due to their high aspect ratio, CNTs usually get caught in the filter and therefore filtering leads to a rather low particle concentration. Therefore, we tested the centrifugation method as an alternative to filtering.

Materials and methods

In the scope of this study, we have tested the printability and compared the performance of more than 26 different CNT based inks. A CNT ink from Bayer (BTS-TD-UP-CC, Bayer Technologies, Eindhoven), 25 inks from Future Carbon with different concentrations, dispersing methods and stabilizing agents as well as in-house prepared inks.

The findings presented in the following paragraphs refer to the best results we have obtained for printability and electronic performance.

A MWCNTs based ink (3 wt. %) from Future Carbon (TUM 19) was centrifuged at 4000 rpm for 30 minutes. The upper 50% of the centrifuged ink was then decanted for inkjet printing. The printing was performed using a nozzle with a diameter of 30µm. Stable jetting behavior was obtained at a voltage of 110 V and a pulse duration of 22 µs. The printing speed was set to 30mm/s.

Results and discussion

Although the low-concentration filtered ink is rather easy to print using a nozzle with a diameter of 30µm, the printed tracks have a width of about 230µm (figure 4.1.a/b) and one time printed tracks are not conductive.

The centrifuged ink has a much darker color than the filtered ink and therefore a higher particle concentration (figure 4.1.c). In spite of the higher particle concentration, the centrifuged ink could also be easily printed using the same nozzle. Stable jetting behavior could be observed for prolonged periods of time (up to 60 minutes).

The tracks printed from the centrifuged ink (line width ~ 80µm, figure 4.1.d) were significantly narrower than the track obtained from the filtered ink (line width ~ 230µm, figure 4.1.b) eventually due to the higher solid content in the centrifuged ink.

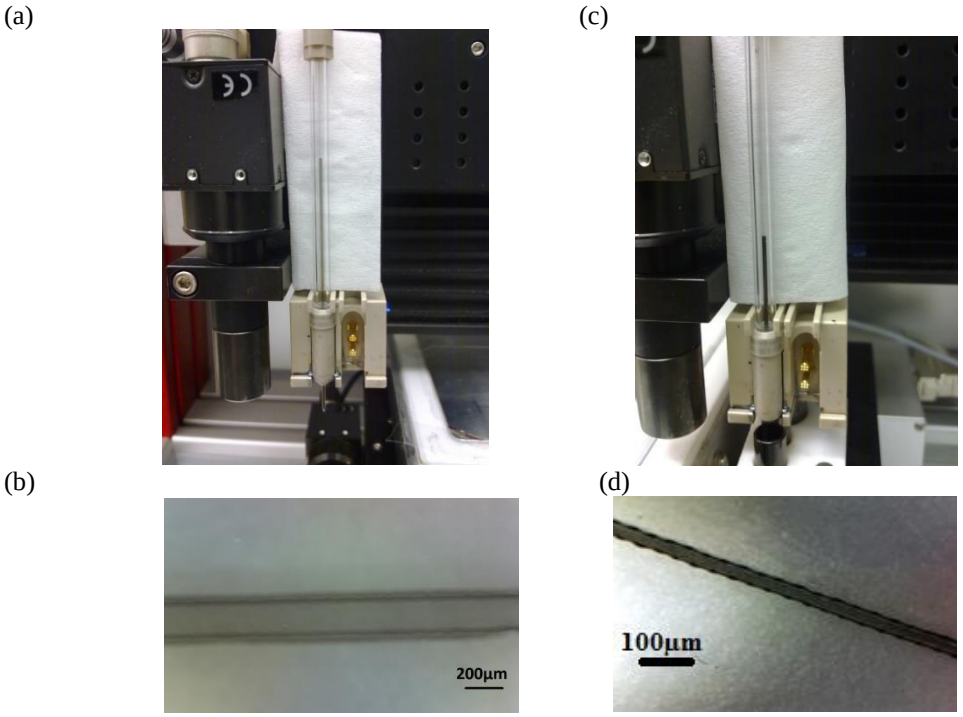

Figure 4.1: Photograph of the inkjet pipette filled with filtered CNT ink (a) and a track printed on polymer substrate using the filtered ink (b). Image of the inkjet pipette filled with centrifuged CNT ink (c) and a track printed on polymer substrate using the centrifuged ink (d). The filtered ink has a lower particle concentration that translates into a lighter color compared to the centrifuged ink and to a lower particle density of the printed track.

Other research groups have also reported on successfully using the centrifugation process before printing CNT-based inks. However, they either used inks with a lower concentration (1 wt.%) combined with a longer centrifugation duration [103] or combined centrifugation and filtering [104]. We found that centrifuging a high concentration (3 wt.%) ink at 4000rpm for 30 minutes and decanting the upper 50% for printing is sufficient to achieve a good printability if combined with optimized printing parameters such as applied voltage and printing speed.
The centrifugation process is efficient for removing unwanted agglomerations and achieving a stable jetting behavior without a drastic reduction of the nanoparticles concentration. The higher particle concentration does not only affect the shape of the printed tracks but has also a significant influence on their electrical performance.

4.2 Electrical performance

Due to the low particles concentration, the tracks printed using the filtered ink had a very poor electrical performance. Electrical conductivity was only obtained with several printing layers and even after 10 printing layers, the tracks still had a very high resistivity of about 800 KΩ/cm due to the poor percolation of the CNTs. As a result of the significantly higher concentration of the nanoparticles, one layer tracks printed using the centrifuged ink had a resistivity of about 60 KΩ/cm. For this reason the printed CNT-based tracks discussed in the rest of this chapter are all printed using a centrifuged ink.

In contrast to the inkjet-printed silver based tracks, as printed CNT patterns are already conductive and do not strictly require a thermal post-printing treatment. However, the resistivity of the printed CNT based tracks is relatively high. The high resistivity of the CNT patterns can have different causes. Although the intrinsic resistivity of CNTs is rather low (10^{-6} Ω cm for SWCNTs and 3 10^{-5} Ω cm for MWCNTs) the resistivity of the single CNTs can be much higher because of the formation of defects and impurities during the fabrication process of the nanotubes.

Ideally CNTs should have all carbon atoms bonded in a hexagonal lattice, however, defects created during mass production introduce pentagons, heptagons and other imperfections that degrade the desired properties [98].
The resistivity of CNT films is also much higher than the resistivity of single CNTs because of the high resistance between overlapping CNTs in the random network (junction resistance) and to their electrical transport properties (relative content of metallic and semiconducting tubes) [26].
Although using longer CNTs may lead to a lower resistivity by limiting the number of CNT junctions per unit area, the length of the CNTs used for inkjet printing should not exceed 5% of the nozzle diameter to avoid nozzle clogging.
The resistivity of the printed CNT patterns can be influenced by the ink composition, the number of printed layers and post-printing processes. Here we discuss different methods to reduce the resistivity of the printed CNT tracks using different methods such as ink centrifugation, increasing the number of printed layers and the removal of the stabilizing surfactants using an acidic treatment.

Materials and methods

The resistance of the CNT samples was measured with a two point measurements along the printed lines using a multimeter. Centrifugation was performed using a tool from NeoLab (D-6015) for 30 minutes. The acidic treatment was performed using nitric acid diluted (1:4) in water. The samples were submerged in the acid for 60 minutes and then rinsed using distilled water and finally dried using a nitrogen gun. The thermal treatment of the samples was performed at 160°C for 60 minutes using a convection oven (B180, Nabertherm, Germany).

Results and discussion

We have compared inks with different nanoparticles formulations: MWCNT-inks containing only multi-walled carbon nanotubes, CNP-inks containing only carbon nanoparticles and MWCNT/CNP-inks containing both types of nanoparticles.
CNP based printed patterns had a higher resistivity then the tracks printed using the MWCNT ink. This result was expected mainly due to the superior intrinsic carrier mobility of the CNTs and to the lower number of junctions per unit area. Azoubel et al. reported on a sheet resistance of less than 16 KΩ/□ for MWCNT tracks with 14 inkjet-printed layers [102] while Torrisi et al. reported on a sheet resistance of 30 KΩ/□ for tracks with 30 layers printed using a graphite nanoparticles based ink [105].
The tracks printed using MWCNT/CNP ink had the lowest resistivity compared to the MWCNTs only and the CNPs only tracks (figure 4.2.a). Although the CNPs themselves do not have a similar electrical performance to the CNTs, they can help bridging the gap between the nanotubes, facilitate the electron transport from a tube to another and therefore enhance the electrical conductivity of the printed layers.
Although we could obtain continuous patterns and a good printability of the ink on polymer substrates, the coffee ring effect could not be completely eliminated. Therefore the CNT network in the middle of the printed line may be relatively sparse in comparison to the edges where most particles tend to accumulate. This effect is widely observed when printing carbon nanoparticles. By enhancing the contact of the CNTs to each other and helping to create electron pathways especially in regions where the CNT network is comparably sparse, the CNPs positively contribute to the electrical performance of the printed patterns.
By controlling the centrifugation parameters, the concentration of the ink and therefore the conductivity of the printed tracks can be enhanced. To ensure a good printability and prevent nozzle clogging, carbon nanoparticle based inkjet inks are usually treated using ultrasonification at high speeds of about 10000 rpm [105, 106].
We observed that by lowering the centrifugation velocity, inks with higher particles concentration can be obtained due to less sedimentation of the nanoparticles. The higher concentration translates in a lower resistivity of the printed tracks as can be seen in figure 4.2.b.
Since all samples show a good printability, we opted for the lowest centrifugation velocity (4000 rpm) in order to print tracks with a relatively low resistivity.

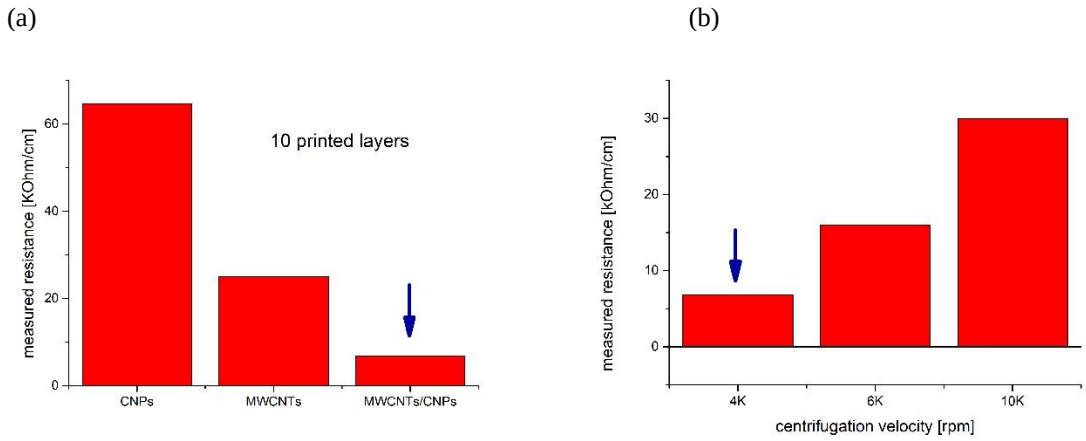

Figure 4.2: Measured resistance of tracks printed using CNT, CNP and CNT/CNP inks (10 printed layers). The CNT/CNP based tracks have a lower resistivity than CNT only and CNP only tracks (a), measured resistance of tracks printed using CNT/CNP inks centrifuged at different centrifugation velocities. A lower centrifugation velocity results in higher ink concentration and thereby leads to printed tracks with lower resistivity (b) the blue arrows point to the options we chose for the further fabrication of carbon based tracks.

In order to investigate the effect of a further lowering of the centrifugation velocity we tested a CNT ink sample that has been centrifuged at 2500 rpm. This sample, however, showed a very poor printability. It is therefore necessary to find a balance between the printing and electrical performance of the ink.
In addition to the pre-printing processes, it is possible to reduce the resistivity of the printed tracks by increasing the number of the printed layers and by using a post-printing acidic treatment.
Printing multiple layers increases the density of the carbon nanotubes network and significantly reduces the resistivity of the printed patterns. We observed that by using 10 printed layers we could reduce the resistivity of the printed tracks by about one order of magnitude as displayed in figure 4.3.

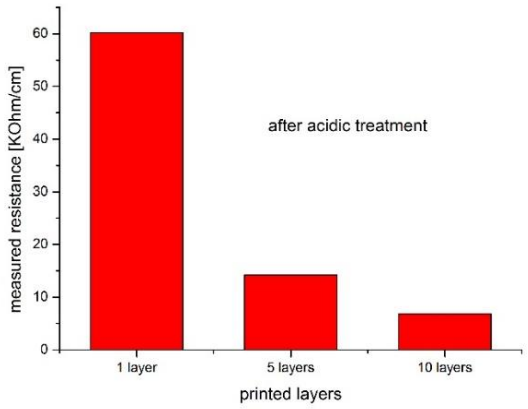

Figure 4.3: Measured resistance of CNT-based tracks with 1, 5 and 10 printed layers after acidic treatment. Printing multiple layers increases the density of the CNT network and significantly reduces the resistivity of the printed tracks.

Similar results were obtained by other research groups who reported on a resistivity reduction with the factor 8 to 10 for five printed layers, however, the obtained resistivity may also depend on the length of the used CNTs [104].
The resistivity of the printed CNT tracks can also be significantly lowered by the decomposition and removal of the dispersing agent using an acidic treatment. Before printing, the surfactant plays a positive role by preventing agglomerations and ensuring the homogeneity and therefore the printability of the ink.

After printing, the surfactant plays a rather negative role by hindering the contact of the nanotubes to each other. The immersion of the printed samples in an acid such as citric acid, nitric acid or sulfuric acid successfully removes the unwanted surfactant and leads to a better conductivity of the CNT based tracks [107].
The removal of the surfactant leads to the densification of the CNT network and therefore reduces the cross-junction resistance between the nanotubes. Some acids such as HNO_3 contribute more effectively than others to the electrical conductivity of the CNTs because they not only remove the surfactant but also can cause p-doping of the nanotubes. Because for CNTs the hole mobility is larger than the electron mobility, using p-dopant oxidizers such as HNO_3, NO_2 or $SOCl_2$ is an effective method to improve the conductivity of the CNT patterns [26]. To investigate the effect of the acidic treatment we submerged printed MWCNTs/CNPs samples in nitric acid diluted (1:4) in water for 60 minutes. A thermal treatment was performed before the submersion in acid mainly to enhance the adhesion of the nanotubes to the substrate. After the acidic treatment we observed a reduction of the resistance approximately to the half as can be seen in figure 4.4.

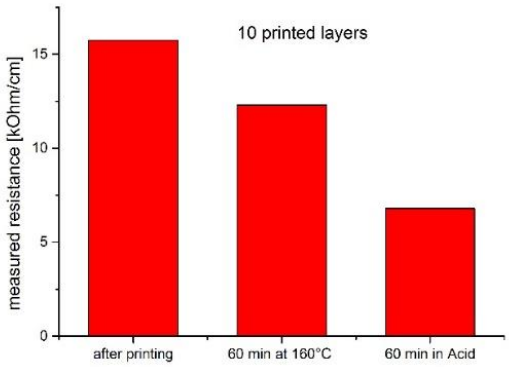

Figure 4.4: Measured resistance of CNT-based tracks with 10 printed layers directly after printing, after 60 minutes at 160°C and after a 60 minutes exposure to an acidic solution. An acidic treatment leads to a densification of the CNT network and therefore to a resistivity decrease with the factor 2.

Using a HNO_3 treatment has been reported by other research groups to lead a resistivity decrease with the factor 2 to 10 of printed CNT based tracks [26]. An oxidizing treatment may be more effective for SWCNTs than MWCNTs because it has been reported to enhance the metallic behavior of SWCNTs [107].

4.3 Mechanical performance

The main reason we have investigated printed CNT based tracks is to fabricate biocompatible cell electrodes for the disposable biochips. These electrodes are intended to be submerged in aqueous solutions for several hours or even days during the cell measurements. Therefore, it is crucial to ensure a good adhesion of the tracks to the substrate and a sufficient shelf life in aqueous media. To prevent device failure during handling or roll-to-roll fabrication, the CNT based tracks printed on flexible substrates need to be bendable.

Materials and methods

Impedimetric measurements were performed using an impedance gain phase analyzer (Solartron) and the IMOLA system [95]. During these measurements, the samples were submerged in an aqueous PBS (Phosphate buffered saline) solution. The measurements were performed at 37°C and with an applied AC voltage of 300mV.

The bending experiments were performed without PBS. A motor was used to bend the printed samples with a bending radius of 1.5 cm and cycle duration of 7 seconds. The impedance of the samples was measured over time using the impedance gain phase analyzer (Solartron) with an applied AC voltage of 300mV.

Results and discussion

Adhesion and shelf life in aqueous media

A quick and simple adhesive tape test (figure 4.5) can deliver a first impression on the adhesion of the printed MWCNT/CNP tracks. In comparison to the silver based tracks described in the previous chapter, the CNT based tracks showed a much better adhesion to the PET substrate after a thermal treatment at a relatively low temperature (160°C). As can be seen in figure 4.5.f, very few particles were transferred to the adhesive tape and the conductivity of the samples was not affected by the test.

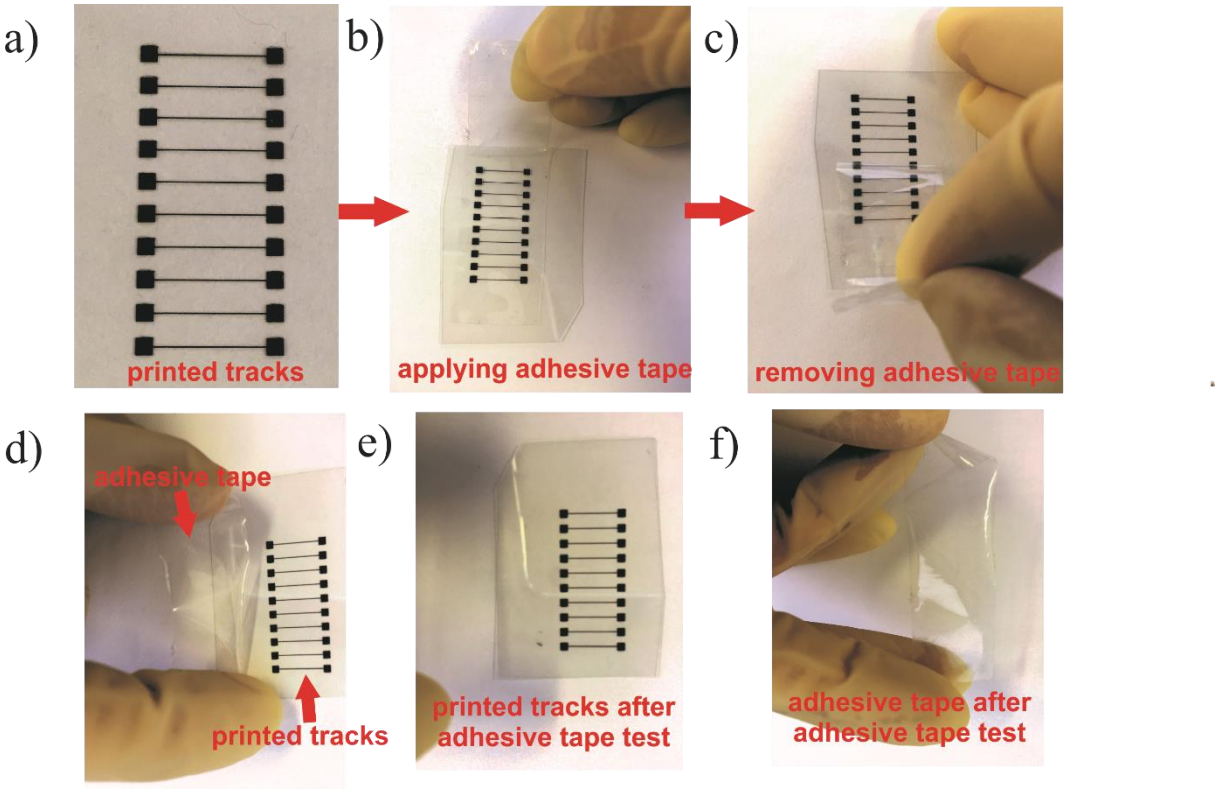

Figure 4.5: Images corresponding to the steps of an dhesive tape test performed on CNT based tracks printed on PET substrate: The adhesive tape test procedure consists in applying an adhesive tape on the printed tracks (a,b), peeling the tape off (c) and then comparing the amount of particles remaining on the substrate to the amount of particles transferred to the adhesive tape (d,e,f). Here, the adhesive tape test reveals a good adhesion of the CNT based tracks to PET substrate after a thermal treatment at a relatively low temperature (160°C).

The impedance measurements also revealed a good adherence of the printed tracks to the PET substrate and no significant impedance change upon exposure to aqueous media was observed for several days as shown in figure 4.6. These samples have a shelf life of at least ten days in aqueous media and with an applied AC voltage with an amplitude of 300mV and are therefore suitable for disposable biochips.

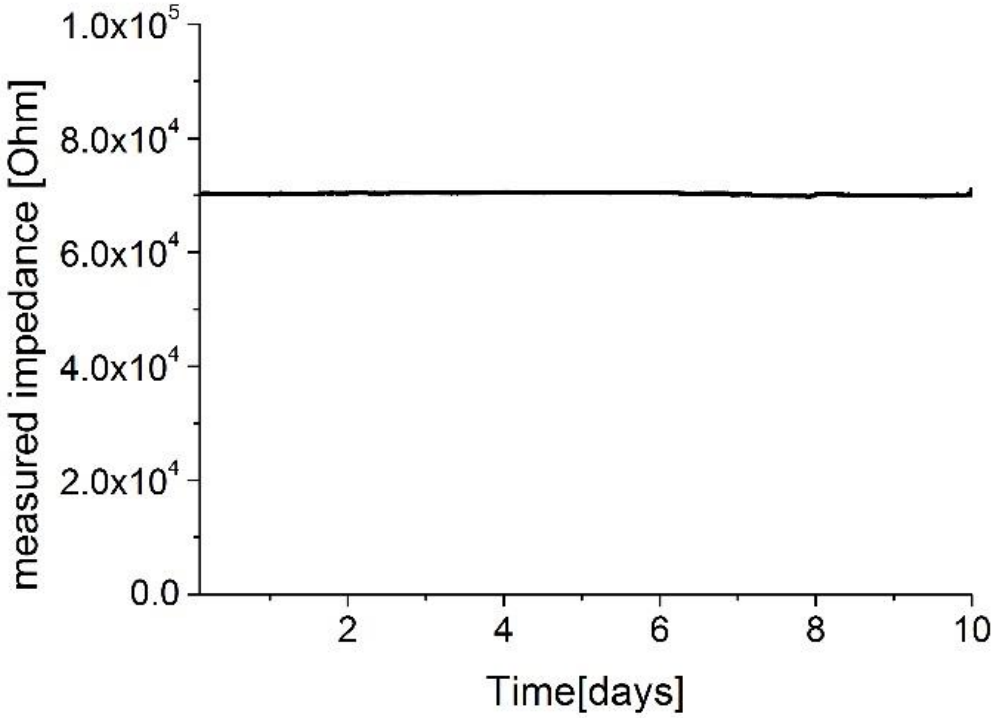

Figure 4.6: Measured impedance of CNT based tracks over time. No significant change in the impedance of the printed CNT tracks was observed upon exposure to aqueous media for several days.

The CNT based samples showed a good adhesion to PET substrate and a promising shelf life already at process temperatures as low as 160°C.
For a further investigation of the stability and shelf life of the inkjet-printed CNT tracks we tested the effect of photonic flash treatment and thermal treatment at 300°C on their mechanical performance. As described in the previous chapter, both photonic sintering and thermal sintering lead to a good adhesion of silver based tracks and enhance their shelf life to several weeks in aqueous media.
Since printed biochips may include silver and CNT based electrodes, the CNT based tracks will also eventually be exposed to treatments originally targeting the sintering of silver nanoparticles such as photonic treatment, thermal treatment at higher temperatures or plasma treatment. It is therefore interesting to investigate the influence of such treatments on the mechanical behavior of CNT based electrodes.
Similar to the silver based tracks, the photonic and thermal treatment at 300°C seem to have a positive impact on the adhesion of the printed samples. As can be seen in figure 4.7, impedimetric measurements show that the CNT based tracks have a shelf life of several weeks in aqueous media.

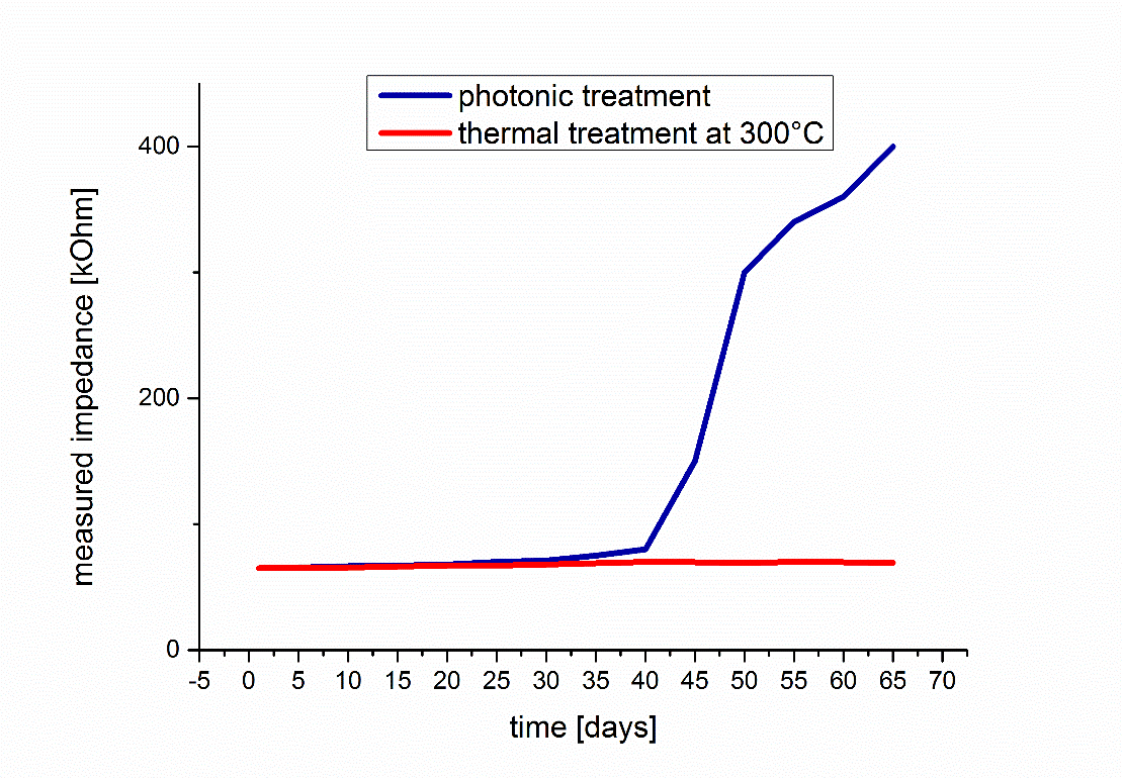

Figure 4.7: Measured impedance of CNT based tracks treated using a photonic treatment (blue curve) and thermal treatment (red curve) over time. After a photonic treatment or a thermal treatment at 300°C, the CNT based tracks display a shelf life of several weeks in aqueous media.

In contrast to photonic and thermal treatment, argon plasma treatment has proven to be strongly damaging for the CNT patterns. These were completely erased of the polymer substrate after a 5 minutes exposure to argon plasma.
Since treatment durations of about 15 to 45 minutes are needed for the sintering of silver nanoparticles, argon plasma seems to be not suitable for the fabrication of flexible biochips containing carbon based electrodes. For this reason, we have investigated the suitability of nitrogen plasma as an alternative to argon plasma.
As opposed to the destructive effect of argon plasma, nitrogen plasma seems to be a rather gentle treatment for the CNT based tracks. We did not observe any damage of the CNT patterns after a 40 minutes exposure to nitrogen plasma. Not only were the CNT tracks mechanically not affected by the nitrogen plasma, we measured a resistivity decrease of 20% after 20 minutes and 35% after 40 minutes exposure to plasma.
Plasma treatment is an efficient method for material surface modification and can be implemented to incorporate foreign atoms in the CNT structure. The chemical doping of carbon based materials is a leading strategy to enrich free charge-carrier densities, improve the electrical conductivity and enhance the metallic behavior of carbon nanotubes. Among different possible dopants, nitrogen is considered to be an excellent element for the chemical doping of carbon based materials. The reason is that nitrogen atoms have a comparable atomic size to carbon atoms and contain five valence electrons available to form strong valence bonds with the carbon atoms [108].
Wang et al. [108] reported on an enhanced electrical performance of graphene based samples caused by nitrogen doping. A plasma exposure of up to 40 minutes was beneficial for the electrical conductivity, however, they reported that for longer exposure durations the effect of the plasma treatment was rather destructive.

Bendability

The impedance of the CNT based tracks stayed constant over time while they are being periodically bent with a radius of 1.5 cm and a cycle duration of 7 seconds for a total of 9400 cycles. The result displayed in figure 4.8 confirms the ductile nature of carbon nanotubes and their suitability for flexible electronics.

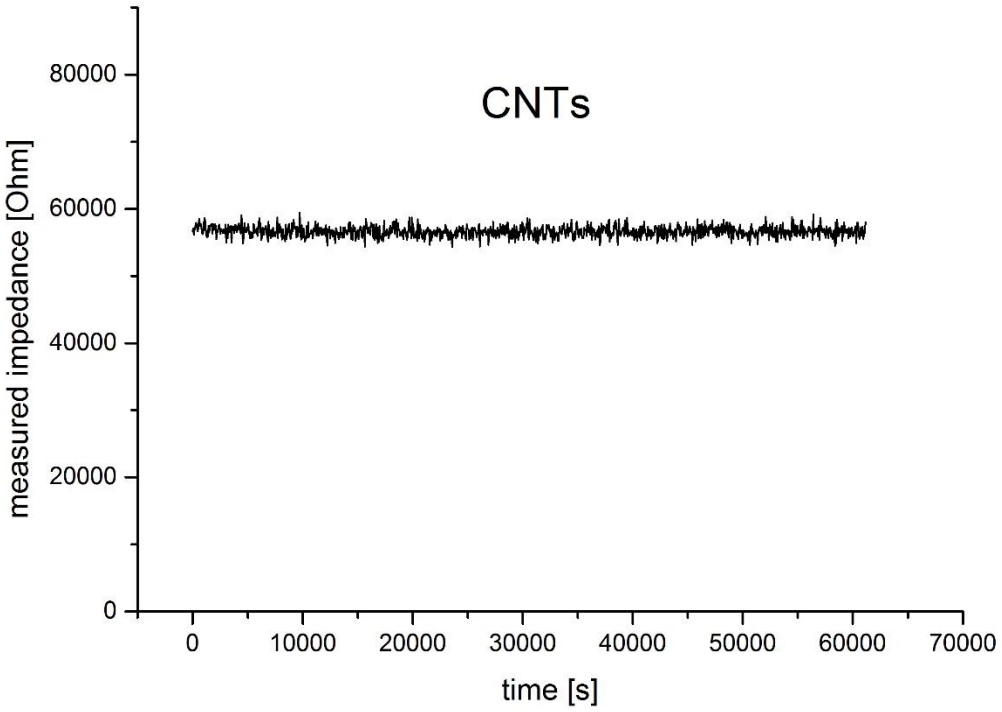

Figure 4.8: Measured impedance of CNT based tracks over time during the bending test. The impedance of CNT samples is stable for up to 9400 bending cycles.

CNTs have been investigated by several research groups as a promising low-cost and ductile replacement to the rather expensive and very brittle ITO especially for applications in electroluminescent devices [26, 102]. Kamyshny et al. reported that a resistivity increase of $\leq 0.5\%$ after 2500 cycles of bending and Azoubel et al. observed no resistivity change after 20 bending cycles at 180°. Different research groups also reported no performance decrease of CNT based devices upon bending confirming their reliability for flexible electronics applications such as electroluminescent devices [102] and transparent conductors [14] in touch screens for smart phones or displays, integrated circuits [99] and thin film transistors [101]. The superior mechanical performance of carbon nanotubes does not only translate in bendability but also in stretchability and therefore opens new opportunities for flexible electronics. Stretchable conducting CNT films have been implemented in various innovative applications such as in stretchable pressure, strain, biological or chemical sensors or even in robotic systems with skin-like capabilities [101].

Biocompatibility

Although the electrical conductivity of inkjet-printed tracks is still at this stage not competing with metals such as silver or copper, they have the advantage to be biocompatible. This quality is especially attractive for applications in the biomedical field. A biocompatibility test according to ISO 10993 validated the biocompatibility of the MWCNT/CNP ink and its suitability for the fabrication of cell electrodes for printed biochips. Figure 4.9 shows uniform growth of cancer cells on a CNT/CNP spot (lower left corner) as well as on the adjacent substrate.

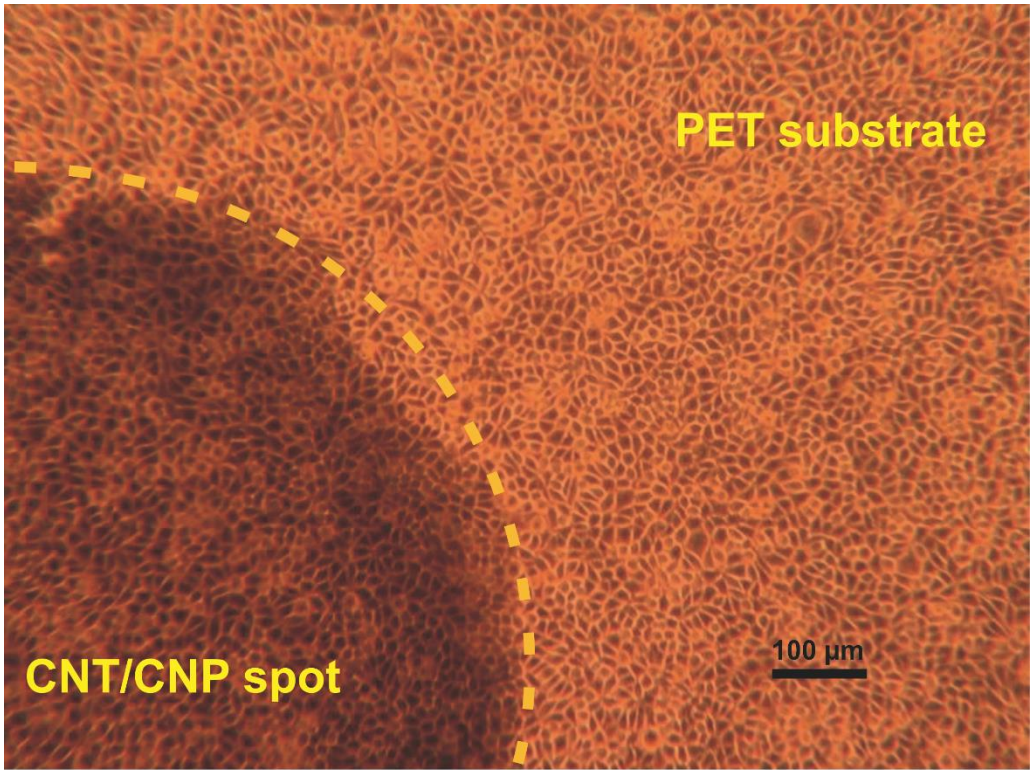

Figure 4.9: Image of cancer cells (L929) growing on a PET substrate with a CNT/CNP spot. The uniform growth of the cells both on substrate and the CNT/CNP spot indicates biocompatibility of these materials.

4.4 Summary

We achieved successful inkjet printing of continuous CNT based tracks on flexible polymer substrates. Although single CNTs have a low intrinsic resistivity, the resistance of the printed CNT track is rater high mainly due to the junction resistance in the random CNTs network and the stabilizing surfactant wrapping the nanotubes. We have demonstrated several methods to reduce the resistivity of the printed CNT network. Instead of using the conventional filtering method, we have shown that centrifugation allows the printing of higher concentration inks and therefore leads to a better electrical performance. Printing several layers leads to a densification of the CNT network and a resistivity decrease up to one order of magnitude for 10 printed layers. We could also significantly reduce the resistance of the printed tracks by removing the stabilizing agent using an acidic treatment. All these method allow to enhance the electrical performance of the CNT tracks without damaging the polymer substrate. The printed CNT samples displayed a good adherence to both PET and PI substrates and had a shelf life of several weeks in aqueous media. Bendability test revealed no significant impedance change after 9400 bending cycles and validated the ductile nature of CNTs and their suitability for flexible electronics. Although the conductivity of the printed CNT samples is not as good as silver, they have the advantage of being biocompatible which makes them very attractive candidates for biomedical applications.

Chapter 5

Inkjet-printed insulating biocompatible polymers

5.1 Insulating polymers for printed electronics

Solution-processable and functional polymers have a great potential for the fabrication of low-cost and printed electronic devices. Partly-printed all-polymer devices such as thin film transistors containing conductive, semi-conductive and dielectric polymers [109] have been reported. However, most research efforts have been dedicated to the printing and patterning of conductive polymers [68, 110] while the insulating polymers are frequently deposited by more conventional means such as spin coating. The reason for that is eventually the poor printability of the insulating polymers. These are difficult to deposit using inkjet printing because most of them are either insoluble or prone to clogging [111, 112]. Also, some polymer dielectrics such as polyimides require high temperatures for cross-linking rendering them unsuitable for thermally-unstable and low-cost substrates such as PET [113]. Recent advances in ink formulations mainly targeting the printability of gate dielectrics for organic thin film transistors [113, 114] have led to successful printing of insulating polymers.
Biocompatible insulating polymers can also be interesting for the fabrication of printed and disposable biochips. The electrodes and contacts in classical biochips are usually fabricated using very expensive, noble and biocompatible metals such as gold and platinum. The fabrication costs can be significantly reduced by using cheaper metals with a good conductivity such as silver or copper. However, these metals are not biocompatible and show toxic and damaging effects upon direct contact with living cells. Printing an insulating polymeric layer on top of non-biocompatible electrodes such as silver-electrodes may help providing a biocompatible environment for the living cells that is necessary for reliable cell measurements.
In this chapter we report on successful inkjet deposition of insulating polymers on printed silver-based electrodes. We investigate the breakdown voltage of the polymers and the biocompatibility of the printed patterns to ensure their suitability for biomedical applications. Here we demonstrate that printable and UV-curable insulating polymers can be implemented to enhance the biocompatibility of silver based electrodes on low-cost PET substrate and present potential candidates for the fabrication of printable and disposable biochips.

5.2 Inkjet printing of insulating polymers

The inkjet printing of insulating polymers can be challenging due to different reasons. Several insulating polymers suffer from solubility and nozzle-clogging issues [112]. Also, the fluid behavior that is most commonly encountered during inkjet printing of polymer solutions is non-Newtonian. Typically, a droplet of polymer solution remains attached to the nozzle by an elongating filament for several hundreds of microseconds. Then, the formation of a pinch point above the main drop triggers the disintegration of the filament into satellite droplets [110]. If the satellite droplets do not merge with the main drop before reaching the substrate, they can lead to a poor printing behavior. This is eventually the reason why rather few inkjettable insulating polymers have been reported and most of them were custom in-home prepared solutions.
We tested the printability of SU-8 polymer based solutions as well as samples of polymer inkjet inks from Altana. SU-8 is a well-known biocompatible epoxy that is commonly used as a photoresist in microelectronic industry and usually deposited using spin coating.

Materials and methods

Solutions of SU-8 polymer (SU-8 2, 40% in Gamma Butyrolacetone) from MicroChem (MicroChem Corp., Westborough, USA) diluted with dichlorobenzene (DCB) (1:1), (1:4) and (1:9) were stirred at room temperature for 30 minutes. Inkjet-printing was performed using a nozzle with a diameter of 70µm, a voltage of 65V, a pulse duration of 20µs and a printing speed of 70mm/s.
The polymer ink (AL13-119-M-A in n-Butylacetat) from Altana (Altana, Wesel, Germany) was printed using a nozzle with a diameter of 70µm at a voltage of 72V, a pulse duration of 18µs and a printing speed of 70mm/s.

Results and discussion

The concentrated SU-8 polymer solution was not printable and droplet formation was not possible even at a high voltage of 250V eventually due to the high viscosity of the solution. On the other hand the solutions of SU-8 diluted with DCB showed a good printability. Stable and reproducible droplet formation could be achieved by diluting the SU-8 solution and reducing its viscosity.
We could also obtain a stable droplet formation using the polymer ink from Altana. No nozzle clogging or drying was observed for prolonged printing durations.
Both the ink form Altana as well as the solutions of diluted SU-8 polymer showed a good printability and desirable Newtonian fluid behavior without the formation of satellite droplets as can be seen in figure 5.1.

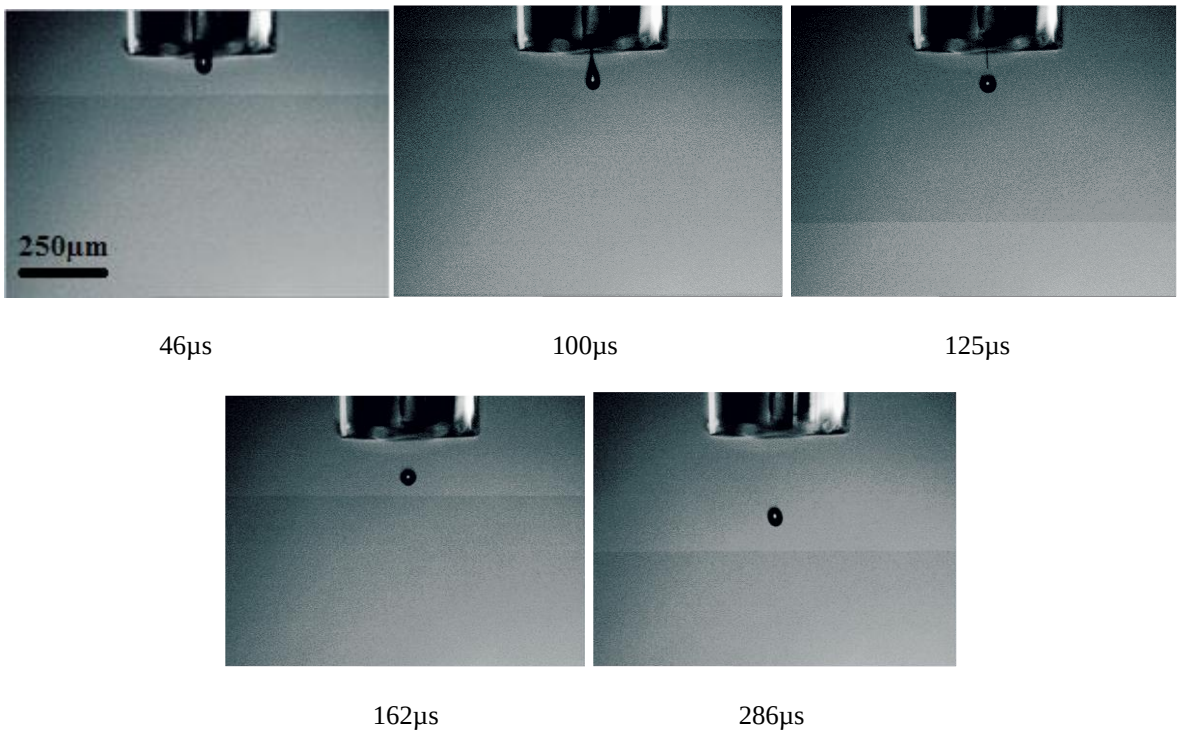

Figure 5.1: Stroboscopic images of droplets produced by inkjet printing. These images show a stable droplet formation and Newtonian fluid behavior during the printing of insulating polymer based inks (here SU-8 (1:1) diluted in DCB).

In addition to good printability, the homogeneity of the obtained polymer layer may have an influence on the performance of the final device. In the next section we compare the dielectric performance of the inkjet-printed SU-8 polymer and the polymer from Altana.

5.3 Breakdown voltage of the inkjet-printed polymers

Characterizing the breakdown voltage of dielectric polymers is necessary to prevent unwanted leakage currents and make sure no insulator failure happens during the measurements. To investigate the breakdown voltage of the inkjet-printed polymers, samples with crossing silver based lines separated with the insulating polymer were printed (figure 5.2). Impedance measurements were conducted to monitor the resistance of the insulating layer while an applied voltage is being increased over time.

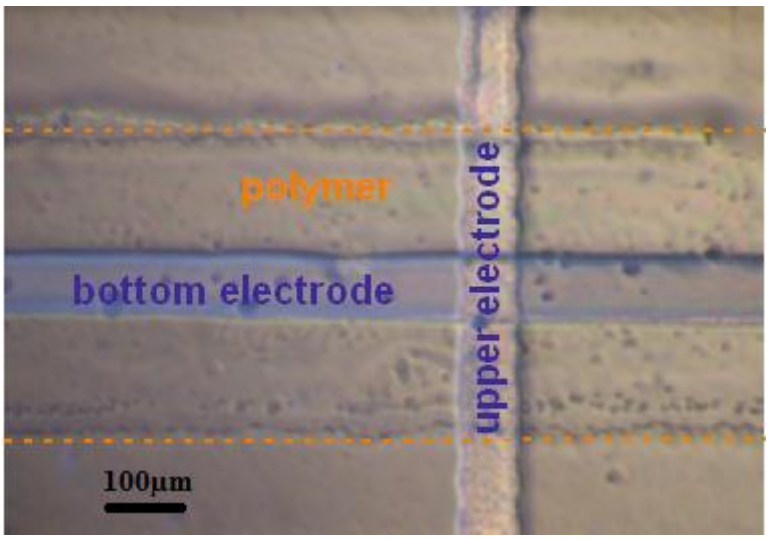

Figure 5.2: Silver electrodes crossing separated with an inkjet-printed polymer for breakdown voltage tests. After printing and sintering the bottom electrode, it is covered by a printed polymer track. Then the upper electrode is printed and sintered.

Materials and methods

Silver nanoparticles based tracks were printed on PET substrate and then chemically sintered. The polymer ink is printed on the bottom silver tracks and then cured. Finally the upper silver based tracks were printed and sintered.
As an insulating polymer, we have used SU-8 polymer diluted (1:1) in DCD (1, 2, 4 and 6 printed layers) and the insulating polymer from Altana (1, 2, 3, 4, 5, 6 and 7 printed layers).
The curing of the SU-8 polymer was performed by heating the sample first at 65°C for 5 minutes and then at 95°C for 30 minutes in the convection oven (B180, Nabertherm, Germany). The samples were then exposed to UV radiation for 15 minutes. To complete the polymerization of the SU-8, the samples were heated again at 95°C for 80 minutes.
The curing of the Altana-polymer was performed by exposure to UV radiations for 4 minutes and 40 seconds.
Two-point impedance measurements were carried out using an impedance gain phase analyzer (SI 1260, Solartron Analytical, UK) at a frequency of 1000 Hz and AC amplitude of 300mV. An applied DC voltage was gradually increased from 0 V up to the breakdown voltage.

Results and discussion

The samples prepared using SU-8 polymer showed a poor dielectric behavior. Different samples had different breakdown voltages ranging from about 300mV to 5 V. No reproducible results could be obtained even for samples with six printed polymer layers.

Optical microscopy images revealed that the inkjet-printed SU-8 film was not homogeneous (figure 5.3) probably due to the formation of air bubbles during the printing process. The inhomogeneous film thickness could be the reason for the non-reproducible breakdown voltage measurements.

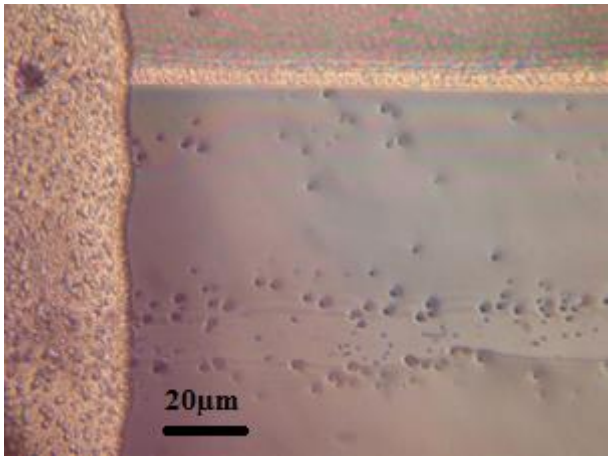

Figure 5.3: Silver electrodes crossing separated with an inkjet-printed polymer on PET substrate (detail of figure 5.2). The inkjet-printed SU-8 film is not homogeneous and may lead to non-reproducible breakdown voltage measurements.

The conventional method for the deposition of SU-8 polymer is spin-coating and is eventually more suitable than inkjet for achieving a homogeneous SU-8 layer.
In contrast to the SU-8 polymer, the insulating polymer from Altana showed a better dielectric performance. Samples with 4 or more printed layers displayed a reproducible (30 measurements per polymer layer thickness) breakdown voltage of 5V (figure 5.4).

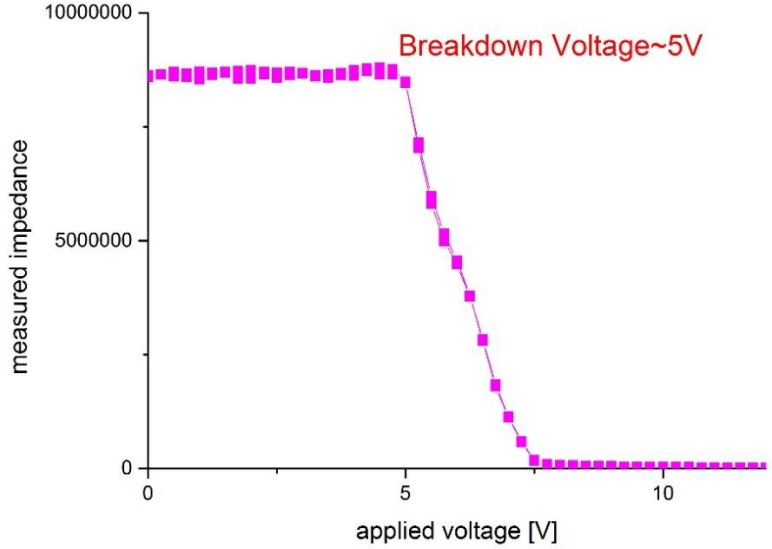

Figure 5.4: Measured impedance of the printed polymer layer versus the applied voltage. A reproducible breakdown voltage of about 5 V could be measured for the inkjet-printed insulating polymer from Altana (here four printed layers).

Since strong electric fields should be avoided during cell assays to prevent cell damage or cell physiology changes [115], the breakdown voltage of 5V of the inkjet-printed polymer can be considered suitable for biochips.

Other research groups also reported a good insulating performance of inkjet-printed polymers. Chung et al. obtained a good dielectric performance by printing two layers of a poly-4-vinylphenol (PVP) solution [114]. However, PVP needs to be annealed at temperatures of at least 200°C and is therefore not suitable for the low-cost polymer substrates such as PET. Dadvand et al. reported on a novel inkjettable spin-on-glass (SOG) based dielectric ink that is cross-linkable at 135°C and shows good dielectric properties. The leakage current of the SOG layer remained at picoampere range even at voltages up to 60V [113]. This SOG dielectric has proven to be efficient for the fabrication of organic thin film transistors and is a promising candidate for low-cost and printed electronics. However, this ink was in-house mixed and is not yet commercially available. It should also be noted that the SOG ink was prepared using an alcohol mixture and may therefore be prone to nozzle-drying and clogging problems. Moreover, experiments conducted at our institute revealed that SOG materials suffer from a poor adhesion to metals (Dr. H. Grothe, private communication, March 15, 2016) and are eventually not suitable as a coating layer for silver electrodes.

5.4 Biocompatibility of the printed tracks

Although the introduction of cheaper metals such as silver or copper in the fabrication of biochips helps reducing the fabrication costs, the major drawback of these metals is that they are not biocompatible. To avoid direct contact with living cells, the silver based electrodes can be covered with a biocompatible polymer. Biocompatibility tests according to ISO 10993 revealed that the inkjet-printed polymer on the silver electrodes conceals the toxic effect of silver and provides a biocompatible environment for the cells.

5.5 Summary

Successful inkjet printing of an SU-8 based solution and a polymer based ink from Altana could be achieved. A Newtonian fluid behavior and stable droplet formation was observed for prolonged printing durations.
The inkjet-printed SU-8 polymer layer suffered from an inhomogeneous thickness and a poor dielectric performance. The polymer ink from Altana showed a remarkably better dielectric performance. For four printed layers we could measure a reproducible breakdown voltage of 5V.
Both dielectric polymers could be cured using a UV-treatment that is suitable for the low-cost PET substrate.
It is possible to integrate cheaper metals such as silver in the fabrication of biochips although they are not biocompatible. Printing a polymer layer to cover the silver electrodes eliminates direct contact between the toxic metal and the cells and therefore provides a biocompatible environment for the living cells.

Chapter 6

Printed biochips with SWCNT based sensors for in-vitro cell monitoring

6.1 Printed biochips for cell monitoring applications

The interfacing of electronic devices and sensors with biomaterials has been a subject of extensive research for decades because of its significant impact on environmental sensing, biological monitoring and medical diagnostics. This has led to the development of high-performance devices that, however, typically suffer from two major drawbacks. These are the expensive production costs and the rigid substrates that limit the application possibilities of the bioelectronics. The emergence of printed electronics and organic bioelectronics materials such as carbon nanotubes changed the direction of future bioelectronics and triggered the development of a new category of flexible, light-weight, ergonomic and wearable devices. In contrast to the planar, rigid and brittle classical biochips, flexible biochips not only have the potential for low-cost fabrication but are also more suitable for the soft and dynamic nature of the human body and biological tissues in general. The fact that flexible biochips allow intimate and conformal integration with biological tissues without causing unwanted irritation or discomfort opens new opportunities for diagnostics and the design of novel bioelectronic devices. Several research groups have been working on flexible and disposable bioelectronics such as chips for protein detection [116], tattoo-like sensors for epidermal pH [19], glucose [18] and lactate [117] monitoring as well as biochips for wireless bacteria detection in tooth enamel [22] and an all-organic sensor for pulse oximetry [23]. Dagdeviren et al. have also reported on flexible chips for piezoelectric energy harvesting and storage from motions of the heart, lung and diaphragm that offer sufficient power outputs for operation of pace-makers, with and without battery assist [118]. However, there have been to date no reports on printed biochips for cell monitoring applications.

Our contribution to the field of printed bioelectronics consists in the fabrication of all-inkjet-printed biochips with novel SWCNT sensors for in-vitro cell monitoring applications that present a potential low-cost alternative to their classical rigid counterparts. To achieve reliable cell measurements, the printed biochips have to fulfill several requirements. They need to have a good conductivity, a good adherence to the substrate and a suitable shelf life for cell measurements. They also have to be flexible to avoid device failure and also biocompatible to allow cell growth for the micro physiological investigations.

In the previous chapters we discussed the fabrication of inkjet-printed silver, CNT and polymer based tracks on flexible substrates as well as their electrical and mechanical performance. Here we show that by using a combination of these materials successful fabrication of disposable biochips can be achieved. The biochips contain two inkjet-printed MWCNT/CNP based interdigitated electrodes (IDES) with 10 printed layers. These IDES structures are biocompatible and can be used as cell electrodes. Eight contact pads and tracks leading from the contact pads to the IDES electrodes are then printed using a silver based ink. After that, the silver contacts should be sintered using a sintering technique that is suitable for the used substrate to achieve a low resistivity. At this point, a sensitive SWCNT based layer can be deposited on the IDES electrodes followed by an acidic treatment to remove the detergent and enhance the densification of the CNT network. Finally, an insulating polymer can be deposited on the silver tracks leading to the cell electrodes. A schematic presentation of the fabrication steps of the printed biochips can be viewed in figure 6.1.

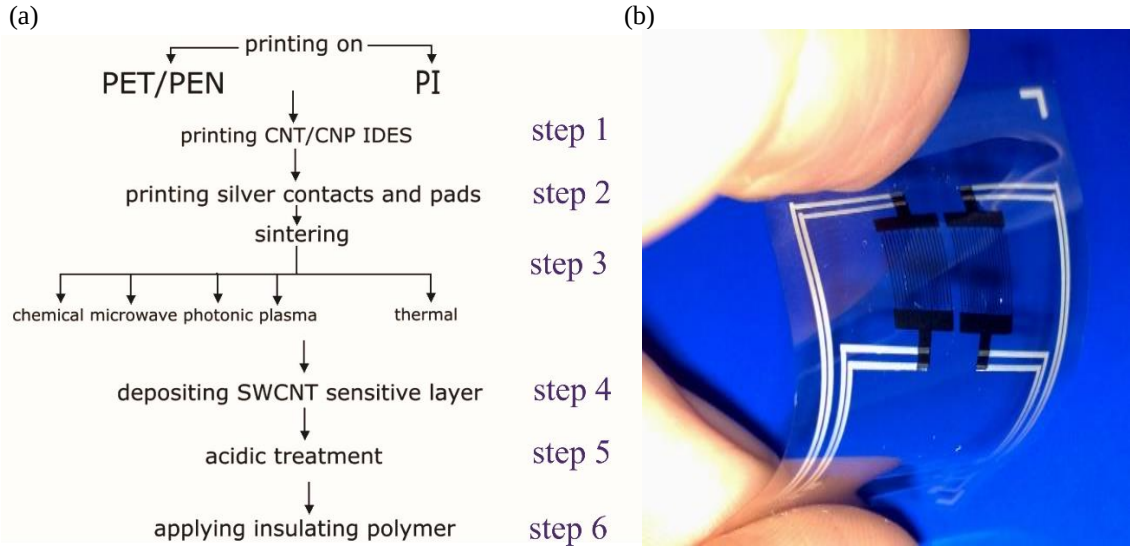

Figure 6.1: Schematic presentation of fabrication steps of the printed biochips (a) Inkjet-printed biochip (steps 1 to 3) (b).

The inkjet-printed biochips on polymer substrates are featured with a good conductivity, bendability, good adhesion in aqueous media as well as a suitable shelf life for cell measurements and biocompatibility. Therefore, they fulfill the requirements needed for in-vitro cell investigations.

In the following sections we investigate the suitability of the printed biochips with novel SWCNT based sensors for cell monitoring applications. For this purpose we test the performance of the on-chip SWCNT sensors as pH and oxygen sensors using impedimetric measurements.

6.2 SWCNT based pH sensors

The classical and most commonly used method for pH measurements is by using a combination of a reference electrode such as an Ag/AgCl electrode and a glass membrane electrode. This method is low-cost, reliable, easy, suitable for fast measurements and has a wide working range. However, the pH-electrode is relatively large and not suitable for small volume samples or integration into sensor chips [119]. These disadvantages make the pH-electrode an ill-suited candidate for our biomedical applications. Extensive research has led to successful design and fabrication of sensors that deliver accurate measurements for small volume samples and have the potential for biological and medical diagnostics.
Among the most investigated pH sensors for biomedical applications are the optical chemical sensors [119, 120] and ion-selective field effect transistors (ISFETs) [121, 122].
The optical chemical sensors can be miniaturized down to submicrometer dimensions, do not require a reference electrode and are stable against electrical and electromagnetic interferences [119]. Wolf et al. have demonstrated the suitability of on-chip optical chemical sensors for the monitoring of living cells and tissues [10]. The limitations of these sensors are the possible bleaching of the dye that may limit the long term stability of the sensor, temperature dependence of the measurements [119], the need for an optical read-out unit and the eventually high material costs.
ISFETs are interesting for sensing applications because their robustness and fast pH response [121]. Maiolo et al. have recently reported on a flexible pH-ISFET with a near-ideal Nernstian response [122]. However, the main disadvantage of ISFETs is the need for a reference electrode that may present a limitation for both the size of the device and its applications.

Owing to their unique electrical, optical, mechanical and structural properties, carbon nanotubes have been the object of extensive research for biological and chemical sensing applications. We report on novel on-chip impedimetric SWCNT based pH-sensors that are easy to integrate in a biochip and do not require a reference electrode.

Materials and methods

A homogeneous aqueous solution of SWCNTs (Southwest Nanotechnologies, semiconducting content >90%) with a concentration of 200µg/ml was prepared. For this purpose 20 mg of carboxymethyl cellulose (CMC) was added to 5 ml distilled water and the solution was stirred overnight (≥12h) at room temperature to dissolve the CMC. 1mg of SWCNTs is then added to the water/CMC mixture followed by sonication for 90 minutes in a bath-sonicator (fabrication steps of the SWCNT solution: courtesy of Dr. Alaa Abdallah, institute for nanoelectronics, TUM).
Using the drop-casting method, a homogeneous SWCNT layer is deposited on the IDES electrodes of the chip. An acidic treatment is then performed to remove the CMC and enhance the densification of the SWCNT network. Therefore, the chips printed on PI substrate are first heated at 250°C for 60 minutes to enhance the adherence of the sensitive layer to the substrate. The chip is then submerged in citric acid for 60 minutes followed by rinsing with distilled water. Finally, the sensors are dried using a nitrogen gun.
For the pH measurements, solutions with different pH values (4, 5, 6, 7, 7.5, 8, 8.5 and 9) were prepared. A standard phosphate buffered saline (PBS) solution with pH value 7.1 was used as the base. The acidic solutions were obtained by adding hydrogen chloride (HCl) and the alkaline solutions were obtained by adding sodium hydroxide (NaOH). The measurements involving only pH 4, pH 7 and pH 9 were performed using standard test solutions purchased from Merck (Merck chemicals GmbH, Germany). For the conductivity experiments, the standard pH solutions were modified using sodium chloride (NaCl) without affecting their pH value (the pH value was controlled with a glass pH electrode) and their conductivity was measured using a conductometer (CG 853, Schott instruments, Germany). For each pH value three solutions with different conductivities were prepared as can be seen in table 6.1:

Table 6.1: Based on the standard pH test solutions, solutions with different conductivities were prepared.

pH value	Conductivity [mS/cm]		
pH 4	6.07	8.55	11.28
pH 7	5.82	7.94	10.67
pH 9	5.65	8.2	10.46

Impedance spectroscopy measurements (EIS) using an impedance gain phase analyzer (SI 1260, Solartron Instruments, Great Britain) were performed with an AC amplitude of 300 mV.
For the inkjet-printing of SWCNTs, the SWCNT solution was centrifuged for 30 minutes at 4000 rpm and then printed using a nozzle with a diameter of 30µm at a printing speed of 30mm/s. The printing voltage was set to 95V and pulse duration to 22µs.

Results and discussion

Stabilization time

After depositing the test solution (in this case a pH4 solution) on to the sensing layer, impedance measurements performed after exposure durations from 1 to 30 minutes revealed that only a slight change of the impedance occurs after 5 minutes and the sensor response stabilizes after about 10 to 15 minutes (figure 6.2).

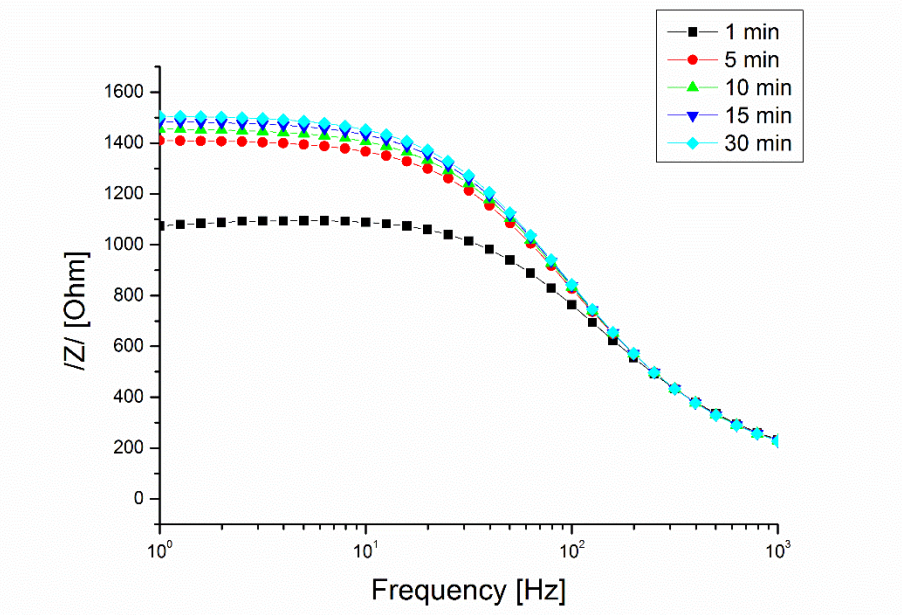

Figure 6.2: Impedance spectra of the CNT sensors after 1 to 30 min exposure time to the analyte (the test solution with pH 4 was used here) [123].

This conditioning period is common to all pH sensors. It does not affect the response time to changes of the pH value. Impedance measurements over time have shown that impedance change from pH4 to pH7 takes about a few minutes.

pH sensitivity

The semiconducting SWCNT network displayed a sensitive response to a wide range of pH values. As shown in figure 6.3, the higher the pH value of the test solution is the higher is the impedance of the SWCNT layer at low frequencies.

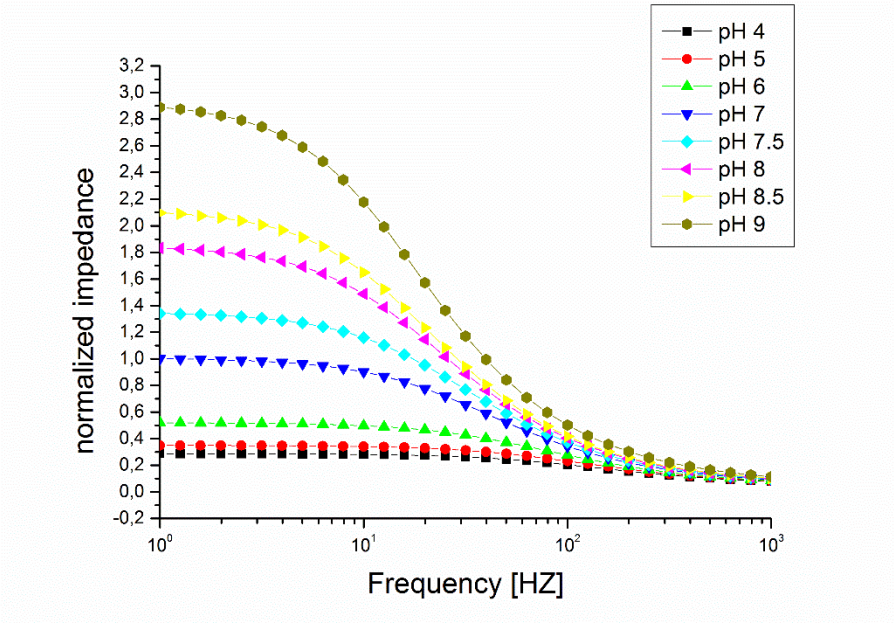

Figure 6.3: Normalized impedance spectra of drop-casted SWCNT sensors depending on the pH value of the test solutions (solutions with pH 4, pH 6, pH 7, pH 7.5, pH 8, pH 8.5 and pH 9) [123].

The pH-dependent charge transport properties of SWCNTs have been examined by several research groups [124, 125, 126] while the observed conductivity changes were attributed to the effect of OH- and H3O+ species present in the test solutions.
In acidic conditions, the SWCNTs are exposed to positive charges leading to protonation and resistivity decrease of the tubes. Opposite effects take place in alkaline conditions where the negative charges result in deprotonation and resistivity increase of the SWCNTs. This behavior is expected due to the fact that SWCNTs are a p-type semiconductor where holes are the charge carriers [127].
Most SWCNT based pH-sensors that have been reported are either ion sensitive field effect transistors (ISFETs) [124, 128] or potentiometric sensors that require a reference electrode [125, 126]. Our impedimetric sensors, however, do not require neither a gate electrode nor a reference electrode. This makes them simpler to fabricate, smaller in size and allows for easier measurements.
The SWCNT based sensors display a good pH sensitivity that is about twice as high compared with sensors based on Poly(3-hexylthiophen-2,5-diyl) (P3HT) polymer as can be seen in figure 6.4 [123].

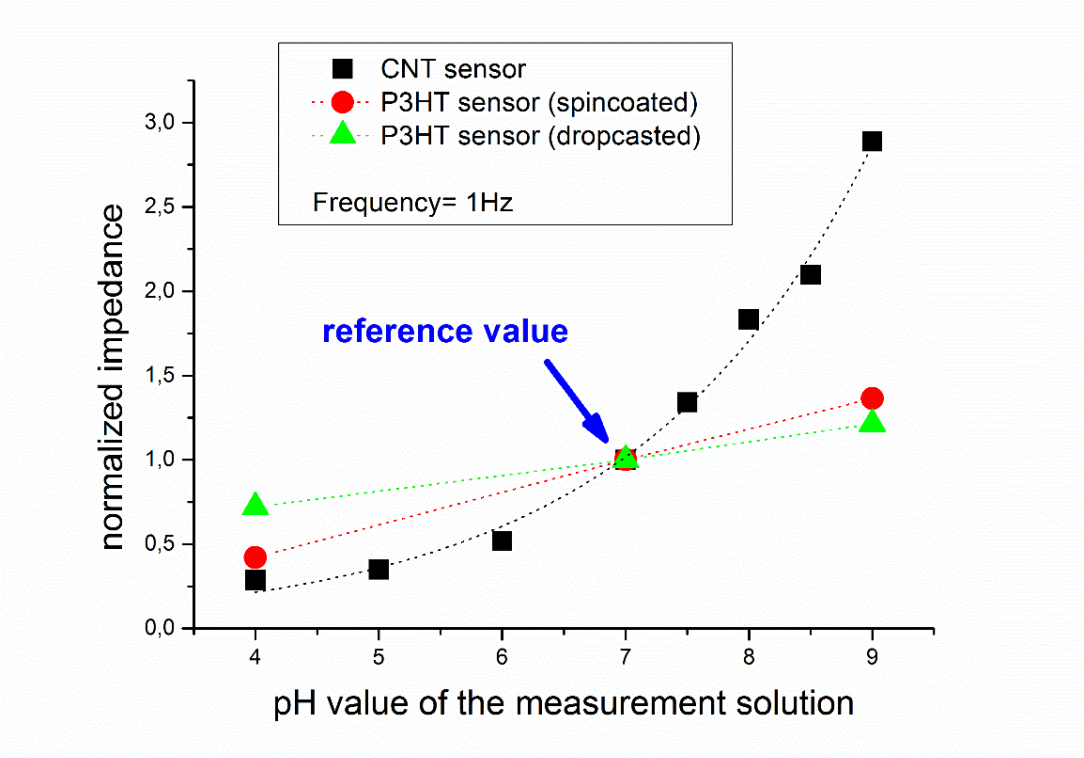

Figure 6.4: Comparison of the normalized impedance values of the pH-sensitivity for CNT sensors and drop-casted and spin-coated P3HT sensors at 1 Hz [123].

Although the sensor response that we have obtained is not linear, our sensors show a higher sensitivity compared to other SWCNT sensors reported in the literature. The reason for the high sensitivity could be that we have used sorted (> 90% semiconducting) CNTs.
Both Keampgen et al. and Gou et al. observed a desirable linear Nernstian response over a wide pH range by coating the CNTs with a conducting polymer such as poly(1-aminoanthracene) (PAA) or Polyaniline (Pani) [125, 127]. However, this step is not necessary for our applications since we are only interested in detecting pH changes over time without the need for the actual pH value (see introduction). We have also conducted control experiments to further evaluate the performance of our sensors and rule out unwanted effects such as sensitivity to conductivity changes of the test solution.

Influence of the conductivity of the test solution

Measurements performed with pH solutions with different conductivities show a negligible sensitivity to changes in the conductivity of the test medium (figure 6.5).

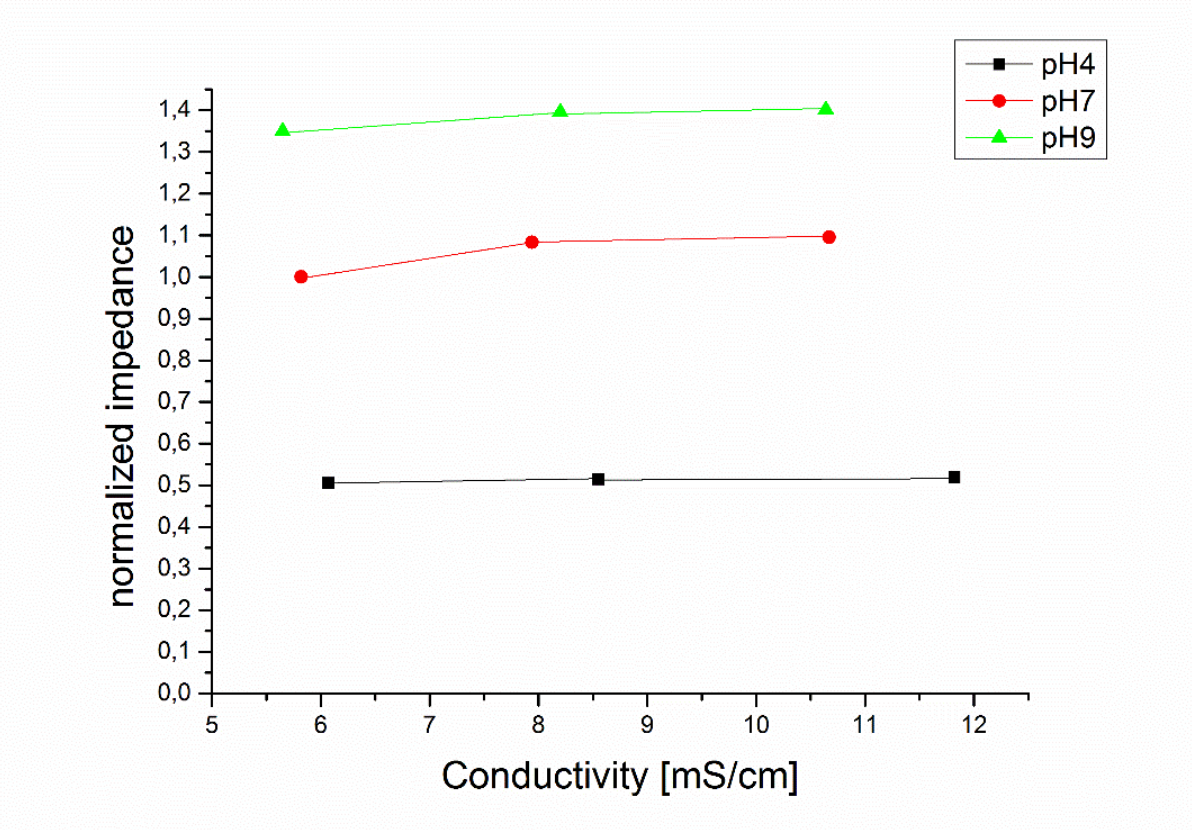

Figure 6.5: Normalized impedance of the drop-casted CNT sensors depending on the conductivity of the test solutions [123].

This result demonstrates that for solutions with an approximately constant conductivity as is the case for blood and cell culture medium, pH-shifts can be accurately detected. Gou et al. have also demonstrated that SWCNT pH-sensor show no response to ions that may be present in cell culture solutions such as Ca^+ and Na^+ ions if the ions concentration is in the range of 10^{-12} to 10^{-6} M, comparable to the range of concentrations of H_3O^+ ions tested [127]. Kaempgen et al. have also demonstrated the selectivity of the SWCNT pH-sensors for H_3O^+ ions against K^+ and Na^+ ions [125]. This validates the suitability of the SWCNT pH-sensors for cell monitoring and biomedical applications.

Influence of the MWCNT/CNP IDES electrodes

Since the printed IDES electrodes of the biochip are also made of carbon nanotubes, it is important to make sure these MWCNT/CNP electrodes do not alter the response of the sensor. The impedimetric measurements revealed no pH sensitivity of the inkjet-printed MWCNT/CNP IDES electrodes and the measured curves for different pH values overlapped as can be seen in figure 6.6.

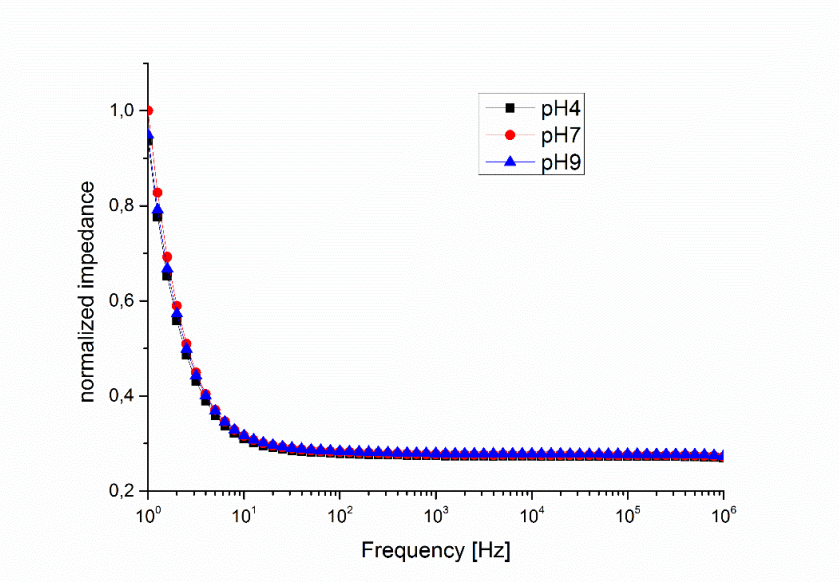

Figure 6.6: Normalized impedance spectra of inkjet-printed MWCNT/CNP IDES electrodes exposed to solutions with different pH values (4, 7 and 9). The almost overlapping curves show that inkjet-printed MWCNT/CNP IDES electrodes are not pH sensitive.

Therefore the uncoated IDES electrodes (see figure 6.1, chapter 6.1) do not interfere with the pH response of the sensor and can be used to monitor the conductivity changes of the sensitive SWCNT layer. The reason behind the poor sensitivity of these electrodes could be the metallic behavior of MWCNTs [100] that may reduce conductivity changes upon exposure to charged species.

pH sensitivity of inkjet-printed SWCNTs

Instead of printing a non-sensitive MWCNT/CNP IDES and then depositing the sensitive SWCNT layer, we tried to directly print SWCNT IDES electrodes. We achieved successful inkjet-deposition of SWCNT IDES electrodes. Although these electrodes are pH-sensitive at low frequencies, their sensitivity is rather low compared with the drop-casted sensors (figure 6.7).

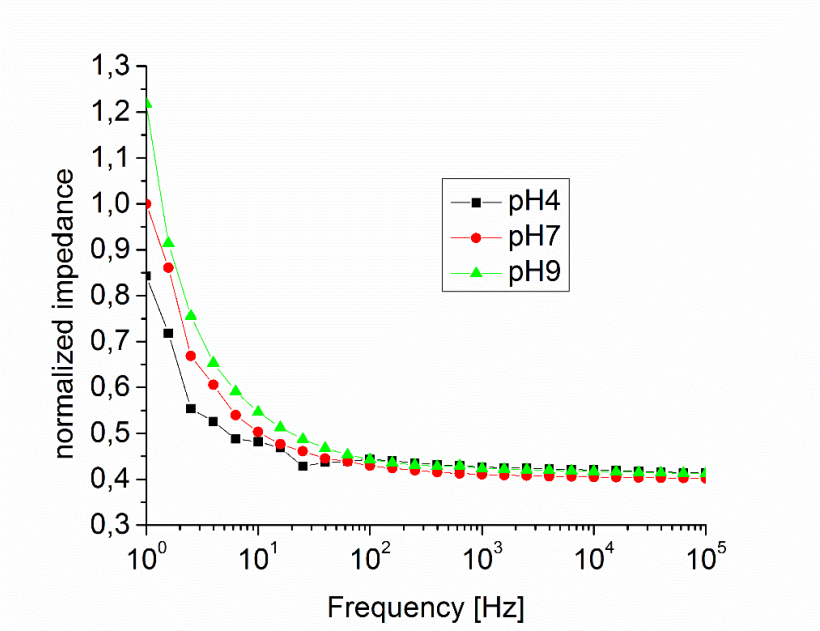

Figure 6.7: Normalized impedance spectra of an inkjet-printed SWCNT IDES at different pH values. The pH-sensitivity at low frequencies is not as pronounced as in the drop-casted SWCNT layer (figure 6.3).

The reasons behind the lower sensitivity of the printed SWCNT IDES in comparison with the drop-casted SWCNT layer could be the higher resistivity of the inkjet-printed electrodes even with 20 printed layers or the lower surface area of the sensor.
The house-prepared SWCNT solution had a significantly lower concentration (0.05 wt. %) in comparison with the ink delivered from Future Carbon (3 wt. %) because it is rather difficult to obtain homogeneous CNT dispersions with high concentrations and no sedimentation or agglomerations that may cause nozzle clogging.
We have also tried depositing the SWCNT layer on the MWCNT/CNP electrodes via inkjet printing. The inkjet-printed structures were successfully tested for pH-sensing. The inkjet-printed sensors, however, were not as sensitive as the drop-casted sensors eventually due to lower SWCNT concentration caused by the centrifugation of the inkjet ink.
These results demonstrate the potential for all-inkjet-printed biochips where the deposition of the sensor material can also take place during the printing process. However, drop-casting remains an easy and fast option that delivers good results.

Memory effect

To evaluate the reproducibility of the measurements and the ability of our sensors to detect pH changes for both increasing and decreasing pH-values, measurements with increasing pH value were first performed (pH 4 then pH 7 and then pH 9) and the measurement with pH 7 was then repeated. Figure 6.8 shows that the impedance values were higher during the second measurement (pH 7 measurements after 10 and 20 minutes overlapped).

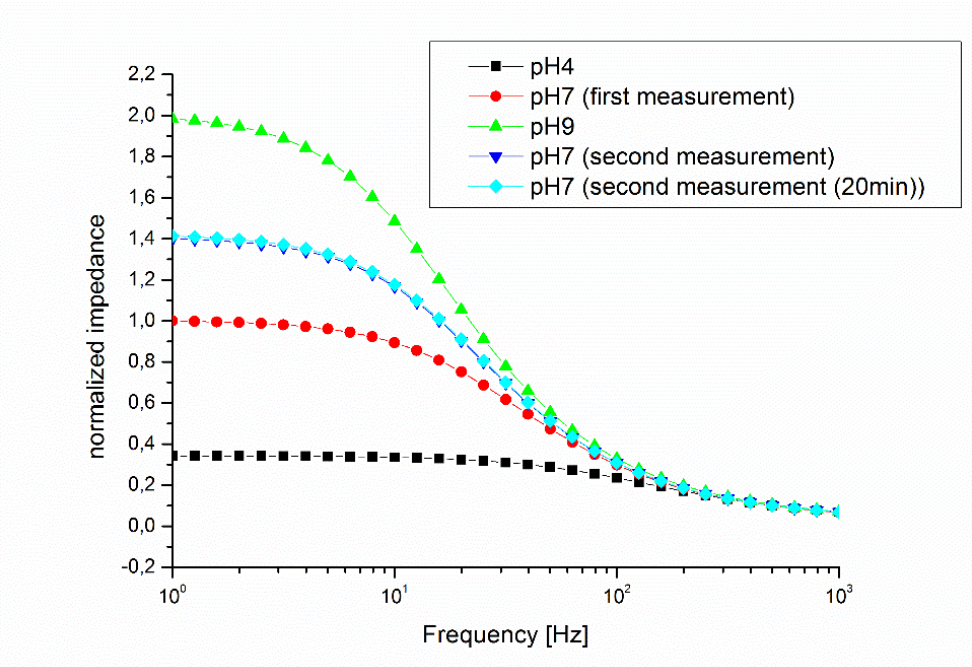

Figure 6.8: Normalized impedance spectra of SWCNT sensors at different pH values. Repeating the pH 7 measurement after a pH 4, pH 7 and pH 9 measurement leads to higher impedance values in comparison with the first pH 7 measurement.

Another pH 7 measurement performed after 20 minutes shows that the impedance values stay constant and do not drift towards the initial values. The memory effect could therefore be caused by irreversible reactions that take place at very high or low pH values. The exposure of SWCNT pH-sensors to extreme pH values of 1 and 13 has been proven to lead to signal drift and sensor damage [125]. However, for biomedical applications the sensors will only be exposed to physiologically relevant and rather mild pH ranges (around pH 7) that are not likely to cause sensor damage.

Performance and stability of the sensors

This work presents only a proof-of-concept study, therefore, no actual reproducibility or aging experiments were performed. However, we did notice some aspects that are relevant for this topic. The impedance values for a given pH value differ from one sensor to another eventually due to varying density of the CNT network since it is rather difficult to deposit the exact number of CNTs for each sensor. This, however, does not present a drawback in our case because we are only interested in detecting pH-changes over time while the impedance value itself is rather irrelevant.
We obtained our best results using freshly prepared pH solutions and noticed that CNTs eventually oxidize over time at ambient atmosphere leading to a poor solubility and decreased sensitivity although such effects may take several months to get noticeable. SWCNT based pH-sensors have been reported in the literature to have a shelf life up to 12 months without any measurable loss in performance [125]. Although some research groups presented SWCNT pH-sensors with the potential for in vivo applications [127, 128] no long term stability in cell culture media has been yet performed. Since our sensors are meant to be disposable, a prolonged shelf life is not required.
We also observed a more pronounced sensing ability for sorted SWCNTs (>90% semiconducting) then for non-sorted CNTs (~70% semiconducting) which is understandable considering that the sensing effect is based on the p-type semiconducting behavior of the SWCNTs.
In addition to the pH sensors, oxygen sensors also belong to the most commonly used sensors for cell monitoring applications. After investigating the pH sensitivity of the SWCNT sensors, in the next section we will discuss their suitability for dissolved oxygen sensing applications.

6.3 SWCNT based oxygen sensors

CNTs have been successfully implemented by several research groups for gas sensing applications and could be used for a variety of applications ranging from sensing of emissions of fossil fuel burning [129] to sensor arrays capable of selective detection when exposed to gas mixtures [130]. Although CNT based sensors for oxygen gas have been demonstrated [131, 132], no investigations have been made towards CNT sensors for dissolved oxygen (pO_2) sensing applications. Here we demonstrate the potential of the impedimetric SWCNT sensors for the detection of pO_2 concentration changes in aqueous media.

Materials and methods

A standard PBS (phosphate buffered saline) solution was bubbled with nitrogen gas for 45 minutes at room temperature in a glove box to reduce the oxygen concentration and then pipetted on to the SWCNT sensor. Electrochemical impedance measurements were performed using an impedance gain phase analyzer (SI 1260, Solartron Instruments, Great Britain) with an AC amplitude of 300 mV at a frequency of 1 Hz. The dissolved oxygen concentration in the PBS solution was monitored by an external sensor (Fibox, PreSens Precision sensing GmbH, Germany).

Results and discussion

When the solution with reduced oxygen concentration is pipetted on to the SWCNT sensor, oxygen from the ambient atmosphere diffuses back into the solution leading to a higher oxygen concentration. The impedance of the sensitive SWCNT layer also increases over time and when the oxygen concentration reaches saturation and stabilizes, the impedance of the sensor also stabilizes (figure 6.9).

(a)

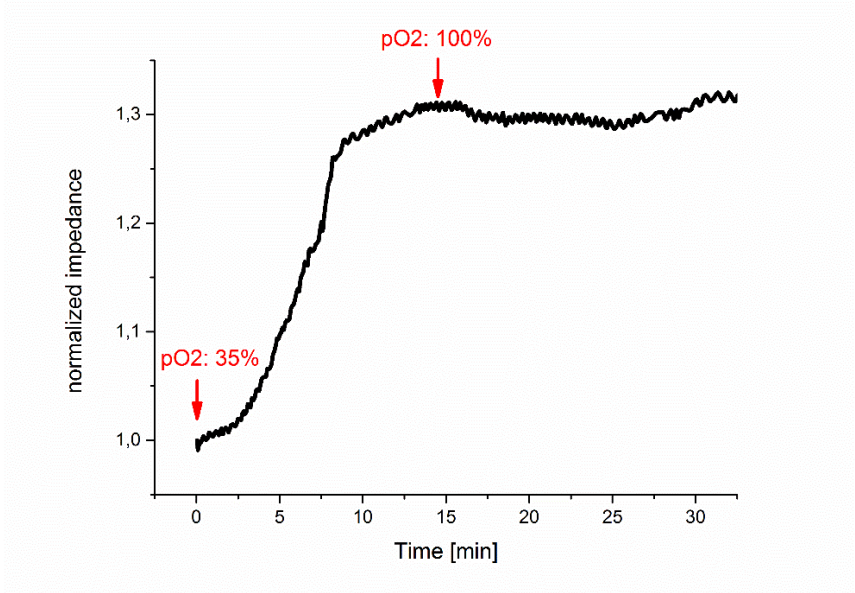

(b)

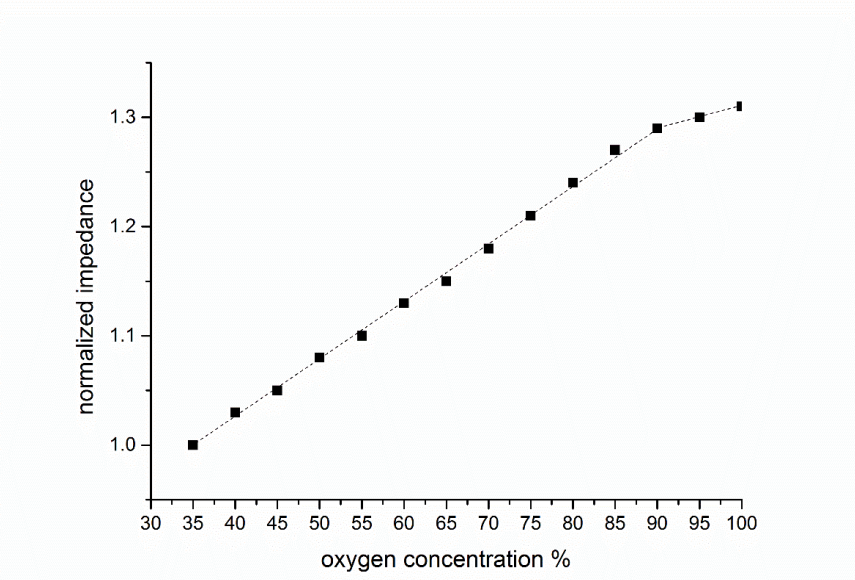

Figure 6.9: Normalized impedance measurement over time during oxygen diffusion from the environment in the PBS. Starting at 35% the dissolved oxygen concentration increases with time and the impedance of the sensitive layer also increases. When the oxygen concentration reaches saturation and stabilizes the impedance of the sensitive layer also stabilizes (a), Normalized impedance of the SWCNT sensor versus the dissolved oxygen concentration. The impedance change caused by oxygen diffusion shows that SWCNTs are suitable for oxygen sensors (b).

These results are coherent with the findings of Kauffman et al. who also observed a conductivity decrease of SWCNT based sensors when exposed to oxygen gas. They attributed the observed conductivity decrease to a possible de-doping of the p-semiconducting SWCNTs caused by the oxygen molecules [131]. Here again, our sensors are not meant to measure the actual oxygen concentration in the test solution but should detect oxygen concentration changes over time. Proving the sensitivity of SWCNTs to oxygen dissolved in aqueous media opens new application possibilities especially in the biomedical field where monitoring cell and tissue oxygenation can be helpful for diagnostics.
Our results demonstrate the potential of the SWCNT sensors for both pH and oxygen sensing applications.

However, being able to distinguish between the two effects can be interesting for some applications where only the pH or oxygen response is required. For example, information about the blood or tissue oxygenation is important for patients suffering from hypoxia with hypovolemia that causes reduction in the transport of O_2 and CO_2 molecules, however, the pH-response in this case is not relevant. Therefore we have tested the influence of a nafion/collodion membrane on the performance of the SWCNT sensors.

6.4 Influence of a nafion/collodion membrane

A nafion and collodion mixture based membrane that is permeable to gases and positive ions was first investigated by Yamauchi et al. [133]. The nafion/collodion membrane is especially attractive for biosensing applications because of its biocompatibility. This membrane has been successfully implemented as a protecting and oxygen permeable membrane for planar oxygen sensors on biochips [134]. We have investigated the influence of this membrane on the performance of the SWCNT sensors.

Materials and methods

To prepare the nafion/collodion membrane, 1 ml of nafion, 3 ml of collodion and 3 ml of undiluted ethanol were mixed at room temperature. Using a pipette (Eppendorf, Eppendorf Vertrieb Deutschland GmbH, Germany) 10µl of the solution was drop-casted on to the SWCNT sensor and then dried at 80°C for 30 minutes in a convection oven. We used the same equipment and parameters for the pH and oxygen sensitivity experiments as in paragraphs 6.2 and 6.3.

Results and discussion

The electrochemical impedance measurements revealed a significant reduction of the pH-sensitivity (figure 6.10) of the SWCNT sensors whereas no noticeable change in the oxygen sensitivity was observed.

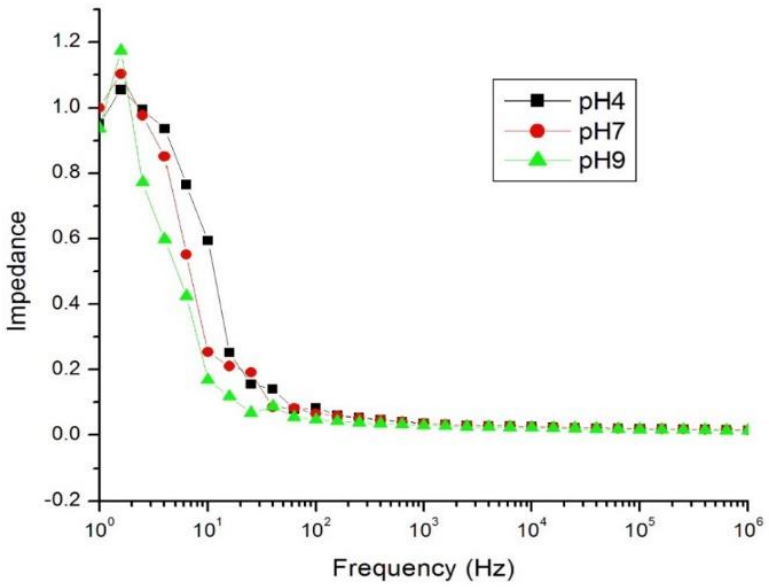

Figure 6.10: Normalized impedance spectra of a SWCNT sensor with a nafion/collodion membrane. The impedance signals obtained with analyte solutions with different pH values (4, 7 and 9) almost overlap at low frequencies. A nafion/collodion membrane strongly reduces the pH-sensitivity of the SWCNT sensor compared to figure 6.3.

This result was expected because the good oxygen permeability of the membrane had been already proven [134].
In spite of its good gas permeability, the nafion/collodion membrane is only selectively permeable to ions and shows a poor permeability to salt that might be improved by increased nafion concentration in the membrane [133].
For applications where only the oxygen response is needed, a nafion/collodion membrane can be used to efficiently suppress the pH-signal.

6.5 Cross-sensitivity to glucose and lactate

The cell metabolism is a rather complex process that does not only affect the pH value and dissolved oxygen concentration in the cell solution. It is also strongly associated with glucose and lactate concentration changes in the microenvironment of the cells.
Metabolite biosensors for glucose and lactate monitoring are being investigated by several research groups [18, 117] because of their importance for diabetic patients and the insight they give on the overall physical performance for athletes, for example.
In our case, however, a sensitivity to glucose or lactate would interfere with the pH and oxygen response of the sensor and is therefore unwanted. For this reason we have tested the cross-sensitivity of the SWCNT sensors to both glucose and lactate.

Materials and methods

We mixed solutions of PBS (phosphate buffered saline) and glucose (D-(+)-Glucose, G7021, Sigma-Aldrich Chemie GmbH, Germany) with different concentrations (10mg/ml, 30mg/ml and 60mg/ml) at room temperature. The solutions were stirred for 5 minutes to dissolve the glucose and obtain homogeneous mixtures.
A similar procedure was performed using lactate (Sodium L-lactate, 98%, L7022, Sigma-Aldrich Chemie GmbH, Germany) to obtain solutions with different lactate concentrations (10mg/ml, 30mg/ml and 60mg/ml).
The solutions were left to react on the sensor for 10 minutes and then electrochemical impedance measurements were performed using an impedance gain phase analyzer (SI 1260, Solartron Instruments, Great Britain) with an AC amplitude of 300 mV.

Results and discussion

The impedance measurements showed that the SWCNT sensors do not have a significant cross sensitivity to glucose and the maximum impedance change at 1 Hz was about 1.9% (figure 6.11.a). Similar results were obtained for the solutions with different lactate concentrations where the maximum impedance change at 1 Hz was only about 3.7% (figure 6.11.b).

(a)

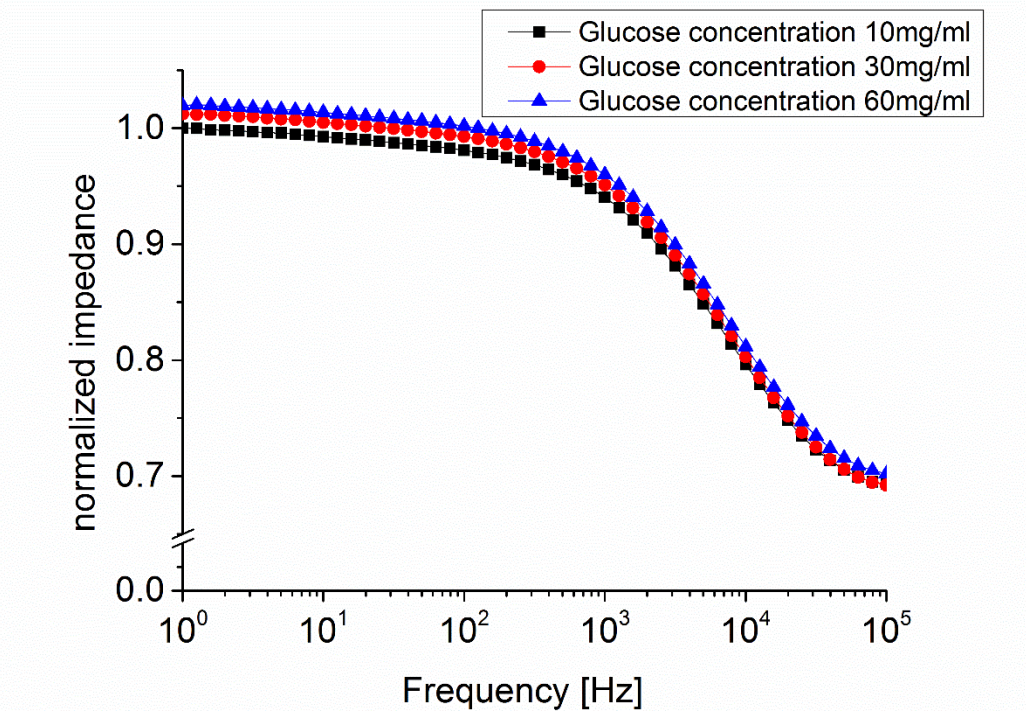

(b)

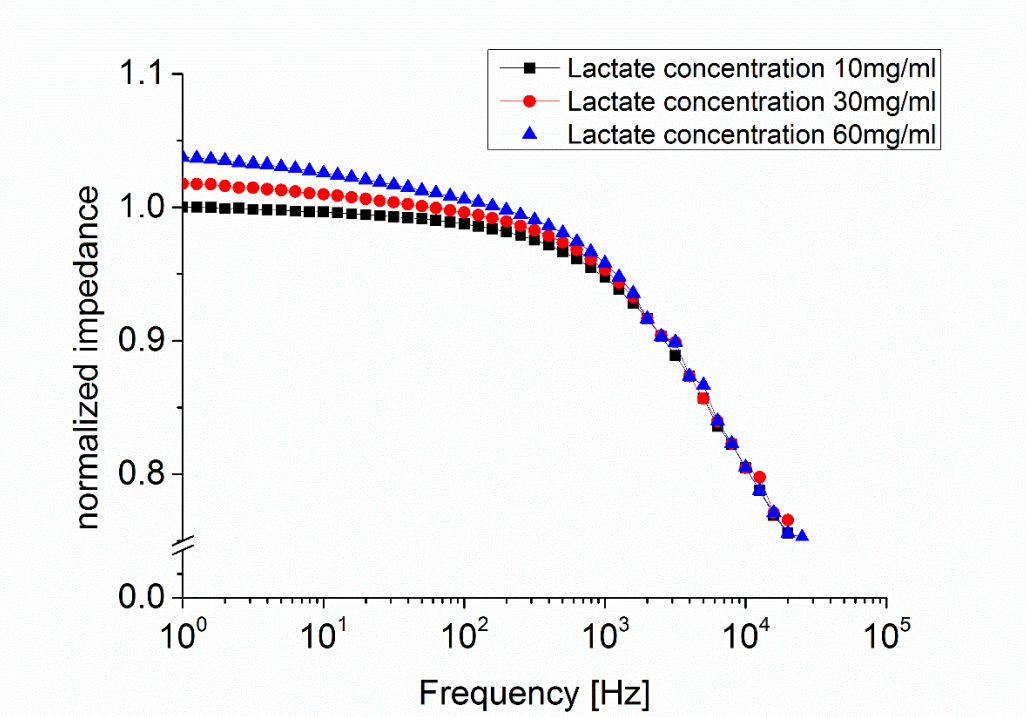

Figure 6.11: Normalized impedance spectra of SWCNT sensors in solutions with different glucose (a) and lactate (b) concentrations. Negligible changes in the impedance reveal no significant cross sensitivity of the SWCNT sensors to both glucose and lactate.

Excluding a cross sensitivity to glucose and lactate is important to ensure no unwanted signals interfere with the sensor response and validate the suitability of the SWCNTs for cell monitoring applications.

6.6 Cell measurements

The cell metabolism usually causes an acidification of the culture medium and a reduction of the dissolved oxygen concentration. The impedance measurements revealed that both the acidification (figure 6.4) and oxygen concentration reduction (figure 6.9) lead to a decrease in the impedance of the sensitive SWCNT layer so even a single SWCNT-sensor can monitor both these vitality signals of living cells together. Also, we have ruled out any cross sensitivity to glucose and lactate. This makes the SWCNT sensors potential candidates for cell monitoring applications.
Since the experiments without cells delivered promising results, we have tested the suitability of the SWCNT sensors for cell monitoring using living yeast cells.

Materials and methods

Using a standard PBS solution, conventional dry yeast and glucose (D-(+)-Glucose, Sigma-Aldrich Chemie GmbH, Germany), we have prepared solutions with different yeast and glucose concentrations. Control measurements were performed using a PBS solution without any additives and a solution with dead yeast cells. The latter solution was obtained by heating a PBS and yeast mixture (8 mg/ml) at about 120°C on a hot plate for 15 minutes while using a thermometer to make sure the solution reached the needed temperature. Solutions with different yeast concentrations (8 mg/ml and 40 mg/ml) and different glucose concentrations (6 mg/ml, 10 mg/ml, 20 mg/ml, 30 mg/ml, 40 mg/ml and 50 mg/ml) were prepared at room temperature.
Electrochemical impedance measurements were performed in an incubator at 37°C using an impedance gain phase analyzer (SI 1260, Solartron Instruments, Great Britain) with an AC amplitude of 300 mV at a frequency of 1Hz.

Results and discussion

The control measurements with the pure PBS solution and the PBS and dead yeast cells solution showed no significant impedance change over time. For the solutions containing living yeast cells, however, an impedance decrease over time was observed (figure 6.12).

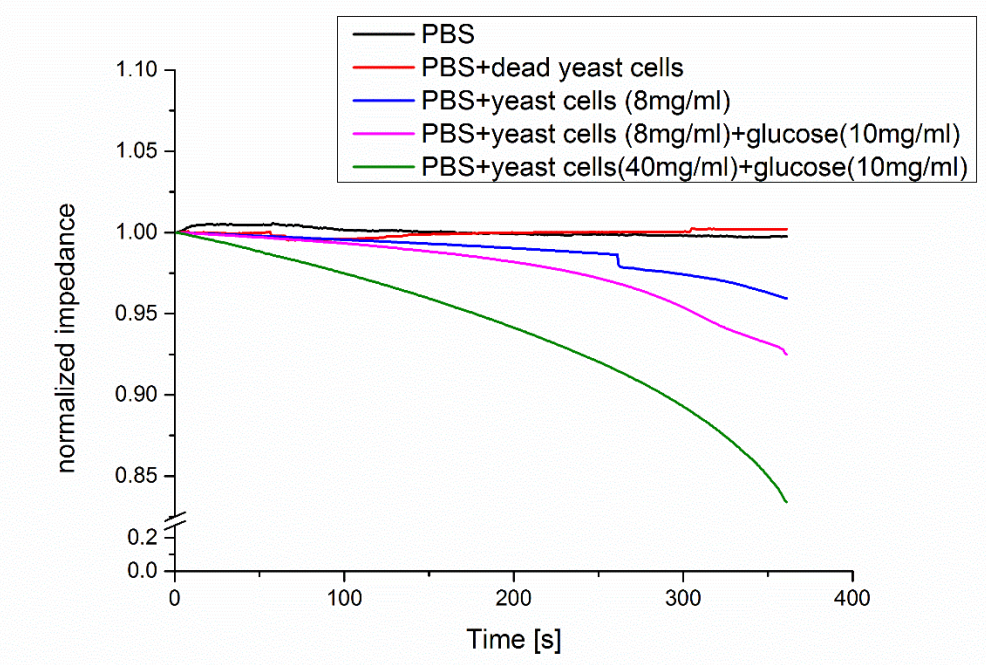

Figure 6.12: Normalized impedance over time of the SWCNT sensor upon exposure to aqueous solutions with different yeast and glucose concentrations. These cell measurements show that the SWCNT biosensors are suitable for detecting cells metabolic activity.

We observed a more pronounced impedance decrease for the solution containing glucose and the solution with higher yeast concentration of up to 20% after 5 minutes. The stronger impedance change is almost certainly associated with stronger cell metabolism resulting in stronger acidification and higher oxygen consumption.
To further investigate the correlation between cells metabolism and impedance change, solutions with different glucose concentrations were left on the sensor for 30 minutes to react. As can be seen in figure 6.13, the higher the glucose concentration in the yeast solutions is the stronger the obtained signals get.

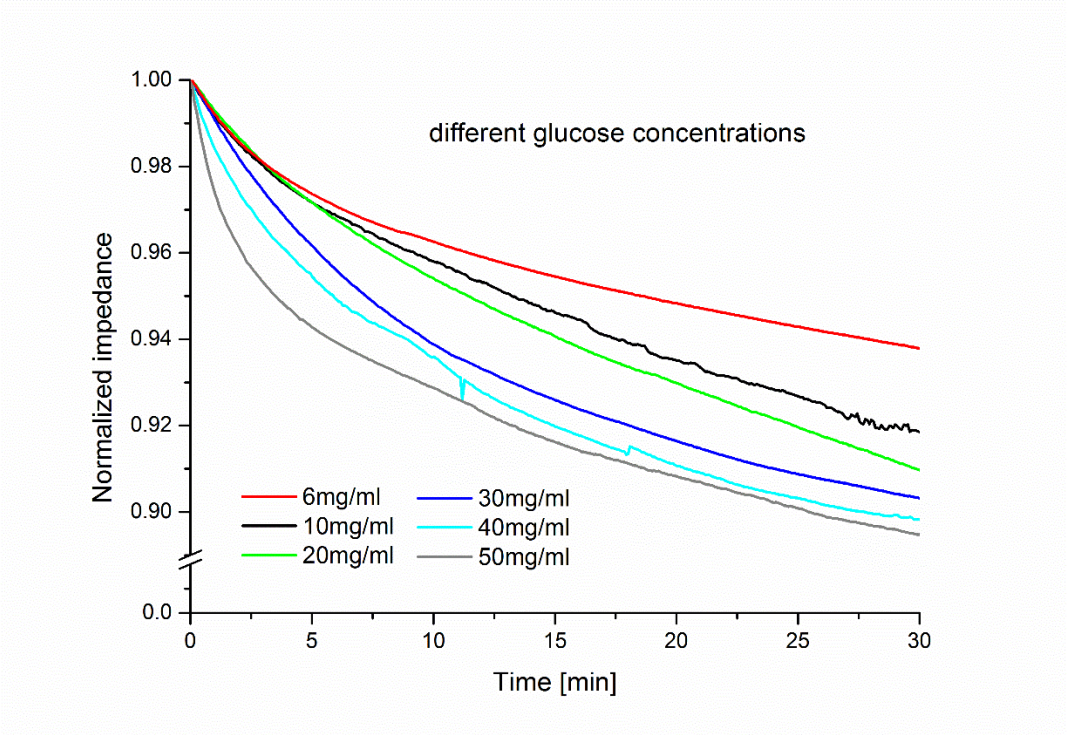

Figure 6.13: Normalized impedance over time of the SWCNT sensor upon exposure to aqueous yeast dispersions with different glucose concentrations. The stronger signal obtained with higher glucose concentrations can be associated with enhanced cell metabolism.

Since a cross sensitivity to glucose has already been excluded (figure 6.11.a), the observed change in signal can be associated with an enhanced cell metabolism. This demonstrates that the SWCNT sensors are suitable for cell monitoring and might be implemented for in-vitro diagnostics.

6.7 Printing of living cells

Inkjet printing is not only interesting for patterned deposition of electrically functional inks but it has also proven to be a powerful tool for controlled deposition of living cells. The inkjet method has therefore opened new possibilities for the biomedical field ranging from the arranging of living cells into tissues with the potential to be implanted in vivo [135] to single cell deposition for a better understanding of heterogeneities of individual cells [136].
This method can also be interesting for the patterned deposition of cells in certain areas of the biochip while avoiding unwanted contamination of other areas.

Previous investigations have been mainly dedicated to the inkjet printing of mammalian [135, 136] or bacterial cells [137]. Since yeast cells can be useful for applications such as investigate synthetic multicellular cell-to-cell communication [137] we have investigated the inkjet deposition of living yeast cells.

Materials and methods

Using a piezoelectric inkjet printer (MD-P-826, Microdrop Technologies, Germany) equipped with a nozzle with an inner diameter of 70µm (ADK-901, Microdrop Technologies, Germany), printing of a yeast suspension was performed with a voltage of 64 V, pulse duration of 18 µs.
The yeast suspension (10mg/ml) was prepared by dissolving dry yeast in a PBS solution at room temperature. Samples with 60 printed drops on filter paper (Whatman GmbH, Dassel Germany) were prepared using different printing frequencies (100, 200, 500 and 1000 Hz) to investigate possible damage of the cells caused by pressure waves at high printing frequencies. The yeast samples were examined using a well-established system for in-vitro diagnostics (IMOLA) [8] where pH and oxygen sensors are used to monitor cell metabolic activities. The cell metabolism results in an acidification of the cells solution and a reduction of the oxygen concentration. These two parameters are monitored over time while the cells are periodically provided with a fresh medium.

Results and discussion

We could deposit yeast cells suspended in a PBS solution using inkjet printing without nozzle clogging (figure 6.14).

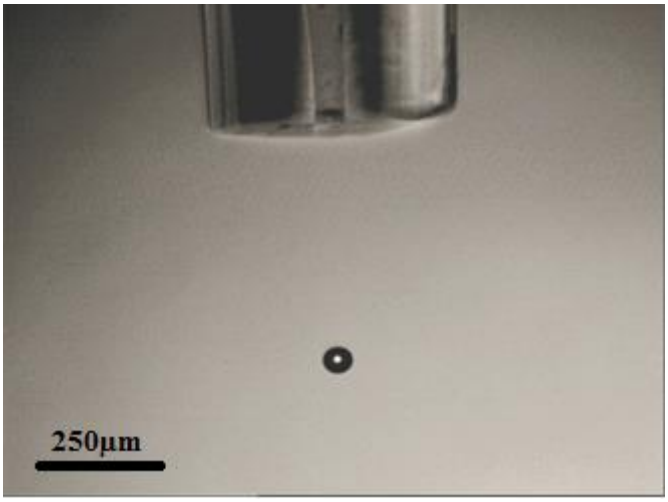

Figure 6.14: Image of droplet generation using a PBS solution with suspended yeast cells. Inkjet printing of yeast cells is possible without nozzle clogging.

The measurements with the IMOLA system revealed that the yeast cells have been safely deposited on the substrate. All samples, including the ones deposited with the highest frequency of 1000Hz delivered a clear metabolic signal (figure 6.15).

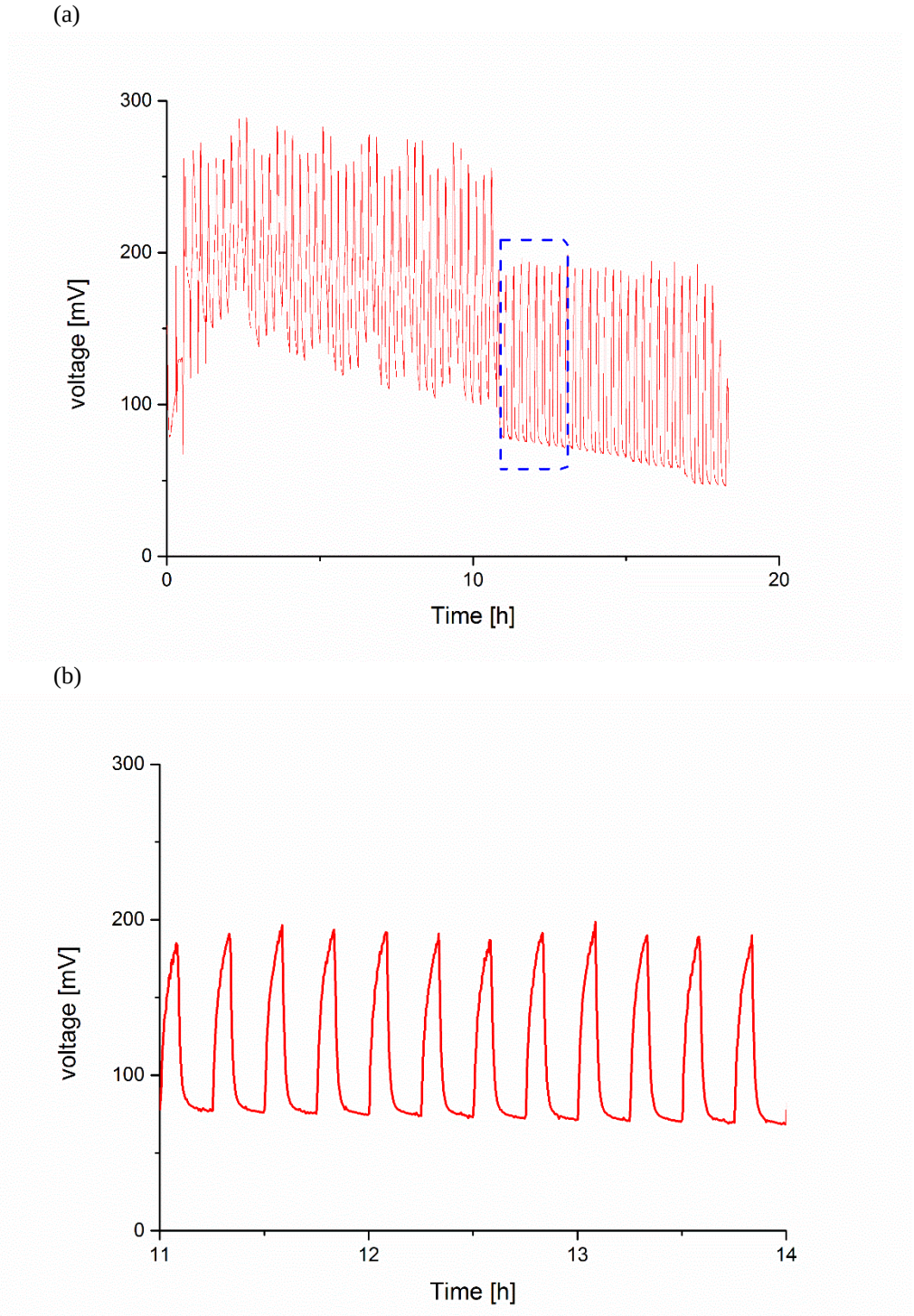

Figure 6.15: Signal voltage over time corresponding to the metabolic activity (pH signal) of inkjet-printed yeast cells (a). Zooming in on the measurement shows the periodic acidification pattern caused by cell metabolism (b).

These results demonstrate that yeast cells can be safely deposited using piezoelectric inkjet printing even when high printing speeds are required. This validates the potential of the inkjet method for the structured patterning of living cells on desired areas of the biochips.

6.8 Conclusions

After the optimization of each material used for the fabrication of inkjet-printed biochips discussed in the previous chapters we could achieve flexible devices with desirable features that have the potential to be a low-cost and disposable alternative to the conventional biochips. We have then investigated a possible application of these biochips for the monitoring of cell metabolic activity using innovative SWCNT sensors. These reference electrode free sensors can easily be integrated into the biochips using drop-casting or inkjet printing and allow for simple measurements where the impedance of the sensitive layer deposited on an IDES electrode is monitored. By monitoring the electronic properties of the SWCNT layer, we have proven its sensitivity for a wide range of pH-values and for oxygen concentration changes in aqueous solutions.

The metabolism of living cells leads to an acidification and oxygen concentration decrease in the solution and in both cases the response of the sensors consisted in an impedance decrease. Therefore, the SWCNT sensors are suitable candidates for cell monitoring that offer the advantage of pH and oxygen sensitivity without the need for two separate sensors for each application. Moreover, due to the impedimetric measurements, no reference electrodes are needed for these applications. It should be noted that these sensors are not meant to deliver an exact value for pH or oxygen concentration but to detect pH and oxygen changes over time. We have also demonstrated that for situations where only the oxygen response is needed, an oxygen permeable nafion/collodion membrane can be used to suppress the pH signal. We have also ruled out the cross sensitivity of the SWCNT sensors to glucose and lactate that are strongly related to cell metabolism.

This preliminary proof-of-concept demonstration indicates the potential of the SWCNT sensor for cell monitoring while challenges such as reproducibility and long term stability still require further investigations. However, results from other research groups have shown that similar sensors can have a shelf life of several months. For example, Gou et al. have achieved a stable pH-sensitivity for over 120 days using SWCNTs that are coated with the conductive polymer poly (1-aminoanthracene) (PAA) and have even demonstrated the potential of their sensors for implantation [127].

Because the measurements without living cells delivered promising results, we have investigated the performance of the SWCNT sensors using living yeast cells. Experiments with yeast cell suspensions confirmed the correlation between enhanced cell metabolism and stronger sensor signal and validated our previous results. Therefore, this proof-of-concept study supports the application of the SWCNT sensors for the monitoring of the metabolic activity of living cells.

Chapter 7

Conclusions and outlook

7.1 Summary and key contributions

The main focus of this thesis is to present a proof-of-concept study for the development of all inkjet-printed, flexible and disposable biochips with novel SWCNT sensors for low cost and reliable microphysiological investigations on living cells. The motivation for this work originated from the high fabrication cost related limitations of the classical rigid biochips and the potential of printed electronics for large area and low cost fabrication. This is an important yet unresolved problem since printed and low-cost biochips for cell monitoring applications that are featured with both biocompatibility and robustness for challenging applications that involve exposure to aqueous media have not been demonstrated earlier.

Since piezoelectric inkjet printing is the main device fabrication method investigated in this thesis, we started by giving an insight into this interesting method. We highlighted the interesting features of inkjet printing in comparison to the main printing techniques and the reasons that drove the evolution of this method from simple graphic art applications to a powerful and popular tool for printed electronics. Unlike graphic art applications that are rather forgiving, printed electronics applications are challenging and necessitate a defect free printing image. We discussed the challenges related to the inkjet printing of electrically functional inks on polymer substrates and the various parameters that need to be optimized in order to obtain an accurate droplet deposition and a good printing image suitable for printed electronics applications.

To obtain printed biochips that display the required properties for cell assays, a combination of different inks with different properties is required. Instead of the expensive noble metals usually implemented for the fabrication of biochips we investigated the performance and suitability of comparably low-cost silver, CNT and polymer based inks.

To achieve silver based tracks, we printed MOD and silver nanoparticles based inks on different polymer substrates. We successfully sintered these tracks to obtain conductive patterns without damaging the thermally instable substrates and compared their electrical and mechanical performance to evaluate their suitability for flexible electronics. Chemically sintered MOD samples on PET substrate showed a good resistivity of 8μΩ cm, however, their mechanical performance and shelf life in aqueous media was not satisfactory. For the silver nanoparticles based tracks, we compared the suitability of various sintering techniques to obtain conductive patterns on PET, PEN and PI substrate. Here we achieved resistivity values as low as twice the resistivity value of bulk silver without damaging the polymer substrates. We noticed that the sintering method has a strong influence on the mechanical performance of the printed tracks. Therefore, choosing the right sintering method is crucial to obtain robust structures that have a good shelf life in aqueous media. For example, using photonic sintering we could enhance the shelf life of printed silver tracks in aqueous media at 38°C and with an applied voltage of 300mV up to eleven weeks. We also noticed that enhancing the thickness of the printed tracks by increasing the number of printed layers leads to a lower resistivity as well as a higher shelf life in aqueous media. We have demonstrated that using alternative sintering techniques such as photonic sintering not only leads to a good electrical and mechanical performance comparable to the classical thermal sintering but it also significantly reduces the sintering time and enhances the potential of inkjet printing for large area and roll-to-roll fabrication.

Inkjet printing of CNT based inks can be quite challenging because these one dimensional nanoparticles can easily clog the inkjet nozzle. We achieved a stable jetting performance for centrifuged CNT based inks.

Using centrifugation instead of the conventional filtering method leads to higher particle concentration and therefore lower resistivity of the printed tracks. Inkjet deposited CNT based tracks suffer from rather high resistivity compared to single CNTs mainly due to the junction resistance in the random CNT network and the effect of the stabilizing surfactant that wraps the CNTs and restrains their interaction. We noticed that enhancing the CNT network density by printing several layers significantly reduces the resistivity of the printed tracks. A resistance decrease up to one order of magnitude was obtained for ten printed layers. The resistivity of the CNT tracks can be further decreased using an acidic treatment to remove the stabilizing surfactant without damaging the polymer substrates. Despite the resistivity decrease achieved by these methods, the resistivity of the CNT based tracks is still much higher than silver based tracks. However, CNTs are especially attractive for biomedical applications because of their biocompatible nature. The CNT samples displayed a good adhesion to the substrate and we could obtain a shelf life of several weeks in aqueous media for tracks printed on PET and PI substrate.

Bendability tests have shown that both silver and CNT based tracks are bendable and no noticeable impedance change was observed after 9400 bending cycles at a bending radius of 1.5 cm. This validates the suitability of these tracks for flexible electronics applications and roll-to-roll fabrication.

To be able to exploit the good conductivity of silver tracks for biomedical applications despite their toxicity, these tracks can simply be covered with a biocompatible polymer. Due to the poor stability and limited availability of insulating polymer based inkjet inks, we tested a house-prepared SU-8 based ink and an ink sample obtained from Altana. We could successfully print both inks without any nozzle clogging or drying issues. The SU-8 polymer based samples were inhomogeneous and suffered from poor dielectric performance. Samples printed using the Altana ink showed a noticeably better performance and we could obtain a reproducible breakdown voltage of 5 V for four printed layers. The curing of these polymers can be achieved by an UV-treatment that does not affect the polymer substrates. Biocompatibility tests have proven that cells can grow on the polymer covered silver tracks. This method is therefore effective for electrical insulating, achieving a biocompatible environment for the living cells and allows the integration of low cost metals in the fabrication of the biochips.

So far we have been focusing on the optimization of each individual material needed for the fabrication of the biochips. Combining these materials we could achieve printed and flexible devices that are featured with good conductivity, mechanical stability, a suitable shelf life in aqueous media and biocompatibility. The printed biochips present therefore a potential low cost and disposable alternative to the conventional rigid biochips. After obtaining biochips that display the desired properties, we have tested a possible application of these chips for cell monitoring using novel SWCNT based sensors. These sensors can easily be integrated into the biochips using drop-casting or inkjet printing to deposit the sensitive layer on the IDES electrodes of the biochip.

Impedimetric measurements without the need for a reference electrode allow to monitor the electronic properties of the sensitive SWCNT layer. We have proven the sensitivity of the SWCNT sensors for a wide range of pH-values and for oxygen concentration changes in aqueous solutions. We observed that the impedance of these sensors decreases with decreasing pH value and with decreasing dissolved oxygen concentration. Therefore the sensors are suitable for the monitoring of the metabolic activity of living cells that results in medium acidification and oxygen consumption. Classical biochips usually have separate sensors to detect the pH and oxygen signal whereas the SWCNT sensors can detect both signals. For applications where only the oxygen signal is relevant, the SWCNT sensor can be covered with an oxygen permeable nafion/collodion membrane that suppresses the pH signal. Similar to the classical biosensor used in rigid biochips, the SWCNT sensors are not meant to deliver an exact value for pH or oxygen concentration but to detect pH and oxygen concentration changes over time.

Since cell metabolism is a complex process that does not only affect the pH value and oxygen concentration but also involves glucose and lactate concentration changes, we have performed measurements using various glucose and lactate concentrations and ruled out the cross sensitivity of the SWCNT sensors to these substances. As the measurements without cells demonstrated the potential of SWCNT sensors for the monitoring of the metabolic activity of cells, we have tested these sensor with living yeast cells. The measurements with living cells proved the correlation between enhanced cell metabolism and more pronounced sensor signal and validated our previous results.
These results demonstrate the potential of the SWCNT sensors for in-vitro cell monitoring for diagnostics, toxicity tests and other cell related screening methods.

7.2 Future work

The steadily growing field of printed electronics regularly offers new ideas for materials and substrates that could be interesting to further improve the fabrication procedure or the performance of the printed biochips. For example silver coated copper nanoparticles based inks have been developed that may be an interesting alternative for silver nanoparticles for an even more cost efficient fabrication of the chips.

This thesis presents a preliminary proof-of-concept study for printed bioelectronic sensor chips, therefore the most critical future work would be a statistical evaluation of performance of a large number of these chips to validate the current results. For this purpose the use of faster printing methods than inkjet at research scale could reduce the fabrication time and facilitate the fabrication of a large number of biochips.

A major challenge for printed electronics is to reach a level of maturity that enables the up-scaling of production processes from laboratory research to high volume industrial applications.
Industrial-scale production usually favors continuous processes such as roll-to-roll fabrication over sheet-to-sheet fabrication. However, the parameters optimized for sheet-to-sheet fabrication might not be directly applicable for large scale production.

While there are various potential methods for the large area fabrication of printed biochips, screen printing is an attractive candidate because it is a well-established, fast and cheap fabrication method. Depending on the mesh-size and fiber diameter of the printing screen, printed structures with a thickness in the range of a few micrometers can be achieved. The surface of the printed tracks in this case is, however, not uniform but clearly shows the imprint of the screen.

Since smooth and homogeneous surfaces with a roughness well below 1 µm are more favorable for the growth of biological cells, screen printing of the sensor structures itself does not seem to be a promising process step at the current state of the art. Here, inkjet-printing or pad-printing would more advantageous due to the inherent submicrometer printing thickness. For printed contact pads or conducting tracks leading to the sensors, however, this restriction is not valid.

All these printing techniques can be applied today for both sheet-to-sheet production as well as roll-to-roll processes. Pilot-scale roll-to-roll production line units (see figure 7.1) that combine printing, drying and/or curing units to enable a good adherence of the just printed structures to the substrate prior to the next process step present an efficient tool to further evaluate the process scalability and ensure a reliable transfer from laboratory to large-scale manufacturing.

A possible solution for mass production therefore could be an arrangement of several such units. Starting with a fast industrial inkjet printing unit (e.g. CERADROP MGI group) for the relatively small IDES structures printed using a CNT/CNP based ink, followed by a photonic sintering unit (e.g. NOVACENTRIX PulseForge unit) for the curing of the printed tracks. The next process unit could add the contact pads and conducting lines by rotary screen printing of silver based paste, followed by a third unit for the application of an insulating polymer layer on the silver based tracks. Finally, the SWCNT based sensitive layer could be deposited by a drop-casting unit.

Figure 7.1: Pilot-scale roll-to-roll production line unit with an integrated printing, drying and photonic curing system from Novacentrix (Novacentrix, Austin).

It should be noted, however, that the future commercial availability of inks and substrates used in this work is not guaranteed due to the still rapidly changing players in the printed electronics market. For a large scale chip production process, therefore, the process parameters for each step should eventually be optimized again for the then available materials and a long-term supply of these has to be ensured.

We have principally shown the potential of the all-printed biochips for large area and roll-to-roll fabrication. Work along this line should be continued to further evaluate the process scalability and ensure a reliable transfer from laboratory to large-scale manufacturing.

Appendix A

Inkjet printer

Inkjet printing is performed using a piezoelectric Autodrop MD-P-826 system (Microdrop Technologies, Norderstedt, Germany, figure A.1). This system is fitted with an AD-k-901 print head (37µl storage volume, figure A.2) that can be moved in the z-direction. The substrates are placed onto a substrate holder that can move in x- and y-direction. The Autodrop system is also equipped with two stroboscopic video cameras to observe and optimize the droplet formation and to control the printing image on the substrate.

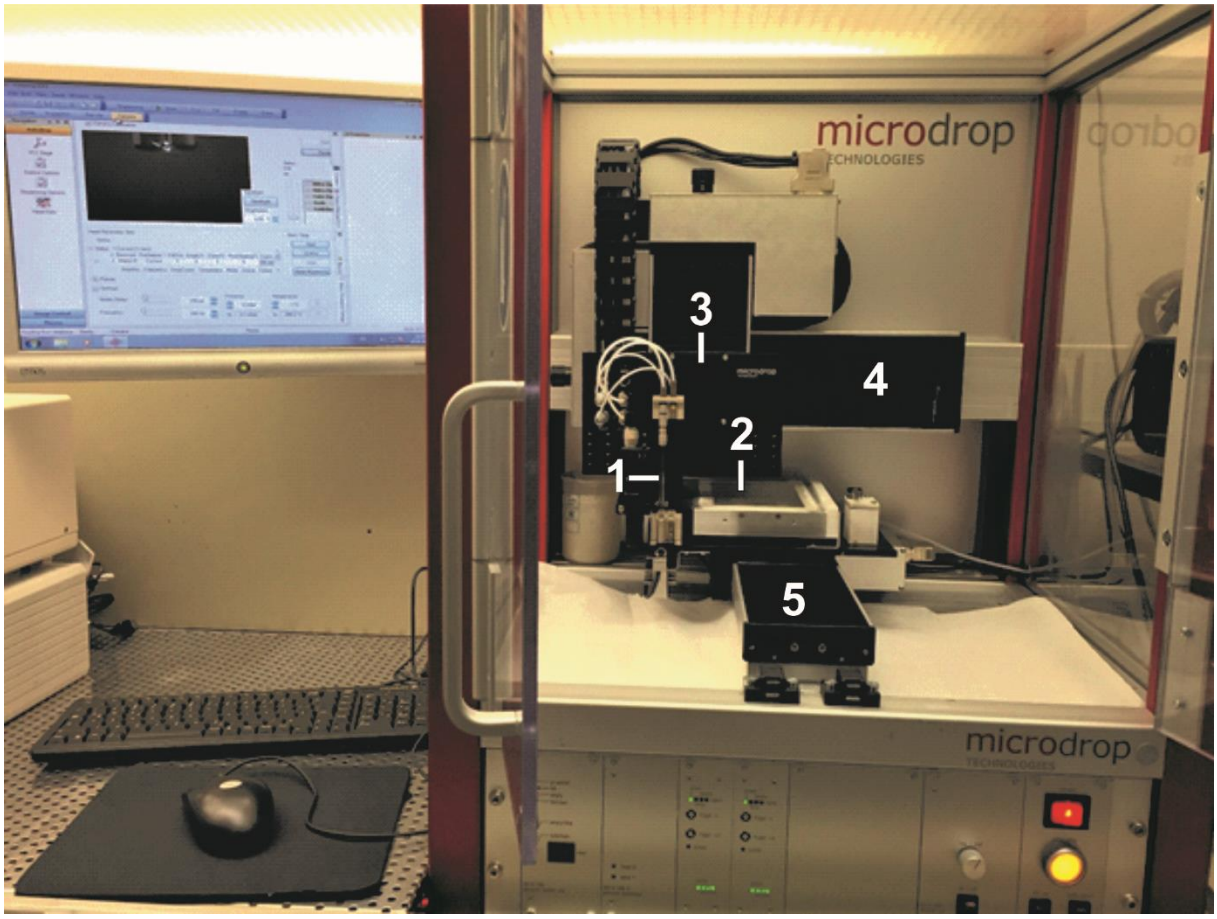

Figure A.1: Piezoelectric Autodrop MD-P-826 system fitted with an AD-K-901 print head. The main assemblies of this system are: 1) AD-K-901 print head, 2) substrate table movable in y-axis, 3) head carrier plate at z-axis, 4) x-axis, 5) y-axis.

The AD-K-901 print head (figure A.2) has standard nozzle diameters of 30µm, 50µm and 70µm. These glass nozzles are able to pipette liquids with viscosities in the range of 1 to 20 mPas.

(a) (b)

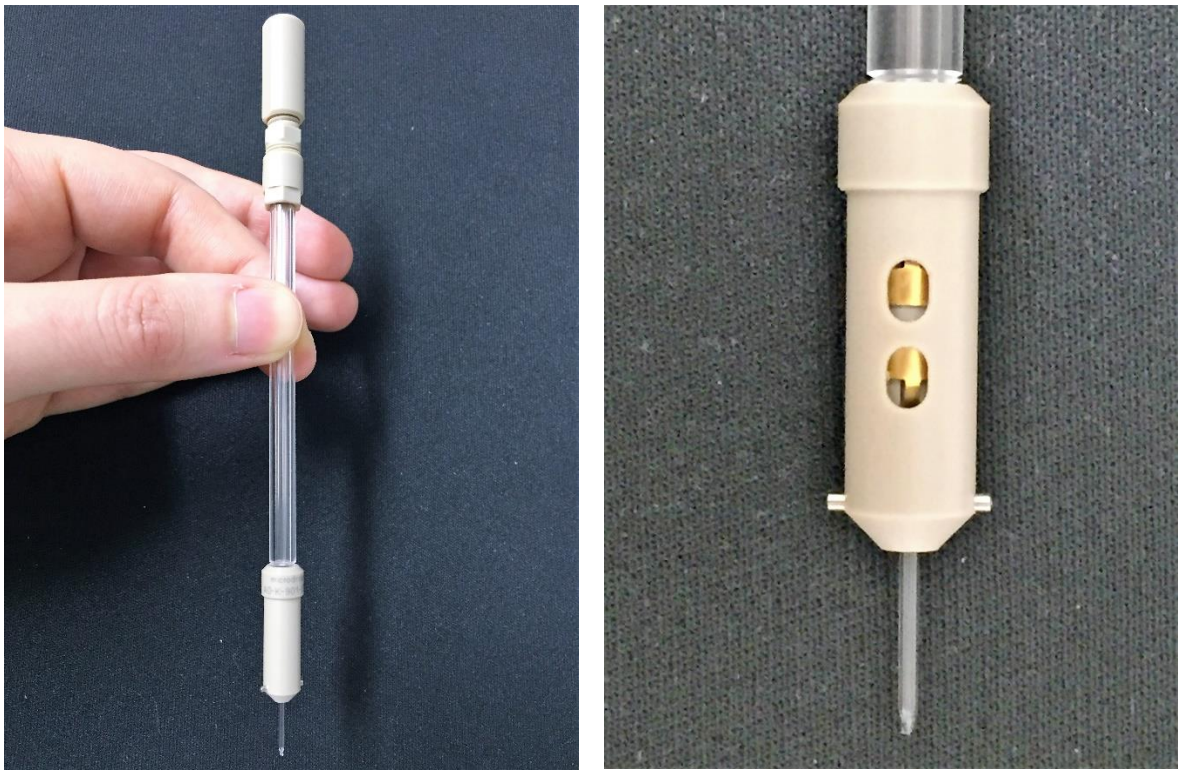

Figure A.2: The AD-K print head (a) is equipped with a piezoelectric droplet generator (b).

Appendix B

Polymer substrates

Substrate types

The substrates used in this work are colorless and flexible polymer substrates.

Polyethylene terephthalate (PET)

PET foils (Hostaphan GN 4600, 175µm thick) were obtained from Mitsubishi Polyester Film (Wiesbaden, Germany). The Hostaphan GN 4600 foils are biaxially oriented with a treated upper side for better adhesion. These foils can be heated at temperatures up to 160°C.

Polyethylene naphthalate (PEN)

PEN foils (Teonex Q65HA, 125µm thick) were obtained from DuPont Teijin Films (Wilton, U.K.). The Teonex Q65 foils are highly transparent, biaxially oriented and have one treated side to provide enhanced adhesion. These foils can be heated at temperatures up to 230°C.

Polyimide (PI)

Colorless PI foils (25µm thick) were obtained from I.S.T (Tokyo, Japan). These foils can be heated at temperatures up to 300°C.

Cleaning and storage

For cleaning, the polymer substrates are submerged in a deconnex/water mixture for 1 minute, washed under running distilled water and then dried using a nitrogen gun. The substrates can then be stored at room temperature and ambient atmosphere for several weeks or until use.

Appendix C

Impedance measurements with the IMOLA system

The Intelligent MObile LAb (IMOLA, figure C.1.a) is a system with an integrated power supply and wireless data transmission initially developed for sensorchip-based analysis of cell metabolic rates. The IMOLA enables pH, oxygen and impedance measurements [8]. Combining six IMOLAs in an incubator to a 6xIMOLA-IVD system (cellasys GmbH, Kronburg, see figure C.1 b) allows the parallel measurement of six multiparametric biomedical sensor chips. The IMOLA-chip shown in figure C.1.a is equipped with an oxygen sensor, two pH sensors and two IDES electrodes. Therefore each IMOLA allows two parallel impedance measurements. Hence, the 6xIMOLA-IVD systems can be used for 12 parallel impedance measurements.

(a)

(b)

Figure C.1: Each IMOLA (a) uses a chip equipped with two IDES electrodes; the 6xIMOLA-IVD system therefore allows 12 parallel impedance measurements (b) (Heinz-Nixdorf Chair for Medical Electronics, TUM).

Originally, the IDES electrodes on the chip shown in figure C.1.a are used for impedance measurements in the IMOLA system. Instead of measuring the impedance of the IDES electrodes, we used the contact pins of the IDES electrodes (figure C.2.a/ C.2.b) to enable 4-point impedance measurements on the printed tracks by connecting a dummy chip (figure C.2.c) to an adaptor (figure C.2.d).

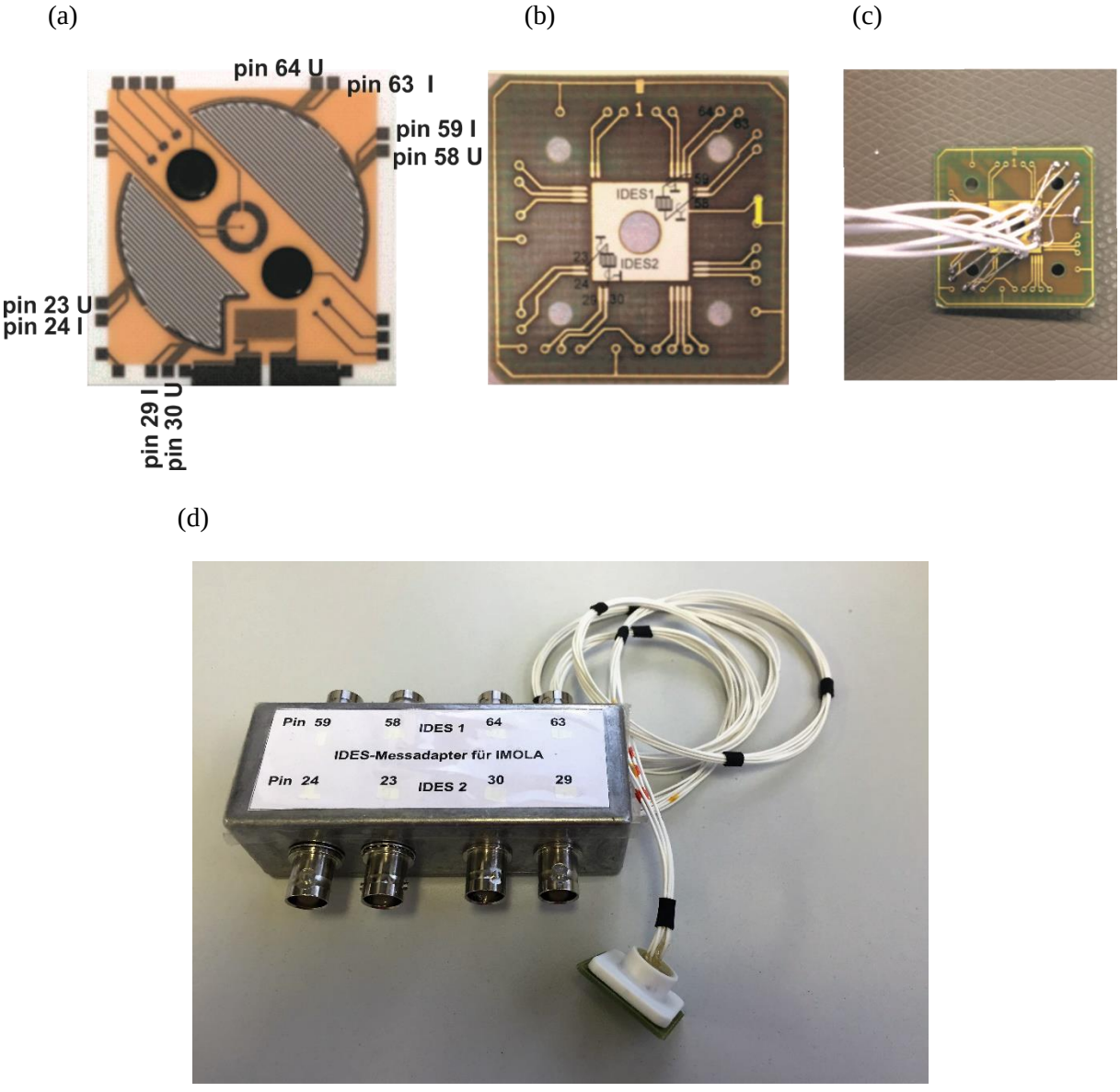

Figure C.2: The pins of the IDES electrodes on the chip (a, b) are used to connect a dummy chip (c) to an adaptor (d) in order to enable 4-point impedance measurements using the IMOLA system to determine the shelf life of the printed tracks.

For example, the pins 24 and 29 of IDES 2 can be used to apply a voltage on the printed tracks and the pins 23 and 30 can be used to measure the current to allow 4-point impedance measurements. Using a dummy chip in each IMOLA connected to an adaptor it was possible to measure the impedance of up to 12 printed structures at the same time for long-term investigations on shelf life of the printed structures in aqueous media.

References

[1] L. Torre, F. Bray, R. Siegel, J. Ferlay, J. Lortet-Tieulent and A. Jemal, “Global Cancer Statistics, 2012”, *CA CANCER J CLIN*, vol. 65, no.2, pp. 87-108, 2015.

[2] J. Elmore, M. Barton, V. Moceri, S. Polk, P. Arena and S. Fletcher, “Ten-year risk of false positive screening mammograms and clinical breast examinations”, *The New England Journal of Medicine*, vol. 338, no. 16, pp. 1089-1096, 1998.

[3] R. Smith, D. Manassaram-Baptiste, D. Brooks, M. Doroshenk, S. Fedewa, D. Saslaw, O. Brawley and R. Wender, “Cancer Screening in the United States, 2015: A Review of Current American Cancer Society Guidelines and Current Issues in Cancer Screening”, *CA CANCER J CLIN*, vol. 65, no.1, pp. 30-54, 2015.

[4] M. Chiriaco, E. Primiceri, A. Monteduro, A. Bove, S. Leporatti, M. Capello, S. Ferri-Borgogno, R. Rinaldi, F. Novelli and G. Maruccio, “Towards pancreatic cancer diagnosis using EIS biochips”, *Lab on a Chip*, vol. 13, pp. 730-734, 2013.

[5] R. Kleinhans, M. Brischwein, P. Wang, B. Becker, F. Demmel, T. Schwarzenberger, M. Zottmann, P. Wolf, A. Niendorf and B. Wolf, “ Sensor-based cell and tissue screening for personalized cancer chemotherapy”, *Med Biol Eng Comput*, vol. 50, pp. 117-126, 2012.

[6] M. Brischwein, E. Motrescu, E. Cabala, A. Otto, H. Grothe and B. Wolf, “Functional cellular assays with multiparametric silicon sensor chips”, *Lab on a Chip*, vol. 3, pp. 234-240, 2003.

[7] J. Wiest, M. Brischwein, J. Ressler, A. Otto, H. Grothe and B. Wolf, “ Cellular Assays with Multiparametric Bioelectronic Sensor Chips”, *Chimia*, vol. 59, no. 5, pp. 243-246, 2005.

[8] J. Wiest, T. Stadthagen, M. Schmidhuber, M. Brischwein, J. Ressler, U. Raeder, H. Grothe, A. Melzer and B. Wolf, “ Intelligent Mobile Lab for Metabolics in Environmental Monitoring”, *Analytical Letters*, vol. 39, pp. 1759-1771, 2006.

[9] B. Becker, S. Etzbach, M. Schmidhuber, D. Grundl, F. Ilchmann, H. Grothe and B. Wolf, “Real-time screening system using living cells for chemosensitivity testing”, *IEEE*, pp. 87-93, 2009.

[10] P. Wolf, M. Brischwein, R. Kleinhans, F. Demmel, T. Schwarzenberger, C. Pfister and B. Wolf, “ Automated platform for sensor-based monitoring and controlled assays of living cells and tissues”, *Biosensors and Bioelectronics*, vol. 50, pp. 111-117, 2013.

[11] R. Kleinhans, “Etablierung und validierung eines prädiktiven metabolischen Chemosensitivitätstests mittels automatisierter chipgestützter analytic”, *Heinz-Nixdorf Chair for Medical Electronics*, TUM, 2016.

[12] A. Haque, M. Chatni, G. Li and D. Porterfield, “Biochips and other microtechnologies for physiomics”, *Expert Rev. Proteomics*, vol. 4, no. 4, pp. 553-563, 2007.

[13] T. Sekitani, U. Zschieschang, H. Klauk and T. Someya, “Flexible organic transistors and circuits with extreme bending stability”, *Nature Materials*, vol. 9, pp. 1015-1022, 2010.

[14] A. Shimoni, S. Azoubel and S. Magdassi, “Inkjet printing of flexible high-performance carbon nanotube transparent conductive films by “coffee ring effect””, *Nanoscale*, vol. 6, no. 19, pp. 11084-11089, 2014.

[15] B. Yoon, C. White, G. Wease, L. Honnappa, S. Tsai, X. Wang and T. Daim, “Technology roadmap for automotive flexible display”, *Springer*, DOI 10.1007/978-3-319-02973-3, chap. 7, 2014.

[16] Q. Lin, H. Huang, Y. Jing, H. Fu, P. Chang, D. Li, Y. Yao and Z. Fan, “Flexible photovoltaic technologies”, *Journal of Materials Chemistry C*, vol. 2, pp. 1233-1247, 2014.

[17] D. Kim, N. Lu, R. Ma, Y. Kim, R. Kim, S. Wang, J. Wu, S. Won, H. Tao, A. Islam, K. Yu, T. Kim, R. Chowdhury, M. Ying, L. Xu, M. Li, H. Chung, H. Keum, M. McCormick, P. Liu, Y. Zhang, F. Omenetto, Y. Huang, T. Coleman and J. Rogers, “Epidermal electronics”, *Science*, vol. 333, pp. 838-843, 2011.

[18] A. Bandodkar, W. Jia, C. Yardimci, X. Wang, J. Ramirez and J. Wang, “Tattoo-based noninvasive glucose monitoring: A proof-of-concept study”, *analytical chemistry*, vol. 87, pp. 394-398, 2014.

[19] A. Bandodkar, V. Hung, W. Jia, G. Valdes-Ramirez, J. Windmiller, A. Martinez, J. Ramirez, G. Chan, K. Kerman and J. Wang, “Tattoo-based potentiometric ion-selective sensors for epidermal pH monitoring”, *Analyst*, vol. 138, pp. 123-128, 2013.

[20] D. Sharp, “Printed composite electrodes for in-situ wound pH monitoring”, *Biosensors and Bioelectronics*, vol. 50, pp. 399-405, 2013.

[21] V. Sanchez-Romaguera, S. Wünscher, B. Turki, R. Abbel, S. Barbosa, D. Tate, D. Oyeka, J. Batchelor, E. Parker, U. Schubert and S. Yeates, “Inkjet printed paper based frequency selective surfaces and skin mounted RFID tags: the interrelation between silver nanoparticle ink, paper substrate and low temperature sintering technique”, *Materials Chemistry C*, vol. 3, pp. 2132-2140, 2015.

[22] M. Mannoor, H. Tao, J. Clayton, A. Sengupta, D. Kaplan, R. Naik, N. Verma, F. Omenetto and M. McAlpine, “Graphene-based wireless bacteria detection on tooth enamel”, *Nature Communications*, vol. 3, pp. 763-771, 2012.

[23] C. Lochner, Y. Khan, A. Pierre and A. Arias, “All-organic optoelectronic sensor for pulse oximetry”, *Nature Communications*, vol. 5, pp. 5745-5752, 2014.

[24] N. Matsuhisa, M. Kaltenbrunner, T. Yokota, H. Jinno, K. Kuribara, T. Sekitani and T. Someya, “Printable elastic conductors with a high conductivity for electronic textile applications”, *Nature Communications*, vol. 6, pp. 7461-7472, 2015

[25] H. Tao, M. Brenckle, M. Yang, J. Zhang, M. Liu, S. Siebert, R. Averitt, M. Mannoor, M. McAlpine, J. Rogers, D. Kaplan and F. Omenetto, "Silk-based conformal, adhesive, edible food sensors", *Advanced Materials*, vol. 24, no. 8, pp. 1067-1072, 2012.

[26] A. Kamyshny and S. Magdassi, "Conductive nanomaterials for printed electronics", *Small*, vol. 10, no. 17, pp. 3515-3535, 2014.

[27] H. Wijshoff, "Structure- and fluid-dynamics in piezo inkjet printheads", dissertation, *University of Twente*, 2008.

[28] J. Perelaer, "Microstructures prepared via inkjet printing and embossing techniques", dissertation, *Technical University Eindhoven*, 2009.

[29] E. Goedde and M. Yuen, "Experiments on liquid jet instability", *Journal of Fluid Mechanics*, vol. 40, pp. 495-511, 1970.

[30] I. Hutchings and G. Martin, "Inkjet technology for digital fabrication", *Wiley*, ISBN 978-0-470-68198-5, 2013.

[31] R. Sweet, "High frequency recording with electrostatically deflected ink jets", *The Review of Scientific Instruments*, vol. 36, no. 2, pp. 131-136, 1965.

[32] B. Derby, "Inkjet printing of functional and structural materials: fluid property requirements, feature stability and resolution", *Annu. Rev. Mater. Res.*, vol. 40, pp. 395-414, 2010.

[33] S. Magdassi, "The chemistry of inkjet inks", *World Scientific Publishing*, ISBN-10 981-281-821-9, 2010.

[34] J. Korvink, P. Smith and D. Shin, "Inkjet-based micromanufacturing", *Wiley-VCH*, ISBN: 978-3-527-31904-6, 2012.

[35] D. Bogy and F. Talke, "Experimental and theoretical study of wave propagation phenomena in drop-on demand ink jet devices", *IBM J. Res. Develop*, vol. 28, no. 3, pp. 314-321, 1984.

[36] H. Klauk, "Organic electronics materials, manufacturing and applications", *Wiley-VCH*, ISBN-13 978-3-527-31264-1, 2006.

[37] K. Suganuma, "Introduction to printed electronics", *Springer briefs in electrical and computer engineering*, ISBN 978-1-4614-9624-3, 2014.

[38] G. Hübner, "Patterning processes and functional printing in conventional print processes", *Workshop functional printing at LOPEC 2015*, 3 March 2015.

[39] A. Hayat and J. Marty, "Disposable screen printed electrochemical sensors: tools for environmental monitoring", *Sensors*, vol. 14, pp. 10432-10453, 2014.

[40] M. Rahman, A. Ahammad, J. Jin, S. Ahn and J. Lee, “A comprehensive review of glucose biosensors based on nanostructured metal-oxides”, *Sensors*, vol. 10, pp. 4855-4886, 2010.

[41] L. Berisha, K. Kalcher, A. Hajrizi and T. Arbneshi, “A new biosensor for glucose based on screen printed carbon electrodes modified with tin (IV)-oxide”, American Journal of Analytical Chemistry, vol. 4, pp. 27-35, 2013.

[42] H. Kang, “Gravure-printed highly scaled organic thin film transistors for low cost and large area electronics”, dissertation, *University of California, Berkeley*, 2013.

[43] H. Kang, R. Kitsomboonloha, J. Jang and V. Subramanian, “High-performance printed transistors realized using femtoliter gravure-printed sub-10 μm metallic nanoparticle patterns and highly uniform polymer dielectric and semiconductor layer”, *Advanced Materials*, vol. 24, pp. 3065-3069, 2012.

[44] E. Secor, S. Lim, H. Zhang, C. Frisbie, L. Francis and M. Hersam, “Gravure printing of grapheme for large-area flexible electronics”, *Advanced Materials*, vol. 26, pp. 4533-4538, 2014.

[45] J. Hast, M. Tuomikoski, R. Suhonen, K. Väisänen, M. Välimeki, T. Maaninen, P. Apilo, A. Alastalo and A. Maaninen, “Roll-to-roll manufacturing of printed OLEDs”, *SID*, no. 18.1, pp. 192-195, 2013.

[46] H. Yan, Z. Chen, Y. Zheng, C. Newman, J. Quinn, F. Dötz, M. Kastler and A. Facchetti, “A high-mobility electron-transporting polymer for printed transistors”, *Nature*, vol. 457, pp. 679-687, 2009.

[47] H. Kempa, M. Hambsch, K. Reuter, M. Stanel, G. Schmidt, B. Meier and A. Hübler, “Complementary ring oscillator exclusively prepared by means of gravure and flexographic printing”, *IEEE Transactions on Electron Devices*, vol. 58, no. 8, pp. 2765-2769, 2011.

[48] P. Harrey, B. Ramsey, P. Evans and D. Harrison, “Capacitive-type humidity sensors fabricated using the offset lithographic printing process”, Sensors and Actuators B, vol. 87, pp. 226-232, 2002.

[49] E. Cantatore, “Applications of organic and printed electronics, a technology-enabled revolution”, *Springer*, ISBN 978-1-4614-3159-6, 2013.

[50] D. Jang, D. Kim and J. Moon, “Influence of fluid physical properties on ink-jet printability”, *Langmuir*, vol. 25, pp. 2629-2635, 2009.

[51] N. Reis and B. Derby, “Ink jet deposition of ceramic suspensions: modeling and experiments of droplet formation”, *Materials Research Society*, vol. 625, pp. 117-122, 2000.

[52] K. Kwon, “Waveform design methods for piezo inkjet dispensers based on measured meniscus motion”, *Journal of Microelectromechanical Systems*, vol. 18, no. 5, pp. 1118-1125, 2009.

[53] Y. Noguchi, T. Sekitani, T. Yokota and T. Someya, "Direct inkjet printing of silver electrodes on organic semiconductors for thin film transistors with top contact geometry", *Applied Physics Letters*, vol. 93, no. 043303, 2008.

[54] L. Creagh and M. McDonald, "Design and performance of inkjet print heads for non-graphic-arts applications", *MRS Bulletin*, pp. 807-811, 2003.

[55] C. Lamont, T. Eggenhuisen, M. Coenen, T. Slaats, R. Andriessen and P. Groen, "Tuning the viscosity of halogen free bulk heterojunction inks for inkjet printed organic solar cells", *Organic Electronics*, vol. 17, pp. 107-114, 2015.

[56] S. Hoath, S. Jung, W. Hsiao and I. Hutchings, "How PEDOT:PSS solutions produce satellite-free inkjets", *Organic Electronics*, vol. 13, pp. 3259-3262, 2012.

[57] D. Soltman and V. Subramanian. "Inkjet-printed line morphologies and temperature control of the coffee ring effect", *Langmuir*, vol. 24, pp. 2224-2231, 2008.

[58] J. Stringer and B. Derby, "Formation and stability of lines produced by inkjet printing", *Langmuir*, vol. 26, no. 12, pp. 10365-10372, 2010.

[59] P. Duineveld, "The stability of ink-jet printed lines of liquid with zero receding contact angle on a homogeneous substrate", *Journal of Fluid Mechanics*, vol. 477, pp. 175-200, 2003.

[60] A. Sharma and G. Reiter, "Instability of thin polymer films on coated substrates: rupture, dewetting and drop formation", *Journal of Colloid and Interface Science*, vol. 178, pp. 383-399, 1996.

[61] C. Redon, F. Brochard-Wyart and F. Rondelez, "Dynamics of dewetting", *Physical Review Letters*, vol. 66, no. 6, pp. 715-719, 1991.

[62] R. Deegan, O. Bakajin, T. Dupont, G. Huber, S. Nagel and T. Witten, "Capillary flow as the cause of ring stains from dried liquid drops", *Nature*, vol. 389, pp. 827-829, 1997.

[63] J. Sun, B. Bao, M. He, H. Zhou and Y. Song, "Recent advances in controlling the deposition morphologies of inkjet droplets", *ACS Applied Materials and Interfaces*, vol. 7, no. 51, pp. 28086-28099, 2015.

[64] H. Hu and R. Larson, "Marangoni effect reverses coffee-ring depositions", *The Journal of Physical Chemistry B*, vol. 110, pp. 7090-7094, 2006.

[65] T. Still, P. Yunker and A. Yodh, "Surfactant-induced Marangoni eddies alter the coffee-rings of evaporating colloidal drops", *Langmuir*, vol. 28, pp. 4984-4988, 2012.

[66] M. Layani, M. Grouchko, O. Milo, I. Balberg, D. Azulay and S. Magdassi, "Transparent conductive coatings by printing coffee ring arrays obtained at room temperature", *ACS Nano*, vol. 3, no. 11, pp. 3537-3542, 2009.

[67] J. Wang, Z. Zheng, H. Li, W. Huck and H. Sirringhaus, “Dewetting of conducting polymer inkjet droplets on patterned surfaces”, *Nature Materials*, vol. 3, pp. 171-176, 2004.

[68] B. de Gans, P. Duineveld and U. Schubert, “Inkjet printing of polymers: state of the art and future developments”, *Advanced Materials*, vol. 16, no. 3, pp. 203-213, 2004.

[69] Z. Liu, Y. Su and K. Varahramyan, “Inkjet-printed silver conductors using silver nitrate ink and their electrical contacts with conducting polymers”, *Thin Solid Films*, vol. 478, pp. 275-279, 2005.

[70] A. Denneulin, J. Bras, F. Carcone, C. Neuman and A. Blayo, “Impact of ink formulation on carbon nanotube network organization within inkjet printed conductive films”, *Carbon*, vol. 49, pp. 2603-2614, 2011.

[71] A. Kamyshny, J. Steinke and S. Magdassi, “Metal-based inkjet inks for printed electronics”, *The Open Applied Physics Journal*, vol. 4, pp. 19-36, 2011.

[72] S. Wünscher, R. Abbel, J. Perelaer and U. Schubert, “Progress of alternative sintering approaches of inkjet-printed metal inks and their application for manufacturing of flexible electronic devices”, *Journal of Materials Chemistry C*, vol. 2, pp. 10232-10261, 2014.

[73] Y. Dong, X. Li, S. Liu, Q. Zhu, J. Li and X. Sun, “Facile synthesis of high silver content MOD ink by using silver oxalate precursor for inkjet printing applications”, *Thin Solid Films*, vol. 589, pp. 381-387, 2015.

[74] W. Shen, X. Zhang, Q. Huang, Q. Xu and W. Song, “Preparation of solid silver nanoparticles for inkjet printed flexible electronics with high conductivity”, *Nanoscale*, vol. 6, pp. 1622-1628, 2014.

[75] V. Abhinav, V. Rao, P. Karthik and S. Singh, “Copper conductive inks: synthesis and utilization in flexible electronics”, *RSC Advances*, vol. 5, pp. 63985-64030, 2015.

[76] G. Jensen, C. Krause, G. Sotzing and J. Rusling, “Inkjet-printed gold nanoparticle electrochemical arrays on plastic. Application to immunodetection of a cancer biomarker protein”, *Physical Chemistry Chemical Physics*, vol. 13, pp. 4888-4894, 2011.

[77] M. Grouchko, A. Kamyshny and S. Magdassi, “Formation of air-stable copper-silver core-shell nanoparticles for inkjet printing”, *Journal of Materials Chemistry*, vol. 19, pp. 3057-3062, 2009.

[78] S. Wünscher, “Sintering and applications of inkjet-printed silver nanoparticles”, dissertation, *Technical University Jena*, 2014.

[79] K. Fukuda, T. Sekine, D. Kumaki and S. Tokito, “Profile control of inkjet printed silver electrodes and their application to organic transistors”, *ACS Applied Materials and Interfaces*, vol. 5, no. 9, pp. 3916-3920, 2013.

[80] Y. Galagan, E. Coenen, R. Abbel, T. Lammeren, S. Sabik, M. Barink, E. Meinders, R. Andriessen and P. Blom, "Photonic sintering of inkjet printed current collecting grids for organic solar cells applications", *Organic Electronics*, vol. 14, pp. 38-46, 2013.

[81] J. Perelaer, P. Smith, D. Mager, D. Soltman, S. Volkman, V. Subramanian, J. Korvink and U. Schubert, "Printed electronics: the challenges involved in printing devices, interconnects and contacts based on inorganic materials", *Journal of Materials Chemistry*, vol. 20, pp. 8446-8453, 2010.

[82] J. Valeton, K. Hermans, C. Bastiaansen, D. Broer, J. Perelaer, U. Schubert, G. Crawford and P. Smith, "Room-temperature preparation of conductive silver features using spin-coating and inkjet printing", *Journal of Materials Chemistry*, vol. 20, pp. 543-546, 2010.

[83] S. Jahn, T. Blaudeck, R. Baumann, A. Jakob, P. Ecorchard, T. Rüffer, H. Lang and P. Schmidt, „Inkjet printing of conductive silver patterns by using the first aqueous particle-free MOD ink without additional stabilizing ligands", *Chemistry of Materials*, vol. 22, pp. 3076-3071, 2010.

[84] S. Wünscher, T. Rasp, M. Grouchko, A. Kamyshny, R. Paulus, J. Perelaer, T. Kraft, S. Magdassi and U. Schubert, "Simulation and prediction of the thermal sintering behavior for a silver nanoparticle ink based on experimental input", *Journal of Materials Chemistry C*, vol. 2, pp. 6342-6352, 2014.

[85] H. Bönnemann and R. Richards, "Nanoscopic metal particles- synthetic methods and potential applications", *European Journal of Inorganic Chemistry*, vol. 2001, no. 10, pp. 2455-2480, 2001.

[86] J. Niittynen, R. Abbel, M. Mäntysalo, J. Perelear, U. Schubert and D. Lupo, "Alternative sintering methods compared to conventional thermal sintering for inkjet printed silver nanoparticle ink", *Thin solid films*, vol. 556, pp.452-459, 2014.

[87] S. Magdassi, M. Grouchko, O. Berezin and A. Kamyshny, "Triggering the sintering of silver nanoparticles at room temperature", *ACS Nano*, vol. 4, no. 4, pp. 1943-1948, 2010.

[88] I. Reinhold, C. Hendriks, R. Eckardt, J. Kranenburg, J. Perelaer, R. Baumann and U. Schubert, "Argon plasma sintering of inkjet printed silver tracks on polymer substrates", *Journal of Materials Chemistry*, vol. 19, pp. 3384-3388, 2009.

[89] J. Perelaer, R. Abbel, S. Wünscher, R. Jani, T. Lammeren and U. Schubert, "Roll-to-roll compatible sintering of inkjet printed features by photonic and microwave exposure: from non-conductive ink to 40% bulk silver conductivity in less than 15 seconds", *Advanced Materials*, vol. 24, pp. 2620-2625, 2012.

[90] S. Hong, J. Yeo, G. Kim, D. Kim, H. Lee, J. Kwon, H. Lee, P. Lee and S. Ko, "Nonvacuum, maskless fabrication of a flexible metal grid transparent conductor by low-temperature selective laser sintering of nanoparticle ink", *ACS Nano*, vol. 7, no. 6, pp. 5024-5031, 2013.

[91] M. Allen, M. Aronniemi, T. Mattila, A. Alastalo, K. Ojanperä, M. Suhonen and H. Seppä, "Electrical sintering of nanoparticle structures", *Nanotechnology*, vol. 19, pp. 175201-175205, 2008.

[92] M. Grouchko, A. Kamyshny, C. Maihailescu, D. Anghel and S. Magdassi, "Conductive inks with a "built in" mechanism that enables sintering at room temperature", *ACS Nano*, vol. 5, no. 4, pp. 3354-3359, 2011.

[93] K. Kim, S. Lee, A. Mishra and G. Yeom, "Atmospheric pressure plasmas for surface modification of flexible and printed electronic devices: a review", *Thin Solid Films*, vol. 598, pp. 315-334, 2016.

[94] S. Wünscher, S. Stumpf, A. Teichler, O. Pabst, J. Perelear, E. Beckert and U. Schubert, "Localized atmospheric plasma sintering of inkjet printed silver nanoparticles", Journal of Materials Chemistry, vol. 22, pp. 24569-24576, 2012.

[95] T. Günay, "Untersuchung von Inkjet-gedruckten Leiterbahnen für Biosensoren", Diplomarbeit, *Heinz-Nixdorf Chair for Medical Electronics*, TUM, 2013.

[96] S. Wünscher, S. Stumpf, J. Perelaer and U. Schubert, "Towards single-pass plasma sintering: temperature influence of atmospheric pressure plasma sintering of silver nanoparticle ink", *Journal of Materials Chemistry C*, vol. 2, pp. 1642-1649, 2014.

[97] J. Perelaer, M. Klokkenburg, C. Hendriks and U. Schubert, "Microwave flash sintering of inkjet-printed silver tracks on polymer substrates", *Advanced Materials*, vol. 21, pp. 4830-4834, 2009.

[98] M. De Volder, S. Tawfick, R. Baughman and A. Hart, "Carbon nanotubes: present and future commercial applications", *Science*, vol. 339, pp. 535-539, 2013.

[99] C. Wang, K. Takei, T. Takahashi and A. Javey, "Carbon nanotube electronics- moving forward", *Chemical Society Reviews*, vol. 42, pp. 2592-2609, 2013.

[100] H. Li, W. Yin, K. Banerjee and J. Mao, "Circuit modeling and performance analysis of multi-walled carbon nanotube interconnects", *IEEE Transactions on Electron Devices*, vol. 55, no. 6, pp. 1328-1337, 2008.

[101] S. Park, M. Vosguerichian and Z. Bao, "A review of fabrication and applications of carbon nanotube film-based flexible electronics", *Nanoscale*, vol. 5, pp. 1727-1752, 2013.

[102] S. Azoubel, S. Shemesh and S. Magdassi, "Flexible electroluminescent device with inkjet-printed carbon nanotube electrodes", *Nanotechnology*, vol. 23, pp. 344003-344009, 2012.

[103] K. Kordas, T. Mustonen, G. Toth, H. Jantunen, M. Lajunen, C. Soldano, S. Talapatra, S. Kar, R. Vijtai and P. Ajayan, "Inkjet printing of electrically conductive patterns of carbon nanotubes", *Small*, vol. 2, no. 8-9, pp. 1021-1025, 2006.

[104] R. Tortorich and J. Choi, "Inkjet printing of carbon nanotubes", *Nanomaterials*, vol. 3, pp. 453-468, 2013.

[105] F. Torrisi, T. Hasan, W. Wu, Z. Sun, A. Lombardo, T. Kulmala, G. Hsieh, S. Jung, F. Bonaccorso, P. Paul, D. Chu and A. Ferrari, "Inkjet-printed graphene electronics", *ACS Nano*, vol. 6, no. 4, pp. 2992-3006, 2012.

[106] E. Secor and M. Hersam, "Emerging carbon and post-carbon nanomaterial inks for printed electronics", *The Journal of Physical Chemistry Letters*, vol. 6, pp. 620-626, 2015.

[107] H. Geng, K. Kim, K. So, Y. Lee, Y. Chang and Y. Lee, "Effect of acid treatment on carbon nanotube-based flexible transparent conductive films", *Journal of American Chemical Society*, vol. 129, pp. 7758-7759, 2007.

[108] Y. Wang, Y. Shao, D. Matson, J. Li and Y. Lin, "Nitrogen-doped graphene and its application in electrochemical biosensing", *ACS Nano*, vol. 4, no. 4, pp. 1790-1798, 2010.

[109] H. Sirringhaus, T. Kawase, R. Friend, T. Shimoda, M. Inbasekaran, W. Wu and P. Woo, "High-resolution inkjet printing of all-polymer transistor circuits", *Science*, vol. 290, pp. 2123-2126, 2000.

[110] E. Tekin, P. Smith and U. Schubert, "Inkjet printing as a deposition and patterning tool for polymers and inorganic particles", *Soft Matter*, vol. 4, pp. 703-713, 2008.

[111] Y. Liu, T. Cui and K. Varahramyan, "All-polymer capacitor fabricated with inkjet printing technique", *Solid-State Electronics*, vol. 47, pp. 1543-1548, 2003

[112] C. Edwards and D. Albertalli, "Application of polymer LED Materials using piezo ink-jet printing", *SID 01 Digest*, no. 38.3, pp. 1049-1051, 2001.

[113] A. Dadvand, J. Lu, C. Py, T. Chu, R. Movileanu and Y. Tao, "Inkjet printable and low annealing temperature gate-dielectric based on polymethylsilsesquioxane for flexible n-channel OFETS", *Organic Electronics*, vol. 30, pp. 213-218, 2016.

[114] S. Chung, S. Kim, S. Kwon, C. Lee and Y. Hong, "*IEEE Electron Device Letters*, vol. 32, no. 8, pp. 1134-1136, 2011.

[115] J. Voldman, "Electrical forces for microscale cell manipulation", *The Annual Review of Biomedical Engineering*, vol. 8, pp. 425-454, 2006.

[116] C. Marquette, F. Bouteille, B. Corgier, A. Degiuli and L. Blum, "Disposable screen-printed chemiluminescent biochips for the simultaneous determination of four point-of care relevant proteins", *Analytical and Bioanalytical Chemistry*, vol. 393, pp. 1191-1198, 2009.

[117] W. Jia, A. Bandodkar, G. Valdes-Ramirez, J. Windmiller, Z. Yang, J. Ramirez, G. Chan and J. Wang, "Electrochemical tattoo biosensors for real-time noninvasive lactate monitoring in human perspiration", *Analytical Chemistry*, vol. 85, pp. 6553-6560, 2013.

[118] C. Dagdeviren, B. Yang, Y. Su, P. Tran, P. Joe, E. Anderson, J. Xia, V. Doraiswamy, B. Dehdashti, X. Feng, B. Lu, R. Poston, Z. Khalpey, R. Ghaffari, Y. Huang, M. Slepian and J. Rogers, "Conformal piezoelectric energy harvesting and storage from motions of the heart, lung and diaphragm", *Proceedings of the National Academy of Sciences*, vol. 111, no. 5, pp. 1927-1932, 2014.

[119] D. Wencel, T. Abel and C. McDonagh, “Optical chemical pH sensors”, *Analytical Chemistry,* vol. 86, pp. 15-29, 2014.

[120] O. Wolfbeis, “Fiber-optic chemical sensors and biosensors”, *Analytical Chemistry*, vol. 74, pp. 2663-2678, 2002.

[121] P. Bergveld, “Thirty years of ISFETOLOGY. What happened in the past 30 years and what may happen in the next 30 years”, *Sensors and Actuators B,* vol. 88, pp. 1-20, 2003.

[122] L. Maiolo, S. Mirabella, F. Maita, A. Alberti, A. Minotti, V. Strano, A. Pecora, Y. Shacham-Diamand and G. Fortunato, “Flexible pH sensors based on polysilicon thin film transistors and ZnO nanowalls”, *Applied Physics Letters*, vol. 105, no. 093501, 2014.

[123] N. Mzoughi, A. Abdellah, Q. Gong, H. Grothe, P. Lugli, B. Wolf and G. Scarpa, “Characterization of novel impedimetric pH-sensors based on solution-processable biocompatible thin-film semiconducting organic coatings”, *Sensors and Actuators B,* vol. 171-172, pp. 537-543, 2012.

[124] J. Back and M. Shim, “pH-dependent electron-transport properties of carbon nanotubes”, *Journal of Physical Chemistry B,* vol. 110, pp. 23736-23741, 2006.

[125] M. Kaempgen and S. Roth, “Transparent and flexible carbon nanotube/polyaniline pH sensors” *Journal of Electroanalytical Chemistry*, vol. 586, pp. 72-76, 2006.

[126] C. Li, K. Han, X. Pham and G, Seong, “A single-walled carbon nanotube thin film-based pH-sensing microfluidic chip”, *Analyst,* vol. 139, pp. 2011-2015, 2014.

[127] P. Gou, N. Kraut, I. Feigel, H. Bai, G. Morgan, Y. Chen, Y. Tang, K. Bocan, J. Stachel, L. Berger, M. Mickle, E. Sejdic and A. Star, “Carbon nanotube chemiresistor for wireless pH sensing”, *Scientific Reports,* vol. 4, pp. 4498-4504, 2014.

[128] D. Lee and T. Cui, “Low-cost, transparent and flexible single-walled carbon nanotube nanocomposite based ion-sensitive field-effect transistors for pH/glucose sensing”, *Biosensors and Bioelectronics,* vol. 25, pp. 2259-2264, 2010.

[129] M. Mittal and A. Kumar, “Carbon nanotube (CNT) gas sensors for emissions from fossil fuel burning”, *Sensors and Actuators B,* vol. 123, pp. 349-362, 2014.

[130] A. Abdelhalim, M. Winkler, F. Loghin, C. Zeiser, P. Lugli and A. Abdellah, “Highly sensitive and selective carbon nanotube-based gas sensor arrays functionalized with different metallic nanoparticles”, *Sensors and Actuators B,* vol. 220, pp. 1288-1296, 2015.

[131] D. Kauffman, C. Shade, H. Uh, S. Petoud and A. Star, “Decorated carbon nanotubes with unique oxygen sensitivity”, *Nature Chemistry,* vol. 1, pp. 500-506, 2009.

[132] P. Collins, K. Bradley, M. Ishigami and A. Zettl, “Extreme oxygen sensitivity of electronic properties of carbon nanotubes”, *Science,* vol. 287, pp. 1801-1804, 2000.

[133] A. Yamauchi, Y. Shin, M. Shinozaki and M. Kawabe, “Membrane characteristics of composite collodion membrane IV. transport properties across blended collodion/nafion membrane”, *Journal of Membrane Science,* vol. 170, pp. 1-7, 2000.

[134] Y. Eminaga, M. Brischwein, J. Wiest, J. Clauss, S. Becker and B. Wolf, “Self calibration of a planar dissolved oxygen sensor”, *Sensors and Actuators B*, vol. 177, pp. 785-791, 2013.

[135] T. Xu, W. Zhao, J. Zhu, M. Albanna, J. Yoo and A. Atala, “Complex heterogeneous tissue constructs containing multiple cell types prepared by inkjet printing technology”, *Biomaterials*, vol. 34, pp. 130-139, 2013.

[136] F. Chen, L. Lin, J. Zhang, Z. He, K. Uchiyama and J. Lin, “Single-cell analysis using drop-on-demand inkjet printing and probe electrospray ionization mass spectrometry”, *Analytical Chemistry*, vol. 88, pp. 4354-4360, 2016.

[137] W. Choi, D. Ha, S. Park and T. Kim, “Synthetic multicellular cell-to-cell communication in inkjet printed bacterial cell systems”, *Biomaterials*, vol. 32, pp. 2500-2507, 2011.

Used symbols and abbreviations

CNT: Carbon nanotubes

MWCNT: Multi-walled carbon nanotubes

SWCNT: Single-walled carbon nanotubes

CNP: Carbon nanoparticles

MOD: metal organic compounds

PET: polyethylene terephthalate

PEN: Polyethylene naphthalate

PI: Polyimide

R2R: Roll-to-roll

IDES: Interdigitated electrodes

We: Weber number, defines the balance between inertial and capillary forces

Re: Reynolds number, defines the ratio of inertial to viscous forces

Oh: Ohnesorge number, characterizes the behavior of liquid drops

Z: dimensionless number, Z= (1/Oh)

$\boldsymbol{\rho}$: density of the ink

$\boldsymbol{\eta}$: viscosity of the ink

$\boldsymbol{\gamma}$: surface tension of the ink

$\boldsymbol{v}$: average velocity of the droplet

a: radius of the printing orifice

$\boldsymbol{v_{min}}$: minimum velocity needed for droplet emission

L: length of the printing nozzle

C: speed of sound in the ink

$\boldsymbol{p_{max}}$: maximum droplet spacing for a line with stable width

$\mathbf{d_0}$: diameter of the droplet in flight

$\mathbf{d_{eqm}}$: diameter of the droplet on the substrate

θ: contact angle of the droplet with the substrate